Crystallization of Alpha-Calcium Sulphate Hemihydrate by Aqueous Reaction of Calcium Chloride with Sulphuric Acid

By

Seref Girgin

Department of Mining, Metals and Materials Engineering
McGill University
Montreal, Quebec, Canada
August 2006

A Thesis submitted to the Office of Graduate and Postdoctoral Studies in partial fulfillment of the requirements of the degree of Doctor of Philosophy

Library and
Archives Canada

Published Heritage
Branch

395 Wellington Street
Ottawa ON K1A 0N4
Canada

Bibliothèque et
Archives Canada

Direction du
Patrimoine de l'édition

395, rue Wellington
Ottawa ON K1A 0N4
Canada

Your file Votre référence
ISBN: 978-0-494-32184-3
Our file Notre référence
ISBN: 978-0-494-32184-3

NOTICE:
The author has granted a non-exclusive license allowing Library and Archives Canada to reproduce, publish, archive, preserve, conserve, communicate to the public by telecommunication or on the Internet, loan, distribute and sell theses worldwide, for commercial or non-commercial purposes, in microform, paper, electronic and/or any other formats.

The author retains copyright ownership and moral rights in this thesis. Neither the thesis nor substantial extracts from it may be printed or otherwise reproduced without the author's permission.

AVIS:
L'auteur a accordé une licence non exclusive permettant à la Bibliothèque et Archives Canada de reproduire, publier, archiver, sauvegarder, conserver, transmettre au public par télécommunication ou par l'Internet, prêter, distribuer et vendre des thèses partout dans le monde, à des fins commerciales ou autres, sur support microforme, papier, électronique et/ou autres formats.

L'auteur conserve la propriété du droit d'auteur et des droits moraux qui protège cette thèse. Ni la thèse ni des extraits substantiels de celle-ci ne doivent être imprimés ou autrement reproduits sans son autorisation.

In compliance with the Canadian Privacy Act some supporting forms may have been removed from this thesis.

While these forms may be included in the document page count, their removal does not represent any loss of content from the thesis.

Conformément à la loi canadienne sur la protection de la vie privée, quelques formulaires secondaires ont été enlevés de cette thèse.

Bien que ces formulaires aient inclus dans la pagination, il n'y aura aucun contenu manquant.

Canada

Abstract

The crystallization of alpha-calcium sulphate hemihydrate with simultaneous regeneration of HCl by controlling the reaction of H_2SO_4 (2.6M-8M) with concentrated $CaCl_2$ (1-3.5M) solution at 80°C was investigated. The research included 3 studies: (a) study of the kinetics and mechanism of $CaSO_4$ dihydrate (DH) conversion to hemihydrate (HH) and anhydrite (AH) in variable composition $CaCl_2$-HCl media; (b) reactive crytsallization of alpha-hemihydrate in a semi-batch reactor configuration following the LaMer Diagram concept; and (c) the study of crystal growth and metal uptake by seeded crystallization with and without the presence of several metal chloride salts. According to the first study, AH is the only stable phase in the range of electrolyte concentration and temperature investigated with DH and HH being either metastable or unstable. In the absence of $CaCl_2$ and at 3M HCl concentration or higher DH converts directly to AH. Maintenance of 0.3M or higher $CaCl_2$ concentration was found to render hemihydrate metastable hence making its production feasible. Solubility estimation of three $CaSO_4$ phases with the aid of OLI Stream Analyser software helped to explain the observed phase transition sequence. SEM characterization further revealed the transition from DH to HH to be governed by the topochemical mechanism.

In the reactive crystallization study H_2SO_4 was the limiting reactant added to the $CaCl_2$ solution up to 0.8 SO_4/Ca molar ratio. The nucleation and growth stages were successfully separated via supersaturation control achieved by regulated addition of the limiting reactant in multiple steps. This separation permitted the growth of the homogeneously nucleated crystals within the metastable zone to needle-shaped hexagonal crystals (acicular habit). Upon recycling (seeding) of the product further growth was achieved, producing crystals with 80 μm – volume based mean crystal diameter- or 100-120 μm length and 10-15 μm diameter. Growth of the seed crystals appeared to follow an agglomeration mechanism. However, in the presence of foreign metal cations (in particular divalent, Mg^{2+}, Fe^{2+}, Ni^{2+} and trivalent, Al^{3+}, Fe^{3+}) crystal growth was severely retarded via their apparent adsorption. Some of the metal cations, namely Na^+, Ni^{2+}, Al^{3+} were found to incorporate into the hemihydrate crystal structure to a variable extent from 0.3g/t for Na to 7g/t for Ni and 11g/t for Al. The chloride uptake was less than 10 ppm.

Resume

La cristallisation du sulfate d'alpha-calcium semi hydraté avec régénération simultanée d'acide chlorhydrique, HCl, par contrôle de la réaction de l'acide sulfurique, H_2SO_4 (2.6M-8M) avec une solution de chlorure de calcium, $CaCl_2$ (1-3.5M) à 80°C était l'objet principal de cette étude. Les trois axes principaux de la recherche étaient les suivant : (a) étude de la cinétique et du mécanisme de conversion du sulfate de calcium $CaSO_4$ dihydraté (DH) en sulfate de calcium semi hydraté (HH) et anhydre (AH) dans un milieu aqueux $CaCl_2$-HCl de composition variable; (b) réaction par cristallisation du composé alpha-semi hydraté dans un réacteur de configuration semi batch en suivant le concept décrit par le diagramme de LaMer; et (c) l'étude de la croissance des cristaux et de l'incorporation de l'espèce métallique par nucléation secondaire cristallisation avec ou sans la présence de plusieurs sels de chlorure métalliques. D'après la première étude, AH est la seule phase stable dans le domaine de concentration en électrolytes proposé et à la température étudiée, DH et HH étant dans un état de phase métastable voire instable. En l'absence de $CaCl_2$, et avec une concentration d'HCl de 3M ou plus, DH est directement converti en AH. L'estimation de la solubilité des trois phases de $CaSO_4$ à l'aide du logiciel OLI Stream Analyser a permis de comprendre la séquence de transition de phases observée. Une étude de caractérisation au MEB a par la suite révélé que la transition de DH à HH était gouvernée par un mécanisme topo chimique.

Dans l'étude portant sur la cristallisation, H_2SO_4 était un réactif limitant ajouté à la solution de $CaCl_2$ jusqu'à obtention d'une fraction molaire SO_4/Ca de 0.8. Les étapes de nucléation et de croissance ont pu être réalisées séparément avec succès via contrôle par super saturation, effectué par addition régulée du réactif limitant en plusieurs étapes. Cette séparation a permis la croissance par nucléation homogène de cristaux en forme d'aiguilles à section hexagonale, au sein de la zone métastable. Un recyclage ultérieur (site de germination) de ces produits a permis l'obtention de cristaux d'un diamètre moyen -calculé à partir du volume- de 80μm, soit d'une longueur de 100-120μm et d'un diamètre de 10-15μm. La croissance des sites de germination semblait suivre un mécanisme d'agglomération. Cependant, en présence de cations métalliques (en particuliers divalents, Mg^{2+}, Fe^{2+}, Ni^{2+} et trivalents, Al^{3+}, Fe^{3+}), la croissance des cristaux était extrêmement retardée à cause de l'adsorption apparente de ces derniers. Il a été découvert que certains cations métalliques, notamment Na$^+$, Ni^{2+}, Al^{3+}, s'étaient incorporés à la structure du cristal semi hydraté avec des taux variant de 0.3g/t pour le sodium à 7g/t pour le nickel et 11g/t pour l'aluminium. L'incorporation du chlore était inférieure à 10ppm.

ACKNOWLEDGEMENTS

First of many thanks for the realization of this work, indeed, goes to Professor George P. Demopoulos, who in the first place gave me the opportunity to pursue my studies under his valuable supervision. In addition to what I have learned about hydrometallurgy from him by his personal attempts, courses and encouragement to publish and present, his scientific enthusiasm, trust and confidence led me to develop my character as a researcher. He taught me not only to "not to believe" in anything but also not to love my ideas that might distract my objectivity. Apart from being a great teacher and supervisor, he was a protecting and caring friend that I could always talk and share. Thanks for everything.

I would also like to thank NSERC, Hatch, Noranda and Process Research Ortech for their support to this project.

Many thanks go to Monique Riendeau, Ed Siliauskas and Helen Campbell for their help with characterization and analysis and to Barbara Hanley and Carol Rousseau for being there with a smiling face when ever I need a solution to my never ending administrative problems.

I deeply appreciate the support and encouragement of my dear friend S. Ilker Birbil.

I am grateful to all Hydrometallurgy group members and graduate and undergraduate students for making worth it through out my study. In particular, the presence of Felipe and Maria in my life was very special. I will never forget Felipe's humour, scientific intelligence, loyal friendship and all the drinking and Maria's cooking for me even when she was 8 months pregnant. Musti deserves many thanks because of taking care of me all these years like a younger but big brother. Thanks to Vincent Menard of New Caledonia (I still don't know if it is a country or not) for sharing all night long discussions and big laughs. Many thanks to Jeff for helping with characterization, Cecile for translating my abstract, Cinziana, Georgiana, Marie-Claude, Terry, Dan, Vera, Jarret and many more for being great colleagues and friends.

I am grateful to my family for being who I am. Especially to my mom who always woke up one hour before me not to let me go to school without breakfast, to my baby sister Hazal who is the biggest joy of my life, and my dad who forced his conditions to provide me a good education. I hope you are in a place where you can be proud of me big man.

Finally I dedicate this work to my wife Helin, who had to sacrifice the most. She followed me by leaving everything behind and did not complain about my sleepless working nights, long experiments and meaningless face when I was thinking about my lab results. I can not thank you enough. This is for you…

CONTENTS

Chapter 1 Introduction

Chapter 2 Theory and Technical Background

Chapter 3 Experimental Techniques and Characterization Methods

Chapter 4 Stability of $CaSO_4$ Phases

Chapter 5 Homogeneous Crystallization

Chapter 6. Seeded Crystallization

Chapter 7. Synopsis

LIST OF FIGURES

LIST IF TABLES

CHAPTER 1

Introduction

Chloride metallurgy becomes increasingly an attractive choice for the processing of metal sulphide or oxide feed stocks due to the unique chemical properties of aqueous chloride solutions [1]. For example one of the unique properties of chloride solutions is the high proton activity of HCl solutions, which increases in the presence of metal chloride salts hence making possible the leaching reaction to be carried out under atmospheric pressure conditions. Another important property is the formation of the metal chloro-complexes that allow for efficient metal separation and recovery schemes to be developed. Chloride hydrometallurgy however, suffers from the corrosive nature of both HCl and chlorine gas. This limitation has now though successfully addressed via the development of corrosion-resistant materials such as plastics, alloys and ceramic components hence removing one of the obstacles of adopting chloride metallurgy [2, 3].

One of the most important applications of chloride hydrometallurgy has been the HCl pickling of steel in the ferrous industry due to its superior properties over sulphuric acid pickling in terms of surface properties and pickling rate [2].

In the case of non-ferrous metal oxide leaching processes, the recent development of the UGS Process by QIT [4] to upgrade its titaniferrous slag by dissolving the Fe, Al and Mg impurities by HCl is another proof of the unique power of chloride metallurgy. Efforts to develop HCl-based leaching methods for laterite ores, like Jaguar Nickel Inc.'s atmospheric chloride leaching process [5], are expected to intensify in the near future.

Similarly chloride metallurgical processes have been developed for the processing of metal sulphides such as CLEAR Process developed and operated earlier by Durval Corp. for the treatment of chalcopyrite concentrates [6] or the atmospheric (HCl-O_2) leaching process patented recently for Pb-Zn sulphides [7].

One critical issue in the successful commercialization of an HCl-based leaching process is the regeneration of the lixiviant [2]. In a process where MgO is used as a neutralizing agent, pyrohydrolysis of the $MgCl_2$ produced after neutralization is technically feasible for HCl regeneration [7]. However in the case of using CaO or $CaCO_3$, pyrohydrolysis is not feasible due to the prohibitive high pyrohydrolysis temperature [2]. Either way, however, pyrohydrolysis is a capital and energy intensive technology that has hampered the commercialization of non-ferrous chloride hydrometallurgical processes. Hence a low cost alternative to pyrohydrolysis as a means of regenerating HCl is required to be developed.

Developing a process that can regenerate HCl from spent $CaCl_2$ solution may solve this important problem of chloride hydrometallurgy. The present work does indeed relate to this issue. In particular the reaction of $CaCl_2$ solution with H_2SO_4 under atmospheric pressure is investigated with the objective to produce the high value material, alpha calcium sulphate hemihydrate (α-$CaSO_4 \cdot 0.5H_2O$ or α-HH), with the simultaneous regeneration of HCl according to the following series of simplified reactions:

$$MeO_{(s)} + 2HCl \rightarrow MeCl_{2(aq)} + H_2O \quad \text{(Leaching of oxides)} \quad (1.1a)$$

$$MeS_{(s)} + 2HCl + 1/2O_2 \rightarrow MeCl_{2(aq)} + S_{(s)} + H_2O \quad \text{(Leaching of sulphides)} \quad (1.1b)$$

$$MeCl_{2(aq)} + CaO \rightarrow MeO_{(s)} + CaCl_{2(aq)} \quad \text{(Neutralization)} \quad (1.2)$$

$$CaCl_{2(aq)} + H_2SO_{4(aq)} + xH_2O \rightarrow CaSO_4 \cdot xH_2O_{(s)} + 2HCl_{(aq)} \quad \text{(HCl regeneration)} \quad (1.3)$$

Reaction (1.3) may lead to the production of gypsum ($CaSO_4 \cdot 2H_2O$, DH), anhydrite ($CaSO_4$, AH) or hemihydrate ($CaSO_4 \cdot 0.5H_2O$, HH). The latter can either be of the beta variety (the well known Plaster of Paris) or the alpha variety. Hence the reaction needs to be properly studied and controlled to determine the conditions under which each of these phases form. Moreover the crystallization of calcium sulphate phases is of importance as the production of well grown crystals will facilitate the downstream separation of the regenerated HCl solution from the calcium sulphate precipitate.

Alpha calcium sulphate hemihydrate is a high value construction and dental material because of its excellent physical properties such as setting time and compressive strength [8]. Table 1.1 compares the prices of $CaSO_4$ materials. Currently α-$CaSO_4 \cdot 0.5H_2O$ production is limited to autoclave processes [9, 10] since it is metastable under certain steam pressure only above the boiling point of water [11]. With the addition of electrolytes, the water activity and consequently the transition temperature of DH to HH drops below the boiling point, hence allowing for the development of an atmospheric production process, which is the subject-matter of this study.

Table 1.1. $CaSO_4$ material prices (2003).

Type	Price,US $/tm 2003
Crude Gypsum [12]	17
Calcined Gypsum [12]	18
By-Product Gypsum [12]	5
Plasters [12]	160
Natural Anhydrite [12]	100
Alpha gypsum [13]	698

Objectives

Although there are a few studies described in the literature involving the production of α-HH in chloride media either by conversion of gypsum to alpha-hemihydrate or by reacting $CaCl_2$ with H_2SO_4, none of them provide sufficient information on the kinetic metastability limits of hemihydrate or the factors controlling the crystal quality. It is, therefore, the basic purpose of this study to establish first how to produce α-HH and then how to improve the quality of the produced α-HH crystals in a system where HCl can also be recycled. More specifically, this thesis seeks to address the following objectives:

(1) To establish an operating window for α-$CaSO_4 \cdot 0.5H_2O$ formation in $CaCl_2$-H_2SO_4 reaction media under atmospheric pressure conditions and to identify crystal phase transformations and mechanisms.

(2) To describe the reactive crystallization chemistry of α-$CaSO_4 \cdot 0.5H_2O$ during $CaCl_2$/H_2SO_4 reaction.

(3) To improve the physical properties (i.e., size, morphology, filtration rate) of produced α-$CaSO_4 \cdot 0.5H_2O$ material by controlling supersaturation, seeding and recycling.

(4) To investigate the effects of metal chloride impurities/admixtures on α-HH crystal properties in order to produce metal and chloride-free crystals.

Thesis Lay-out

The thesis has been organized into a number of chapters as follows: The literature Review given in Chapter 2 provides information on crystallization and precipitation chemistry emphasizing the metastability and supersaturation characteristics of solutions. In this part, nucleation, crystal growth and other factors affecting crystal quality are discussed. After that, a brief introduction of the various $CaSO_4$ crystal phases is given with focus on the differences of alpha and beta forms of calcium sulphate hemihydrate. This is followed by a discussion of the thermodynamic stability and solubility of $CaSO_4$ phases. Finally the chapter includes a review of the laboratory and industrial methods available for the production of α-$CaSO_4 \cdot 0.5H_2O$ and the application properties of the latter.

Chapter 3 describes the experimental set-up, procedure and materials used during experimental studies and the methods used for analysis and characterization.

Chapter 4 presents the results of stability tests, where dihydrate-hemihydrate-anhydrite conversion was monitored as a function of electrolyte concentration and time. Besides, Chapter 4 discusses the transformation mechanisms of above-mentioned phases.

Chapter 5 deals with the detailed investigation of the crystallization of α-HH by the reaction of $CaCl_2$ with H_2SO_4 in a semi-batch reactor configuration. An operating window for HH production is proposed as a function of final $CaCl_2$/HCl concentration and time. The system is analysed in terms of separation of homogeneous-heterogeneous nucleation stages during the progress of the reaction. In addition, crystal quality properties such as size, shape and filtration rate are determined and correlated to supersaturation-effecting parameters such as H_2SO_4 concentration, addition rate and method (i.e. titration versus stepwise addition).

Chapter 6 focuses on the conditions of improving final product quality with the use of seed (lab made and commercial α-HH) and recycling and presents the findings of the tests where the effect of several metal chlorides on crystal growth and impurity uptake was investigated.

Finally the thesis ends with Chapter 7, where a global summary of the main findings of the study is presented along with the original contributions made to knowledge and some ideas for future work.

References

[1] Muir, D.M., “Basic principles of chloride hydrometallurgy” in Chloride Metallurgy 2002, Eds. Peek, E., Van Weert, G., CIM, Montreal, QC, 2002, 759-778.

[2] Van Weert, G. and Peek, E.M.L., “Reagent recovery in chloride hydrometallurgy--some missing links”, Hydrometallurgy, 29, 1992, 513-526.

[3] Babale, D.D., Wandji, R., and Bessiere, J., “Concentrated hydrochloric acid media: acid-base, oxidation-reduction, and solvation properties”, J. Chem. Eng. Data, 35, 1990, 345-347.

[4] Hudon ,G., Pepin, Y., Turgeon, J-F., “Impact of mortar properties on the integrity of an autoclave brick lining system”, in Pressure Hydrometallurgy 2004, Eds. M.J. Collins and V.G. Papangelakis, CIM, Montreal, QC, 2004, 651-662.

[5] Harris, G.B., Magee, T.J., Lakshmanan, V.I., “The Jaguar Nickel Inc. Cechol Laterite Project-Atmospheric chloride leaching process”, in International Laterite Nickel Symposium 2004, Eds. W.P. Imrie, D.M. Lane, TMS, Warrendale, PA, 2004, 219-241.

[6] Dutrizac, J.E., "The leaching of sulphide minerals in chloride media", Hydrometallurgy, 29, 1992, 1-45..

[7] Allen, C., Kondos, P., Payant, S., Van Weert, G., Van Sándwich, A., "Production of zinc oxide from complex sulphide concentrates using chloride processing", US Patent, No. 6,395,242, 2002

[8] Ling, Y., Demopoulos, G.P., Giove, A., Filippou, D., "Technical evaluation and characterization of alpha calcium sulphate materials", in 7th Science and Technology Conference on Gypsum and Fly Ash, Toronto, Ontario, 2002, 6-1 to 6-14.

[9] Engert, H. J. and Koslowski, T., New gypsum binder alpha 2000, ZKG International, 51(4), 1998, 229-237.

[10] Brosig, A., "Calcining technologies for the conversion of FGC gypsum into alpha and beta hemihydrate", in 6th International Conference on Natural and Synthetic Gypsum, Process Research Ortech, Toronto, Ontario, 2000, 26-1 to 26-7.

[11] Martynowicz, E.T.M.J., "Impurity uptake in calcium sulphate during phosphoric acid processing", Ph.D. Thesis, Delft University Press, Delft, NL, 1994.

[12] http://tx.technion.ac.il/~cvrkost/ChemicalGypsum/sld007.htm

[13] http://www.sculpt.com

CHAPTER 2

Theory and Technical Background

2.1. Introduction

This chapter reviews the theoretical background and technical literature relating to the crystallization/production of alpha-calcium sulphate hemihydrate in aqueous chloride solutions. In terms of theory, the crystallization fundamentals are discussed by focusing on supersaturation as crystallization driving force, nucleation and growth mechanisms and kinetics and crystal quality control under the effect of supersaturation and admixtures. In terms of technical literature, the main $CaSO_4$ phases are introduced and the stability and solubility of $CaSO_4$ phases as relating to chloride systems are reviewed. Finally information is provided on the production methods of alpha-$CaSO_4$ hemihydrate and its application properties.

2.2. Crystallization Fundamentals

The process of formation of crystals from a supersaturated solution is a non-equilibrium process and generally is defined by the following steps: (1) Solvated ions and molecules partially desolvate and then associate to form ion pairs, complexes or higher aggregates; (2) the ionic and molecular aggregates gather to form crystal nuclei; (3) crystal nuclei grow to crystals.

2.2.1. Supersaturation and Metastability

Supersaturation is the driving force for crystallization and defined as the concentration of component ions (solute) in the solution in excess of the solubility concentration. Supersaturation can be induced in a solution by temperature change, evaporation of the solvent, changing the solvent composition and finally chemical reaction [1]. Solubility (saturation concentration) is the equilibrium condition between solid solute and solution and can be expressed thermodynamically as the equivalence of the chemical potential of the solute in the solution and chemical potential of the solute in solid form [2].

$$\mu_{1,\ \mathrm{solid}} = \mu_{2,\ \mathrm{solution}} \qquad (2.1)$$

The thermodynamic driving force for crystallization can be, therefore, expressed as the difference of these two chemical potentials [3, 4, 5]:

$$\Delta\mu = \mu_1 - \mu_2 = \mu_1{}^0 + RT\ln(a_1) - \mu^0{}_2 - RT\ln(a_2) \qquad (2.2)$$

where; $\Delta\mu<0$ in an instantly crystallizing system and μ^0 is the standard chemical potential ($J.mol^{-1}$), R is the universal gas constant ($8.3144\ J.mol^{-1}.K^{-1}$), T is the absolute temperature (K), a_1 and a_2 are the activities of the solute in solution and the solute in equilibrium with its crystal form, respectively. Rearrangement of equation 2.2 gives;

$$\Delta\mu/RT = \ln(a/a_{eq}) = \ln S \qquad (2.3)$$

where a_{eq} is the activity of the saturated solution and S is saturation ratio (a measure of supersaturation). Equation 2.3 can be recast as:

$$S = \exp(\Delta\mu/RT) \qquad (2.4)$$

Spontaneous crystallization is favoured in the cases where, saturation ratio (S) is greater than 1; that gives negative Gibbs free energy change ($\Delta G < 0$) according to;

$$\Delta G = -RT\ln(a/a_{eq}) = -RT\ln(S) \qquad (2.5)$$

Apart from $S=a/a_{eq}$ expression, supersaturation can practically be defined in terms of solution concentrations ratio;

$$S = C/C_{eq} = m/m_{eq} \qquad (2.6)$$

where C = molarity (mol/L of solution), m = molality (mol/kg of solvent), or concentration difference. In this thesis, the former definition is used;

$$\Delta C = C - C_{eq} \tag{2.7}$$

More strictly speaking, S is expressed with the aid of the solubility product of the compound. Thus assuming a compound having the general formula $C_kA_m \cdot nH_2O$, where C and A are the respective cation and anion, then the saturation ratio becomes:

$$S = \frac{a^k_C . a^m_A . a^n_{H2O}}{K_{sp}} \tag{2.8}$$

There is a maximum level of supersaturation that can be achieved before the solution becomes unstable. Mullin [2] expressed the states of solutes in solution as a function of supersaturation as illustrated in the case of a system in which solubility changes with temperature (Figure 2.1.)

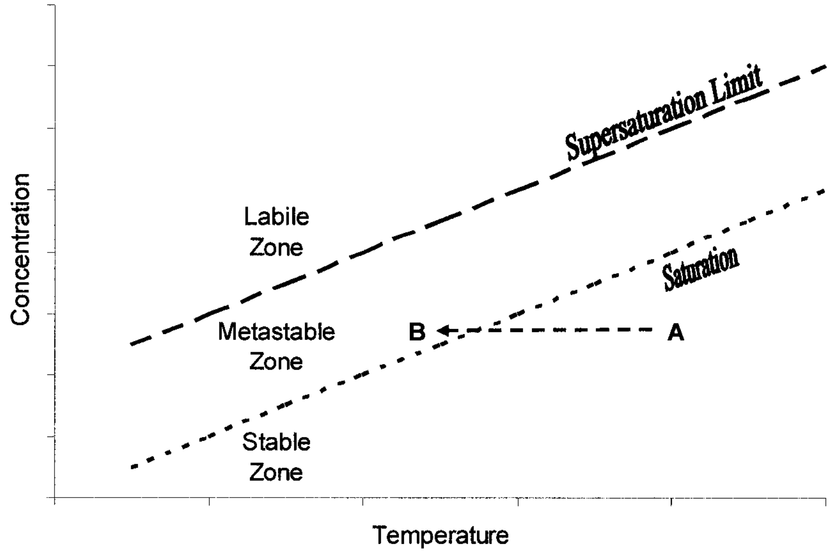

Figure 2.1.Solubility-supersaturation diagram [2]

Stable zone indicates the region below saturation, i.e. no crystallization occurs in that region. Labile (unstable) zone is the region for self-nucleation (spontaneous precipitation) due to the high supersaturation. However at intermediate supersaturation, solutions are metastable. The metastable zone is located between saturation and spontaneous (i.e., homogeneous) crystallization lines. Addition of crystal seed in the metastable zone enables the growth of crystals due to maintaining negative values of ΔG in this zone. In other words, exceeding the saturation level of a solution (decreasing the temperature from point A to B as in Figure 2.1) will not end up with spontaneous crystallization but crystallization will proceed only on the surface of seed crystals. The time required for the initiation of crystallization will be shorter when the temperature is significantly decreased below B, i.e. when a higher supersaturation is generated. Therefore, the higher the supersaturation, the smaller the metastability.

The supersaturation limit (Figure 2.1.) above which spontaneous nucleation occurs (labile zone) is designated as $S_{cr,homo}$.. In most of the precipitation processes, say gypsum precipitation or neutralization, exceeding the $S_{cr,homo}$ concentration (superaturation limit) has the disadvantage of producing very fine sized metastable or poorly crystallized solids, which are not easy to deal with in industrial conditions (i.e. because of slow settling rates). The most effective route recommended for the achievement of well grown and clean crystalline particles is to maintain $S < S_{cr,homo}$ with simultaneous addition of seed material, i.e. to work within the metastable zone (Figure 2.1.). Step-wise addition of precipitating agent is an advantageous method for supersaturation control Figure 2.2. [6].

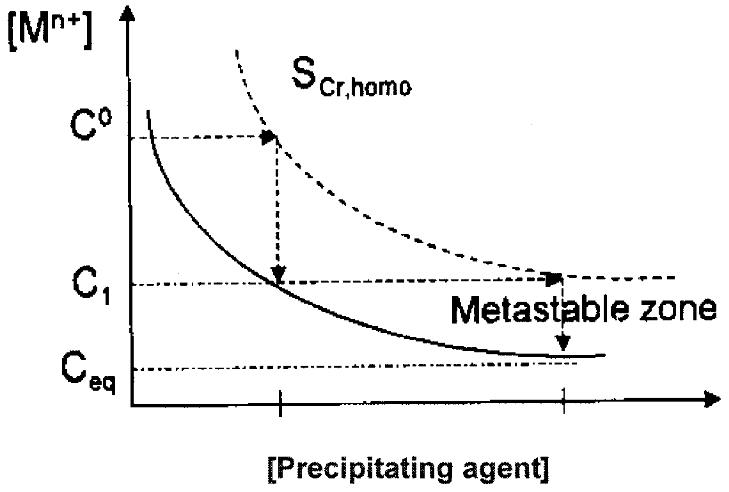

Figure 2.2. The method for step-wise precipitation within the metastable zone [6].

2.2.2. Nucleation

Ions are solvated in solution with water. An increase in the solute concentration leads to the formation of electrically neutral ion pairs. As supersaturation increases, the monomeric ion pairs of the solute aggregate and form polymeric clusters, which upon assuming a critical size become nuclei.

Nucleation of a solute from a solution may occur by different mechanisms [2, 7, 8]. General classification of nucleation processes is represented in Figure 2.3. Of these mechanisms homogeneous nucleation out of solution and surface nucleation on crystal surface (seed) are the most important.

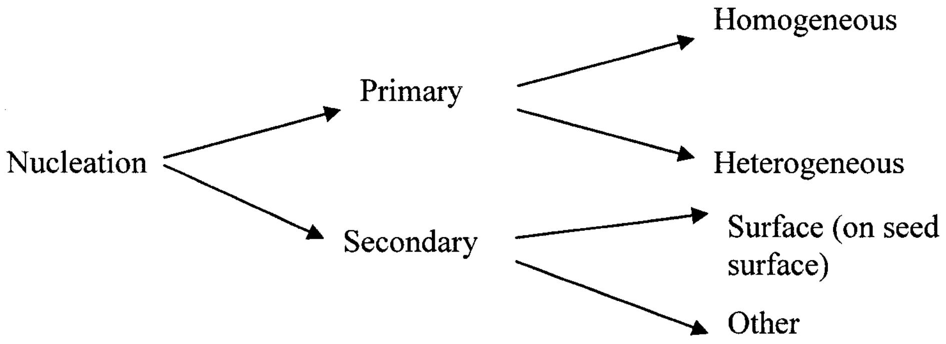

Figure 2.3. Nucleation mechanisms.

Homogeneous-Primary Nucleation: In homogeneous-primary nucleation, formation of a new solid phase takes place in the absence of any solid phase. According to classical nucleation theory, Volmer and Weber in 1926 (as reviewed by Thijssen *et al.* [9]) proposed that the formation of a new phase is initiated by the generation of a very fine embryo within bulk supersaturated (metastable) solution. Formation of these embryos is a result of density or composition variations, which may also lead to their decomposition. Therefore, a stable nucleus can be formed by the addition of each embryo unit (A) successfully and reach a critical cluster size:

$$A_1 + A = A_2 \qquad A_2 + A = A_3 \qquad A_{n-1} + A = A_n \text{ (critical cluster)} \tag{2.9}$$

Formation of such a cluster can be achieved by required free energy change (ΔG), which can be expressed as the balance of the free energy change (ΔG_V) for phase transformation (liquid-solid transformation-volume function) and the free energy change (ΔG_S) for the formation of the nucleus surface (surface area function) [10];

$$\Delta G = \Delta G_S + \Delta G_V \tag{2.10}$$

The free surface energy change (ΔG_S) increases with the variation of interfacial tension (γ_{SL}) between solid surface and surrounding solution. The energy change is positive and added to the system, while the change in free-volume energy is (ΔG_V) is negative. If the nucleus shape is assumed to be spherical, Gibbs free energy change required to form a nucleus of given size can be written as:

$$\Delta G = 4\pi r^2\gamma + (4/3\pi r^3)\Delta G_v \tag{2.11}$$

where r is the nucleus radius, γ is the specific surface energy. According to equation 2.11 on one hand, generation of small number of molecules (i.e. small magnitude of ΔG_V) leads to a positive free energy change, hence eventually dissolving unstable nuclei. However, on the other hand, exceeding a certain size the free energy change becomes negative, hence, spontaneous nucleation occurs (Figure 2.4).

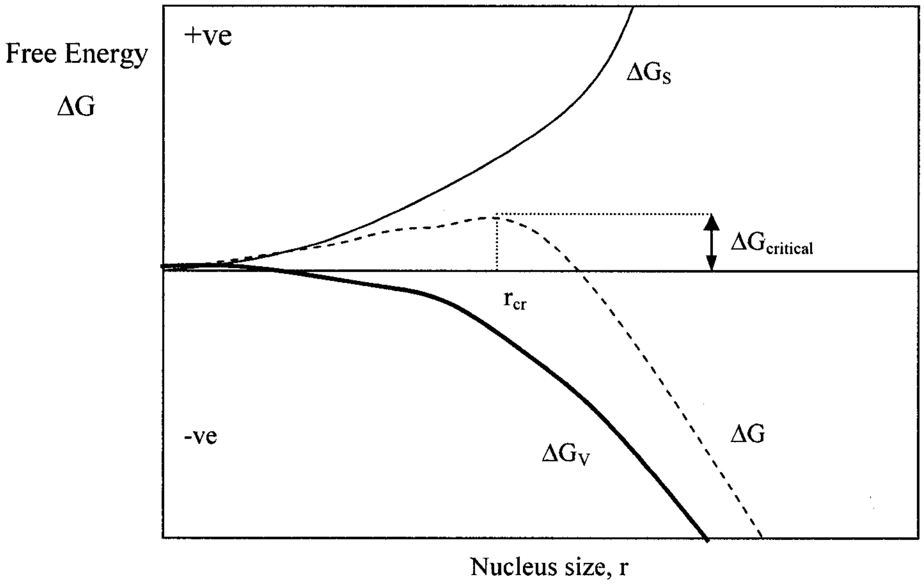

Figure 2.4. Free energy diagram for homogeneous nucleation [2].

The critical radius of a thermodynamically stable nucleus can be determined by minimizing the free energy function [2] (Eq. 2.11):

$$d(\Delta G)/dr = 8\pi r_{cr}\gamma + 4\pi r_{cr}^2\,\Delta G_v = 0 \qquad (2.12)$$

Solving the equation for r_c gives:

$$\Delta G_v = -2\gamma/r_{cr} \qquad (2.13)$$

By substituting ΔG_V in equation 2.11, we get:

$$\Delta G_{critical} = 4\pi r_{cr}^2\,\gamma/3 \qquad (2.14)$$

The growth of critical nucleus is a function of supersaturation and can be expressed by Gibbs-Thompson equation;

$$\ln C/C_{eq} = \ln S = 2\gamma\nu/kTr_c \qquad (2.15)$$

where C is the concentration, ν is the molecular volume ($m^3.mol^{-1}$) and k is the Boltzmann constant ($1.3806503*10^{-23}$ $J.K^{-1}$). Substituting r_{cr} from equation 2.15 in 2.14 gives:

$$\Delta G_{critical} = 16\pi\gamma^3 v^2/3(kT\ \ln S)^2 \qquad (2.16)$$

The nucleation rate, J_{homo} ($nuclei.s^{-1}.cm^{-3}$) is governed by Arrhenius-type equation [11];

$$J_{homo} = A\exp(-\Delta G/kT) \qquad (2.17)$$

where A is the pre-exponential (frequency) factor. Therefore replacing $\Delta G_{critical}$ term in equation 2.16 with the one in Eq. 2.17 gives:

$$J_{homo} = A\exp[-(16\pi\gamma^3v^2)/3k^3T^3(\ln S)] \qquad (2.18)$$

Equation 2.18 clearly suggests that the homogeneous nucleation rate increases with increasing supersaturation and temperature and decreases with increasing surface energy. Considering the fact that the rate of nucleation is the number of nuclei formed per unit time per unit volume (more commonly used units are: # of nuclei.s^{-1}.cm^{-3}), high supersaturation will cause the formation of a vast number of nuclei and thus, a fine sized product, which might be undesirable from precipitation process control point of view.

Heterogeneous - Primary Nucleation: Heterogeneous nucleation occurs in the presence of foreign solid surfaces such as dust particles, reactor or impeller surfaces and crystal seed of a different material. Since it is impossible to remove all solid matter from solutions [1], formation of a new solid phase is often governed and catalyzed by the presence of another solid phase in the system. The catalytic effect of such surfaces is due to the decrease in the energy barrier. This decrease in free energy is related to the contact angle in foreign solid-crystal-solution interface (Figure 2.5) [5]:

$$\Delta G_{hetero} = \phi.\Delta G_{homo} \qquad \text{where } \phi < 1 \qquad (2.19)$$

$$\phi = [(2 + \cos\theta)(1 - \cos\theta)^2]/4 \qquad (2.20)$$

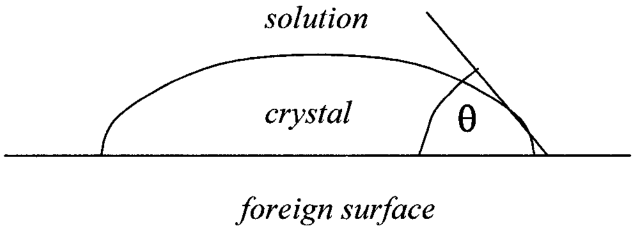

Figure 2.5. Expression of contact angle in foreign surface-crystal-solution interface.

The heterogeneous nucleation rate can be expressed by free energy change similar to homogeneous nucleation [5]:

$$J_{hetero} = \Omega_{hetero} \exp(-\Delta G_{hetero}/kT) \tag{2.21}$$

where $\Omega_{hetero} < \Omega_{homo}$. There are several expressions in the literature describing the heterogeneous nucleation rate however, difficulty of quantitative testing of these complex theoretical predictions causes controversy in terms of explaining the effect of parameters on heterogeneous nucleation rate. For example Mersmann [1] based on his theoretical predictions, emphasizes the effect of supersaturation along with several parameters (i.e. surface tension, diffusivity, molar density, volumetric surface of foreign particles, adsorption constant, contact angle and surface diffusion coefficient) on nucleation rate. On the other hand, based on qualitative analysis, another group of researchers pointed out that the number of crystals formed in a heterogeneous nucleation system is constant and is not affected by supersaturation [12, 13].

Secondary (Surface) Nucleation: Secondary nucleation is the formation of new solid crystals in a supersaturated solution due to the presence of a parent solid phase. Secondary nucleation occurs at lower supersaturation than required for homogeneous nucleation. The formation of the secondary nuclei is related to initial (dust) breeding, needle breeding and collision breeding mechanisms as well as impurity concentration gradient and fluid shear nucleation mechanisms [11].

In initial breeding, secondary nucleation is activated by very fine seed crystals, more specifically the crystallite sites on the seed crystal surface. These crystallites are larger in size than critical nucleus. At high supersaturation, formation of needle-like or dendritic crystals takes place. These crystals also act as nucleation sites and the phenomenon is called needle breeding. In addition to these mechanisms, high agitation rates may cause the fragmentation of crystals which may act as nucleation sites as well. Nucleation in such a way is referred as collision or attrition breeding. Finally, due to the microabrasion of adsorbed layer of non-crystallised solute, contact nucleation occurs upon crystal-crystal, crystal-crystallizer wall or crystal-stirrer contact.

Impurity concentration gradient nucleation is based on the complexity of the structure of the solution near the crystal surface, where high local supersaturation might occur and impurities are incorporated into the crystal surface, hence, improving the possibility of secondary nucleation. Another source of liquid phase secondary nucleation is fluid shear nucleation and it is caused by relatively high fluid velocity in comparison to crystal velocity thus, removing some of the "adsorbed" layer of clusters from the surface leading to subsequent nucleation in solution similar to homogeneous nucleation at high supersaturation.

Secondary nucleation is the most likely mechanism to occur under low supersaturation regime. Figure 2.6 compares nucleation rates for homogeneous, heterogeneous and secondary (surface) nucleation as a function of supersaturation [14] and it is clearly seen that surface nucleation demands the lowest superaturation for high nucleation rates. It can be further seen, in analogy to $S_{cr,homo}$ that there exist $S_{cr,hetero}$ (above which heterogeneous nucleation occurs) and $S_{cr,surf}$ (above which surface nucleation occurs).

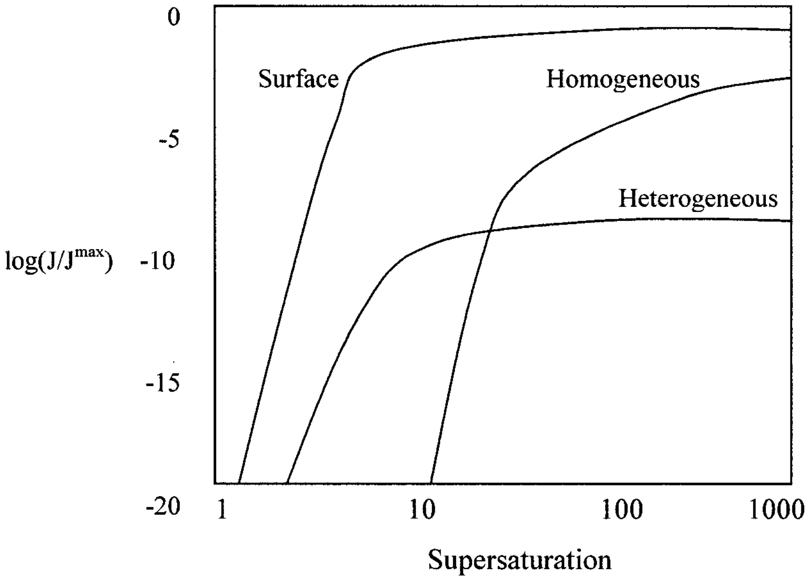

Figure 2.6. Nucleation rates for different mechanisms as a function of supersaturation [14].

2.2.3. Crystal Growth

For better control of crystallization processes in terms of producing crystals with appropriate size, separation of homogeneous nucleation and growth stages by supersaturation control is an important requirement. The LaMer diagram (Figure 2.7) expresses this requirement with the aid of solute concentration vs. time relationship. Slow addition of precipitating agent leads to exceeding $S_{cr,\ homo}$ causing a short-lived homogeneous nucleation event followed by a decrease of supersaturation due to the consumption of solute by precipitation inside the metastable zone, where growth of the initially formed nuclei takes place. In this manner, control of particle size via supersaturation regulation is achieved [15].

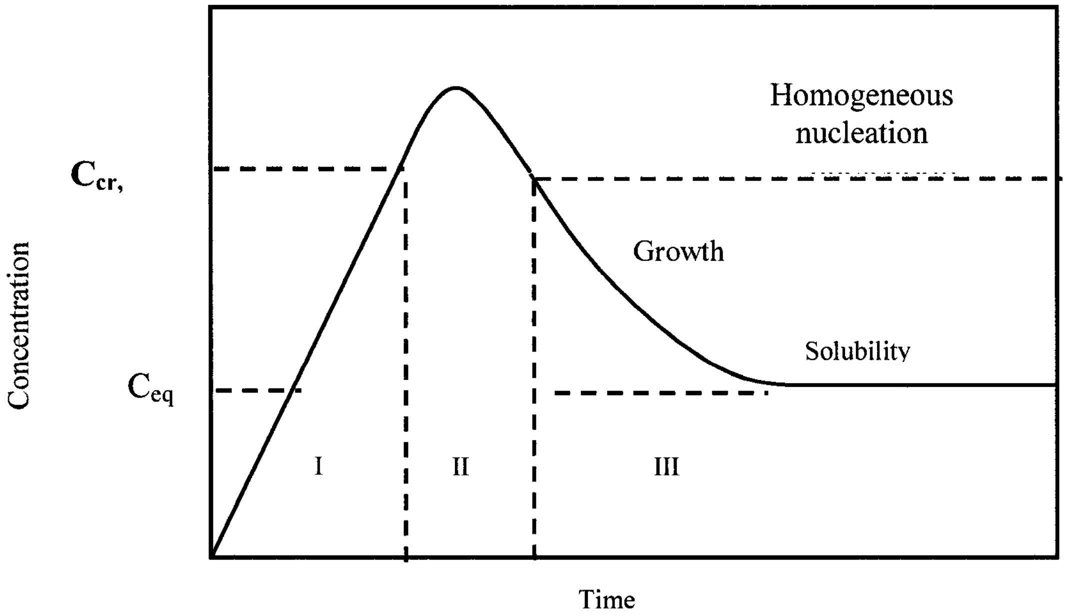

Figure 2.7. The LaMer diagram.

Growth of a crystal out of a supersaturated solution is a complicated process due to several steps taking place before a growth unit from the solution attaches to the crystal lattice [1]. In a crystal growth system, where ionic solute species is the case, the following steps can be considered [2];

(1) Bulk diffusion of solvated ions through the diffusion boundary layer and through the adsorption layer.
(2) Surface diffusion of solvated or unsolvated ions.
(3) Partial or total desolvation of ions.
(4) Integration of ionic species into the lattice structure.
(5) Counter-diffusion of solute through the adsorption layer being replaced by released water and water release through the boundary layer.

Based on these steps, diffusion (mass transfer) and surface integration (reaction) have great importance in terms of growth rate control. The growth rate can be expressed by the change of certain dimension of the crystal with time (G-linear growth rate) or by the increase of mass of the crystal per unit surface area. Both expressions are useful in terms of mass balance or crystal size and shape control.

Crystal Growth by Diffusion: If the integration reaction is faster than diffusion, crystal growth is governed by the diffusive-convective transport of solute units. Diffusivity of a solute is reported to be not only dependent on temperature but also on concentration, dissociation or being multi-component [1].

Crystal Growth by Integration: In an integration system molecules of solute tend to integrate to the energetically most favourable site, which is known as kink site. This is the site where solute molecules have the maximum number of neighbours. According to Kossel [16], a mononuclear layer grows stepwise on the surface of a perfect crystal (Figure 2.8). A monomolecular layer with a flat surface (P′) is located on the surface of the crystal (P). The incomplete axis of P′ forms a S-S′ step and has one or more than one kink (K). Open kink site is the most available position for the attachment of a unit molecule from the solution due to its high binding energy. It should also be noted that, after a crystal has been growing steadily, new molecules are added only at kinks in steps present on the closed packed faces of growing crystal. Molecules adsorbed to locations other than the kink sites do not belong to the crystal [17].

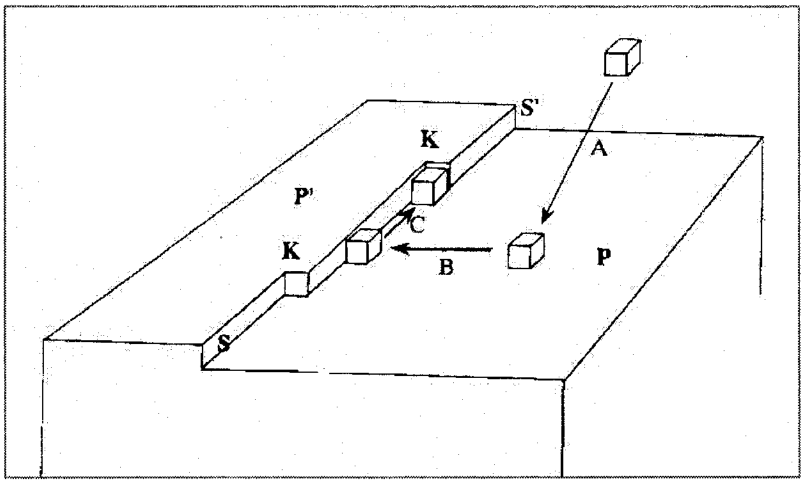

Figure 2.8. Kossel model of crystal growth [16]

In addition to mononuclear-one dimensional integration, two dimensional growth occurs on a flat surface by continuous adsorption of molecules and formation of two-dimensional aggregates by collision. Nuclei are formed and subsequently spread rapidly (due to lower energy requirements). This type of integration, also known as the birth-and-spread model, is not favoured at low supersaturations [16].

Another commonly accepted model for surface integration is Burton-Frank-Cabrera –BCF-(screw dislocation) model [11]. Ideally crystal surfaces are flat and are not available for integration of a growth unit with high surface energy. However in practice, crystals have lattice imperfections. Presence of such imperfections in the form of spiral dislocations creates steps, thus a source of available integration sites.

Crystal Growth Kinetics: The crystal growth rate (n), can simply and often be expressed by the use of overall molar flux according to the following equation;

$$n = k_g(\Delta C)^g \qquad (2.25)$$

where k_g is the growth rate constant and g=2 at low supersaturation and g=1 at high supersaturation; $1<g<2$ is expected in most cases. If the growth rate is limited by diffusion then;

$$n_{dif} = k_d(C-C_I)^g \qquad (2.26)$$

where C is the bulk solute concentration and C_I is the concentration at the interface (concentration gradient at diffusive-convective layer). If the integration is the limiting step;

$$n_{int} = k_r(C_I - C_{eq})^r \quad (2.27)$$

where r is the reaction order. In a diffusion process C_I-C_{eq}<< C-C_I, and in an integration controlled process C-C_I<<C_I-C_{eq}. On the other hand, if k_d and k_r are only temperature dependent, the rate equation can fit to an Arrhenius-type equation;

$$k = A\exp(-E_A/RT) \quad (2.28)$$

where E_A is the activation energy. A crystal growth expression that includes the effect of temperature and supersaturation, therefore, can be expressed as;

$$G = A\exp(-E_A/RT)\Delta C^g \quad (2.29)$$

As is clearly seen from the equation, growth rate is positively affected by supersaturation as long as number of nucleating particles is constant.

2.2.4. Factors Affecting Crystal Quality

There are several factors in a precipitation process that affect crystal growth and quality. For example along with supersaturation and admixtures, which will be discussed in more detail in this section, "growth rate dispersion" may occur due to the change in activity [18] and position [19] of dislocations at constant supersaturation, temperature and hydrodynamic conditions. Also "size dependent growth" may occur as a result of different growth rates of different-sized crystal systems. Recrystallization by fluctuating temperature and concentration, ripening, hydrodynamics-mixing and agglomeration are the other factors that may play important role on the quality of final product [5 ,11].

Supersaturation: As mentioned earlier the dependency of growth rate G and nucleation rate J on supersaturation is different. At low supersaturation, the precipitation process is governed by surface or heterogeneous nucleation and the number of crystals formed is determined by the number of active surface nuclei. The crystal growth mechanism, under these conditions, significantly determines the final crystal shape. Integration-controlled growth at low supersaturation generates compact shapes (e.g. cubes) due to the fact that a minimum overall energy of the crystal surface is maintained, which is feasible under "quasi-stationary" conditions at very slow growth. Gypsum precipitation by $CaCl_2$-H_2SO_4 reaction at 20°C-40°C reported to produce plate-like crystals at low supersaturation, while elongated gypsum needles were obtained at high supersaturation [20].

Elongation of crystals at high supersaturation is related to preferential very high growth rates of crystal faces, which interferes with the transfer of the released heat of crystallization from crystal to bulk solution. This results with diluted solution around the crystal faces. Since crystal edges are surrounded by less diluted solution, diffusion will take place in these locations and crystals will elongate [5].

Admixtures: The crystal growth rate is influenced by any trace component in the solution. These trace components are called additives if they are used intentionally for a reason, or known as impurities if their presence is unintentional. These components are called "admixtures".

These components are known to cause growth-retardation via their adsorption onto the crystal surface and the blocking of the penetration of growth units [1]. Since the penetration requires a different path, the step becomes rounded and consequently incorporation of growth units to the sites becomes slower, thus decreasing the overall growth rate. Once the admixture concentration reaches a critical value, the distance between adsorbed admixture molecules become smaller than the nuclei and the growth process stops for a period of time until another site becomes available for growth [5]. This phenomenon is very well exemplified with the effect of phosphoric acid-based organic additives on gypsum crystal habit, which is usually needle-shaped but with the aid of additives plate-like crystals are obtained. Furthermore, at certain concentration of additive, growth may stop for a certain time. This stoppage time is reported to increase with increasing additive concentration [21].

The presence of admixtures not only causes the retardation of crystal growth but there are cases, where the crystal growth rate is improved by addition of inorganic admixtures, which decrease the interfacial tension, providing thus greater surface nucleation in the birth and spread mode of growth. Due to the same effect step packing is narrowed in the BCF model, which results in increasing growth rate. For example NaCl is reported to have a positive effect on gypsum growth rate [22] as do Cu^{+2} and Zn^{+2} on $CuSO_4 \cdot 5H_2O$ at certain concentration [23].

2.3. $CaSO_4$ Phases

Calcium sulphate is a commonly found mineral in nature and occurs in sedimentary deposits. $CaSO_4$ materials are also produced in several industrial processes such as flue gas desulphurization, phosphoric acid production and desalination.

Calcium sulphate dihydrate (gypsum-$CaSO_4 \cdot 2H_2O$), hemihydrate ($CaSO_4 \cdot 0.5H_2O$) and anhydrite ($CaSO_4$) are the three principal modifications of calcium sulphate.

Hemihydrate has the forms of α-hemihydrate and β- hemihydrate. Alpha hemihydrate is also called alpha-gypsum in some commercial applications while β- hemihydrate is commonly known as Plaster of Paris. Apart from crystallinity or crystal size, the differences that make α-HH a better building material than β-HH upon hydration [24] can be traced to thermodynamic factors [25] and preparation factors [26].

In terms of preparation factors, the formation of α-hemihydrate is favoured in aqueous environment by dehydrating gypsum in the presence of electrolytes in acidic solutions, in water or in steam over the atmospheric pressure On the other hand the formation of β- hemihydrate is favoured when gypsum is dehydrated via heating with insignificant (or no) water vapour (in dry atmosphere) [27].

Differential thermal analysis (DTA) indicates that dehydration of alpha and beta forms of hemihydrate (HH) exhibit different characteristics. In the case of beta-HH, dehydration occurs in two stages. However for the alpha variety, transformation to anhydrite III (soluble anhydrite or γ-$CaSO_4$) occurs at 200-250°C spontaneously followed by anhydrite II (insoluble anhydrite or β-$CaSO_4$) transformation. These two transitions take place at 100°C and 300°C for beta hemihydrate [28].

One of the most significant differences between the two forms of hemihydrate was displayed by Follner *et al.* [27] using Proton Nuclear Magnetic Resonance (^{1}H NMR). In this method, where dipole interactions between neighbouring hydrogen protons can be monitored, the strong peak observed at 0 kHz for β- hemihydrate indicates an isolated group with more than 2 hydrogen protons. Such difference between alpha and beta forms, according to the authors, means different surroundings of the hydrogen protons, therefore, different behaviour upon hydration.

Based on the findings of ^{1}H NMR and DTA analysis, the authors [27] questioned the nature of hydrogen bonding that had been suggested by Bezou et al. [29]. In particular, Follner *et al.* [27] concluded that oxonium ions (i.e. $H_5O_2^+$ or $H_7O_3^+$) are more likely to occur than normal hydrogen bonds in the case of beta-HH.

2.3.1. Stability of $CaSO_4$ Phases

A prerequisite in understanding the crystallization behaviour of $CaSO_4$ modifications is the examination of the thermodynamic stability (activity-solubility-stability) of the three above-mentioned phases. The temperature border between the stability regions of $CaSO_4{\cdot}2H_2O$ (dihydrate, DH) and $CaSO_4$ (anhydrite-AH) in water varies between 40-60°C according to several investigators [30-36]. The region of kinetically feasible but thermodynamically unstable (metastable) $CaSO_4{\cdot}0.5H_2O$ (hemihydrate-HH) borders stable AH and unstable DH region at around boiling point in water. With an increase in electrolyte concentration, the transition temperature of $DH_{(stable)}$ to $AH_{(stable)}$ or $DH_{(metastable)}$ to $HH_{(metastable)}$ drops significantly (Figure 2.9) [30, 37, 38]. Therefore it may be possible to produce HH below the boiling point, which avoids the application of an autoclave process. On the other hand, formation of a least stable phase, say HH, before the stable phase obeys "Ostwald rule of stages" [39]. Ostwald discovered that, in highly supersaturated solutions, the first homogeneously precipitating phase is the metastable phase rather than the thermodynamically stable phase.

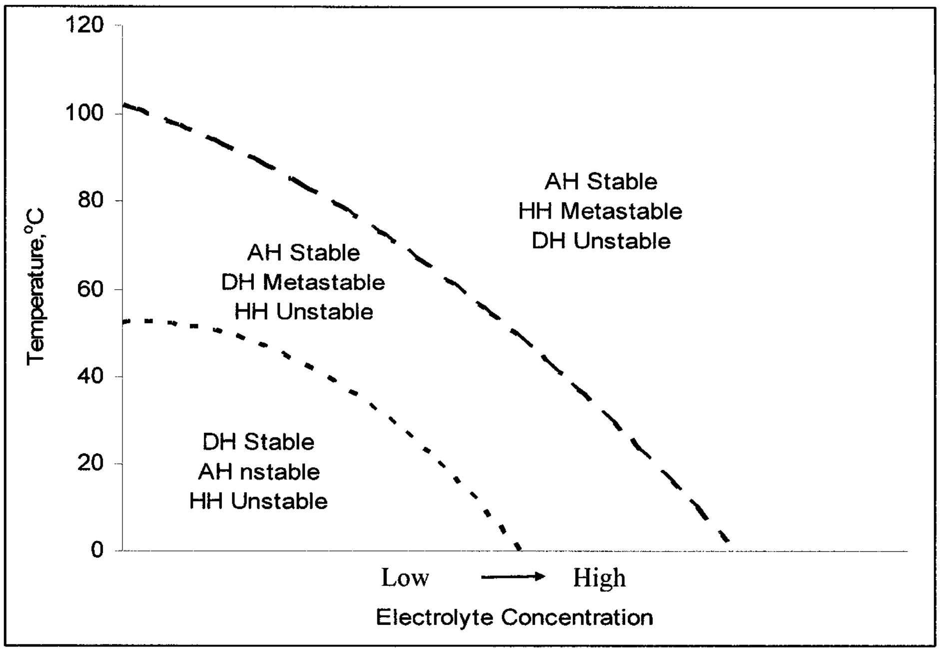

Figure 2.9. Stability of $CaSO_4$ phases as a function of temperature and electrolyte concentration (adapted from [37]).

The effect of solution composition and temperature on the stability of different $CaSO_4$ modifications can be explained by considering the solubility of these phases. In Figure 2.10 the solubility products of the 3 phases in water as a function of temperature are shown. Intersecting points of the lines indicates the phase transition temperatures of $CaSO_4$ modifications in pure water. Phase transition between HH and DH occurs at 377K (104°C) when the water activity is assumed to be 1 [40]. The water activity decreases in concentrated solutions of various electrolytes, such as $CaCl_2$ and HCl [41].

Since the solubility product is a function of temperature and the phase transition temperature is determined by water activity, the HH and DH stability may be related to the water activity. Figure 2.11 clearly illustrates the drop in phase transition temperature due to decrease in water activity [42]. Therefore, the variation of transition temperatures of different $CaSO_4$ modifications as a function of electrolyte concentration can be explained by the decreasing water activity at increasing electrolyte concentrations.

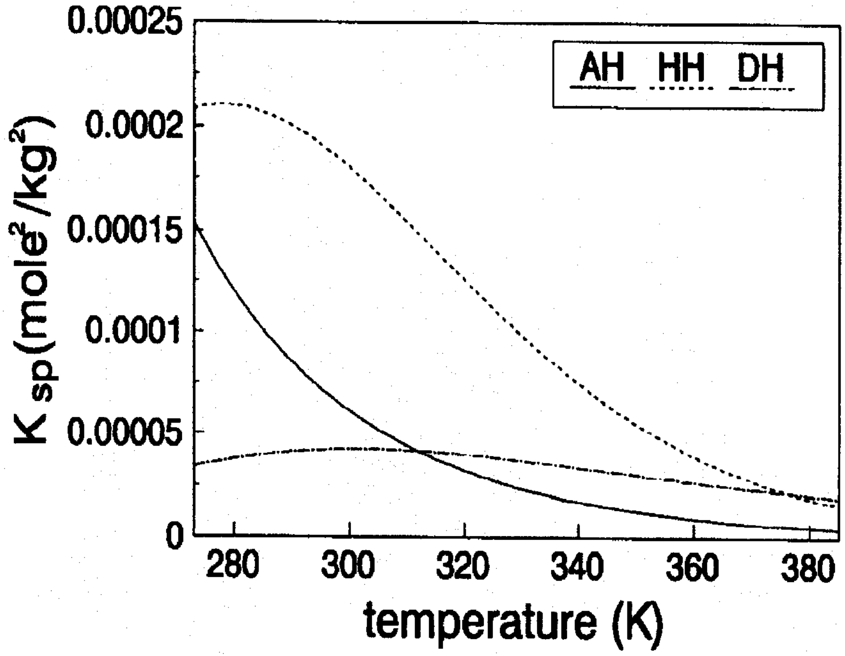

Figure 2.10. The solubility products of $CaSO_4$ modifications in water as a function of temperature [40].

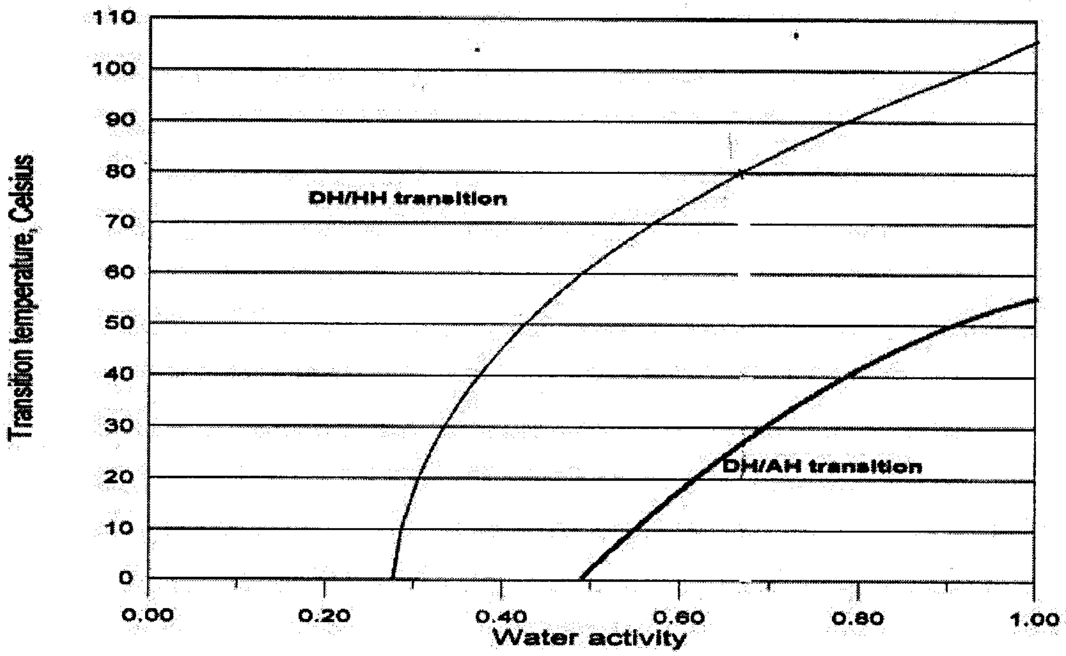

Figure 2.11. Effect of water activity on HH/DH transition temperature [42].

2.3.2. Solubility of $CaSO_4$ Phases

As stated earlier (equation 1.1 in Chapter 1.), the HCl concentration increases and the $CaCl_2$ concentration decreases during the progress of reaction of $CaCl_2$ with H_2SO_4. The solubility of $CaSO_4$ hydrates in the mixed $CaCl_2$-HCl electrolyte system therefore becomes important from a supersaturation control and $CaSO_4$ phase transition point of view.

Till recently there was limited data available on $CaSO_4$ solubilities in aqueous chloride systems. This has changed with a parallel study just completed at McGill University [43]. In the context of the present study, the solubility of $CaSO_4$ dihydrate as a function of HCl and/or $CaCl_2$ solution at 80°C is presented in Figure 2.12 [44-45]. The solubility of $CaSO_4$ in HCl, which is very important from HCl regeneration point of view, gives a peak around 3M concentration and at higher concentrations drops significantly. Besides, since the solubility of $CaSO_4$ in $CaCl_2$ solution is very low due to the common ion effect, the presence of $CaCl_2$ in 1M HCL solution causes the $CaSO_4$ solubility to drop drastically. Absence of HCl favours very low $CaSO_4$ solubility due to the same affect, as well.

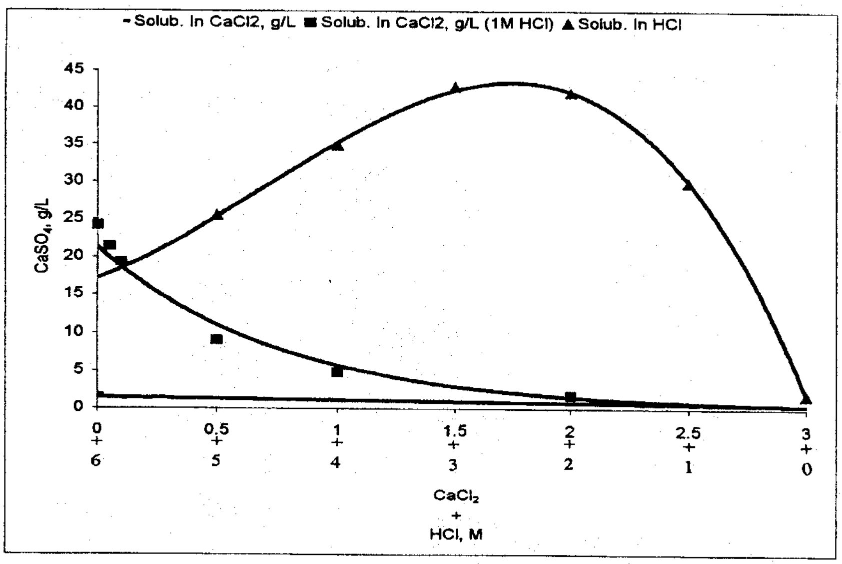

Figure 2.12. The solubility of $CaSO_4$ dihydrate in HCl, $CaCl_2$ and $CaCl_2$-1M HCl solutions (80°C).

2.4. Alpha-$CaSO_4$ Hemihydrate Production

2.4.1. Laboratory Methods of Alpha-HH Production in Chloride Media

Atmospheric production of alpha $CaSO_4$ hemihydrate in aqueous chloride solutions has been the subject of several previous works. In addition, the production of hemihydrate from phosphoric acid in phospogypsum process [37, 46, 47] and by reaction of lime with H_2SO_4 [48], has been reported but none of them is known to have reached commercial status.

Studies dealing with hemihydrate production from chloride media mostly involve the curing of synthetic or natural gypsum in chloride salts. Sukimoto et al. [49] studied the hydration and dehydration properties of $CaSO_4$ phases equilibrated in the environment of NaCl, NH_4Cl, $NaNO_3$, NH_4NO_3 and CH_8COONH_4. Zurz et al. [50] reported the production of α-HH by the transformation of flue-gas gypsum under non-autoclave conditions ($T<110^oC$) in concentrated salt solutions such as NaCl, NH_4Cl, NH_4NO_3, $Mg(NO_3)_2$, $CaCl_2$, $MgCl_2$, $NaNO_3$ and $MgSO_4$ and evaluated the produced material in terms of physical application properties. Hina and Nancollas [51], in a recent patent, gave extensive information on a method of making α-HH by the equilibration of DH in inorganic salts such as NaCl, KCl, $NaNO_3$, $MgCl_2$, $CaCl_2$ at around 90^oC (85-98^oC). In connection to present study, the $CaCl_2$ salt concentration was varied between 3-6M and DH kept for equilibration up to 3 hours. Succinic, mallic and tartaric acids were the investigated organic crystal morphology modifiers, which were reported to have a crystal growth retarding effect.

Yasue and co-workers [52] and Berrie and Woolie [53] were found to be the only investigators who have worked on preparation of α-HH by reactive crystallization in chloride solutions. In the former study, Yasue *et al.* investigated the effect of supersaturation degree on crystal properties of HH produced from the reaction system of $CaCl_2$ / H_2SO_4 and $Ca(NO_3)_2$ / H_2SO_4 at 100^oC. Berrie and Woolie, on the other hand, described in a patent the spontaneous alpha-HH production at 90^oC via fast (1.25 min. titration and 3 min. equilibration) reaction of $CaCl_2$ with H_2SO_4. Confirmatory tests by present author showed, however, that the produced material was dihydrate rather than hemihydrate and gelatinous in nature rendering its separation from the mother solution impractical.

2.4.2. Industrial Production of Alpha-$CaSO_4$ Hemihydrate

Commercial production of alpha-$CaSO_4$ hemihydrate has always been realized in autoclaves. Two major methods used for the commercial production of alpha hemihydrate are known, namely: the SICOWA-Promineral process and the Omega Process.

The former method practiced in Germany (two variants of it exist i.e. SICOWA-Promineral and Salzgitter Anlagenbau) involves the conversion of FGD gypsum to alpha-HH by treatment in a steam chamber at elevated temperature (≈130-150°C) and pressure (≈1.4 bars-2.8 bars). The autoclaving operation is followed by dewatering, drying and grinding [54 ,55].

The second method (the Omega Process) is based on the pressure oxidation (≈1.4 bars-4.1 bars air pressure) of $CaSO_3$ slurry generated by the neutralization of coal combustion products (sulphur dioxide) at 100-150°C. The autoclaving product is subjected to dewatering and size reduction prior to its use [56].

2.4.3. Applications and Properties of Alpha-$CaSO_4$ Hemihydrate

Alpha-$CaSO_4$ hemihydrate, as a plaster material, has found several applications due to its excellent physical properties such as early and final compressive strength, setting time and expansion etc. Such superior properties over beta-hemihydrate (Plaster of Paris) along with better workability, fire resistance and versatility enabled alpha-hemihydrate plaster to find applications in several fields such as pastes, mortars, casting and statuary materials, concrete, dental materials, ceramics (i.e. pottery plaster), and even in special effect supplies [42, 57]. Among several application properties of plaster materials, consistency, setting time and compressive strength are the most important ones and they are interrelated (Figure 2.13). Consistency is the volume of water required to form a paste with certain viscosity [58]. The higher the consistency the lower the strength and longer the setting time of the plaster.

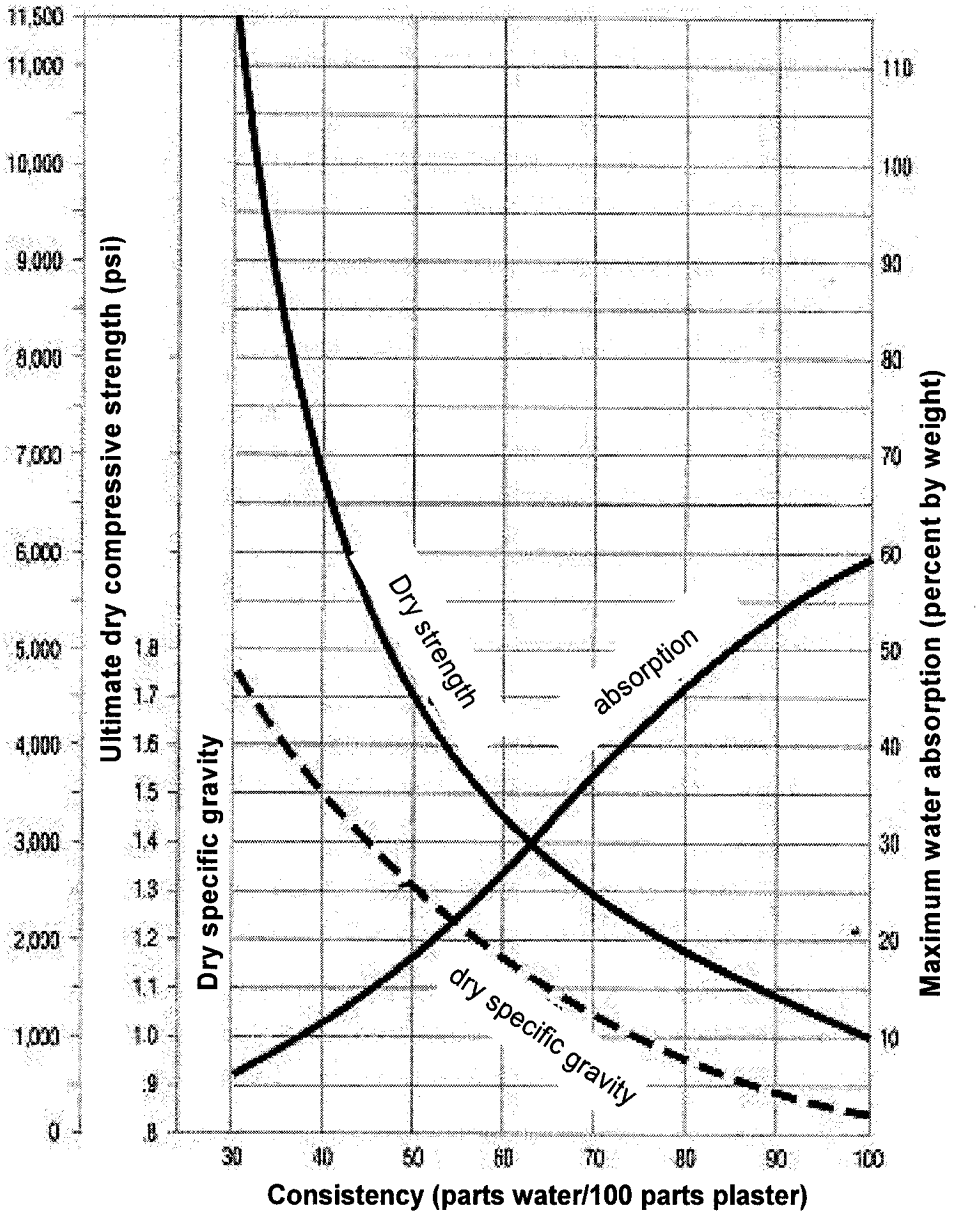

Figure 2.13. Interrelation of application properties of α-HH [58]

Table 2.1 summarizes and compares the application properties of several plaster materials, which were produced with different methods. The superior mechanical strength of α-HH, when compared to that of the most common plaster material (β-HH) is clearly evident. This explains the interest in seeking to develop a method for the production of α-HH under atmospheric pressure conditions.

Table 2.1. Comparison of application properties of various plaster materials

Material	Consistency, g water/100g plaster	Vicat Setting Time, min	Compressive strength, psi	Ref.
Glass-reinforced α -HH			3200-4000	59
Whipmix-dental Laboratory plaster	45	15	4174	42
Omega-Eastroc-BPB Alpha-hemihydrate	41	15	6461	42
BPB-Westroc Alpha-hemihydrate	50		3745	42
Autoclave made α-HH	49	11	3118±450	50
Atmospheric α-HH (42% $Mg(NO_3)_2$)	60	9	3031±508	50
Atmospheric α-HH			2900-4351	51
Atmospheric α-HH	52-70	12-16	2415-3045	42
Plaster of Paris			900	59
Reagent grade β-HH	61	12	1938	42
Gypsum board			420-1400	59

References

[1] Mersmann, A., "Crystallization Technology Handbook", 2nd Edition, Marcel Dekker Inc., New York, NY, 2001.

[2] Mullin, J.W., "Crystallization", 3rd Edition, Butterworth-Heinemann, Oxford, UK, 1993.

[3] Sohnel, O., Garside, J., Jancic, S.J., "Crystallization from solution and thermodynamics of electrolytes", Journal of Crystal Growth, 39, 1977, 307-314.

[4] Mullin, J.W., Sohnel, O., "Expression of supersaturation in crystallization studies", Chemical Engineering Science, 32, 1977, 683-686.

[5] Sohnel, O., Garside, J., "Precipitation-Basic principles and industrial applications", Butterworth-Heinemann Ltd, Oxford, UK, 1992.

[6] Demopoulos, G.P., "Precipitation in aqueous processing of inorganic materials: A unified colloid-crystallization approach to the production of powders with controlled properties", in Processing Materials for Properties, Eds: H. Henein and T. Oki, TMS, Warrendale, Pa, 1993, 537-540.

[7] Nyvlt, J., "Nucleation and growth rate in mass crystallization", Progress in Crystal Growth and Characterization, 9, 1984, 335-370.

[8] Garside, J., "Industrial crystallization from solution", Chemical Engineering Science, 40, 1985, 3-26.

[9] Thijssen, H. A. C., Vorstman, M. A. G., Roels, J. A., "Heterogeneous primary nucleation of ice in water and aqueous solutions", Journal of Crystal Growth, 3-4, 1968, 355-359.

[10] Gibbs, J.W., "On the equilibrium of heterogeneous substances', Collected Works, Longsman-Green, New York, NY, 1928.

[11] Myerson, A.S., "Handbook of Industrial Crystallization", 2nd Edition, Butterworth-Heinemann Ltd, Woburn, MA, 2002.

[12] Mealor, D., Townshend, A., "Homogeneous nucleation of some sparingly soluble salts", Talanta, 13, 1966, 1069-1074.

[13] Garten, V.A., Head, R.B., "Nucleation in salt solutions", Journal of Chemical Society, Faraday Trans. I, 69, 1973, 514-520.

[14] Dirksen, J.A., Ring, T.A., "Fundamentals of crystallization: kinetic effects on particle size distribution and morphology", Chemical Engineering Science, 46(10), 1991, 2389 – 2427.

[15] Sugimoto, T., "Precipitation of monodispersed colloidal particles", Advances in Colloid and Interface Science, 128, 1987, 65-108.

[16] Sawada, K., "Mechanism of crystal growth of ionic crystals in solution", in Crystallization Processes, Ed: H. Ohtaki, John Wiley & Sons Ltd., Toronto, Ontario, 1998, 39-47.

[17] Cabrera, N., Vermilyea, D.A., "The growth of crystals from solution", Growth and Perfection of Crystals, Eds: R.H. Dorimulus, B.W. Roberts, D Turnbull, John Wiley & Sons Ltd., New York , NY, 1958, 393-410.

[18] Davey, R.J., Ristic, R.I., Zizic ,B., "The role of dislocations in the growth of ammonium dihydrogen phosphate crystals from aqueous solutions", Journal of Crystal Growth, 47, 1979, 1-4.

[19] Chernov, A.A., Rashkovich, L.N., Vekilov, "Steps in solution growth: dynamics of kinks, bunching and turbulence", Journal of Crystal Growth, 275, 15, 2005, 1-18.

[20] Deckers, J.M., Lash, J.E., Burns, G., "Heats of crystallization of $CaSO_4.2H_2O$", Bulletin des Societes Chimiques Belges, 93, 1984, 271–279.

[21] Tadros, M.E., Mayes, I., "Linear growth rates of calcium sulphate dihydrate crystals in the presence of additives", Journal of Colloid and Interface Science, 72, 1979, 245-254.

[22] Brandse, W.P., van Rosmalen, G.M., Brouwer, G., "The influence of sodium chloride on the crystallization rate of gypsum", Journal of Inorganic and Nuclear Chemistry, 39, 1977, 2007-2010.

[23] Weijen, M.P.J., van Rosmalen, G.M., “The role of additives and impurities in the crystallization of gypsum”, in Industrial Crystallization 84, Eds; Jancic S.J., and de Jong, E.J., Elsevier, Amsterdam, NL, 1984, 61-66.

[24] Coburn, A., Dudley, E., Spence, R., “Gypsum Plaster: Its Manufacture and Use”, Intermediate Technology Publications, London, UK, 1989.

[25] McAdie, H.G., “The effect of water vapour upon the dehydration of $CaSO_4 \cdot 2H_2O$”, Canadian Journal of Chemistry, 42, 1964, 792-801.

[26] Bensted, J., Varma, S.P., “Investigation of the α and β forms of calcium sulphate hemihydrate” Cement Technology, March/April 1972, pp 67-70.

[27] Follner, S., Wolter, A., Preusser, A., Indris, S., Silber, C., Follner, H., “The setting behaviour of alpha and beta $CaSO_4 \cdot 0.5H_2O$ as a function of crystal structure and morphology”, Crystal Research and Technology, 37, 2002, 1075-1087.

[28] Lehmann, H., “Die phasenbeziehungen im system $CaSO_4$-H_2O”, Tonind.-Ztg., 91(1), 1967, 6-12.

[29] Bezou, C., Nonat, A., Mutin, J.C., Christensen ,N.A., Lehmann, M.S., “Investigation of the crystal structure of γ-$CaSO_4$, $CaSO_4 \cdot 0.5H_2O$ and $CaSO_4 \cdot 0.6H_2O$ by powder diffraction methods”, Journal of Solid State Chemistry, 117(1), 1995, 165-176.

[30] Dahlgren, S.E., “Calcium sulphate transitions in superphosphate”, Fertilizer Materials, 8 (5), 1960, 411-412.

[31] Hardie, L.A., “The gypsum-anhydrite equilibrium at one atmosphere pressure”, American Mineralogist, 52(1-2), 1967, 171-200.

[32] Blount, C.W., Dickinson, F.W., “Gypsum-anhydrite equilibria in systems calcium sulphate-water and calcium sulphate-sodium chloride-water”, American Mineralogist, 58(3-4), 1973, 323-331.

[33] Innorta, G., Rabbi, E., Tomadin, L., "The gypsum-anhydrite equilibrium by solubility measurements", Geochimica et Cosmochimica Acta, 44(12), 1980, pp 1931-1936.

[34] Langmuir, D., Melchior, D., "The geochemistry of calcium, strontium, barium and radium sulphates in deep brines from the Palo Duro Basin, Texas", Geochimica et Cosmochimica Acta, 49(11), 1985, 2423-2432.

[35] Raju, K.U.G., Atkinson, G., "The thermodynamics of "scale" mineral solubilities: (3) Calcium sulphate in aqueous NaCl", Journal of Chemical and Engineering Data, 35(3), 1990, 361-367.

[36] Li, Z., and Demopoulos, G.P., "Model-based construction of calcium sulphate phase transition diagrams in the $HCl-CaCl_2-H_2O$ system between 0-100°C", Industrial and Engineering Chemistry Research, 45, 2006, 4517-4524.

[37] Martynowicz, E.T.M.J., Witkamp, G., Rosmalen, G.M., "The effect of aluminum fluoride on the formation of calcium sulphate hydrates", Hydrometallurgy, 41, 1996, 171-186.

[38] Ling, Y., Demopoulos, G.P., "Phase transformation relationships in the $CaSO_4-H_2SO_4-H_2O$ system", in EPD Congress 2004, Ed: M.E. Schlesinger, TMS, Warrendale, Pa, 2004, 477-487.

[39] Nývlt, J., "The Ostwald rule of stages", Crystal Research and Technology, 30, 1995, 443-449.

[40] Martynowicz, E.T.M.J., "Impurity uptake in calcium sulphate during phosphoric acid processing", Ph.D. Thesis, Delft University Press, Delft, NL, 1994.

[41] Demopoulos, G.P., "Aqueous processing and its role in the production of inorganic materials and environmental protection", Canadian Metallurgical Quarterly, 37, 1998, 1-18.

[42] Ling, Y., "Direct production of alpha-calcium sulphate hemihydrate from sulphuric acid", Ph.D. Thesis, McGill University, Montreal, QC, 2004.

[43] Li, Z. "$CaSO_4$ solubilities in concentrated aqueous chloride solutions", Ph.D. Thesis, McGill University, Montreal, QC, 2006.

[44] Li, Z., Demopoulos, G.P., "$CaSO_4$ solubilities in concentrated aqueous chloride solutions", in Chloride Metallurgy 2002, Eds: E Peek, G. Van Weert., CIM, Montreal, QC, 2002, 561-574.

[45] Li, Z., Demopoulos, G.P., "Solubility of $CaSO_4$ phases in aqueous HCl + $CaCl_2$ solutions from 283 K to 353 K", Journal of Chemical Engineering Data ,50, 2005, 1971-1982.

[46] Van der Sluis, S., Witkamp, G.J., van Rosmalen, G.M., "Crystallization of calcium sulphate in concentrated phosphoric acid", Journal of Crystal Growth, 79, 1986, 620-629.

[47] El Moussaouiti, M., Boistelle, R., Bouhaouss, A., Klein, J.P., "Crystallization of calcium sulphate hemihydrate in concentrated phosphoric acid solutions", Chemical Engineering Journal, 68, 1997, 123-130.

[48] Ling, Y. and Demopoulos, G.P., "Preparation of alpha-calcium sulphate hemihydrate by reaction of sulphuric acid with lime", Industrial and Engineering Chemistry Research, 44, 2005, 715-724.

[49] Sukimoto, S., Hara, N., Mukaiyama, H., "Effects of salts on the formation of α-calcium sulphate hemihydrate in aqueous salts under the atmospheric pressure", Gypsum and Lime, No. 199, 1995, 363-370.

[50] Zurz, A., Odler, I., Thiemann, F., Berghofer, K., "Autoclave-free formation of α-hemihydrate gypsum", in Journal of American Ceramic Society, 74, 1991, 1117-1124.

[51] Hina, A., G.H. Nancollas, "Alpha calcium sulphate hemihydrate and a method of making alpha calcium sulphate hemihydrate", World Patent no. WO0179116, 2001-10-25.

[52] Yasue, T., Kojima, Y., Kishimato, Y., Arai, Y., "Precipitation of alpha gypsum hemihydrate and control of its crystal shape under atmospheric pressure", Gypsum and Lime, No. 239, 1992, 230-237.

[53] Berrie, J.S., Wooley, G.E., "Manifacture of alpha calcium sulphate hemihydrate", U.S. Patent no. 4,120,737, Oct. 17, 1978.

[54] Engert, H. J. and Koslowski, T., "New gypsum binder alpha 2000", ZKG International, 51(4), 1998, 229-237.

[55] Brosig, A., "Calcining technologies for the conversion of FGC gypsum into alpha and beta hemihydrate", in 6th International Conference on Natural and Synthetic Gypsum, Process Research Ortech, Toronto, Ontario, 2000, 26-1 to 26-7.

[56] College, J., The Omega Process: Direct conversion of calcium sulphite to alpha hemihydrate, in 6th International Conference on Natural and Synthetic Gypsum, Process Research Ortech, Toronto, Ontario, 2000, 25-1 to 25-11.

[57] Echterhagen, R., Schlieper, H., Kirchen, G., Morgenroth, H., Wiesgickl, G., "Alpha-hemihydrate- a high value building material made from gypsum, experiences concerning processing, product development and market applications", in 5th International Conference on FGD and Synthetic Gypsum, Toronto, Ontario, 1997, 8-1 to 8-15.

[58] http://www.usg.com (United States Gypsum Company).

[59] http://www.sculpt.com.

CHAPTER 3

Experimental Techniques and Characterization Methods

3.1. Introduction

The experimental work reported in this thesis consists of 4 main parts: (i) Investigation of stability of $CaSO_4$ phases by curing calcium sulphate dehydrate in $CaCl_2$/HCl solutions (Chapter 4), (ii) Homogeneous crystallization tests based on the reaction of $CaCl_2$ with H_2SO_4 (Chapter 5), (iii) Investigation of the role of seeding/recycling and metal chlorides on calcium sulphate hemihydrate crystal growth and foreign metal uptake (Chapter 6).

The procedure applied in each chapter has similarities and differences. The differences are presented in the experimental part of each chapter. This chapter covers the basic common features of typical tests and briefly introduces the materials, experimental set up and characterization techniques employed.

3.2. Materials

All the chemicals used in this study were ACS (American Chemical Society) reagent grade with the exception of alpha-calcium sulphate hemihydrate. The alpha-calcium sulphate hemihydrate used as seed material in chapter 6 marked as "Omega" was a sample of a commercial material produced by Omega Process [1, 2] at East Roc in the USA. Table 3.1 summarizes the name, formula, purpose of use, provider and purity of the rest of the chemicals used in the experimental studies.

The water used in all experimental work for solution preparation, dilution, crystal washing etc. was double distilled water unless other wise specified.

Table 3.1 Chemical reagents employed in experimental studies.

Compound Name	**Formula**	**Purpose**	**Provider**	**Purity (Concentration)**
Sulphuric Acid	H_2SO_4	Crystallization	Fisher Scientific	95-98% (d=1.84 g/cm^3)
Hydrochloric Acid	HCl	Crystallization	ACRÖS Organics	37.5% (d=1.18 g/cm^3)
Nitric Acid	HNO_3	Crystal dissolution	Fisher Scientific	68-70%
Calcium Chloride	$CaCl_2\cdot 2H_2O$	Crystallization	Fisher Scientific	100%
2-Propanol (isopropanol)	$(CH_3)_2CHOH$	Material handling, Particle size analysis	Fisher Scientific	99.9% (d=0.7855 g/cm^3)
Calcium Sulphate dihydrate	$CaSO_4\cdot 2H_2O$	Stability	Fisher Scientific	d = 2.32 g/cm^3
Calcium Sulphate hemihydrate (Plaster of Paris)	β-$CaSO_4\cdot 0.5H_2O$	Characterization	Fisher Scientific	99-100%
Magnesium Chloride	$MgCl_2\cdot 6H_2O$	Crystallization (as impurity)	A&C American Chemicals Ltd.	99-100%
Ferrous Chloride	$FeCl_2\cdot 4H_2O$	Crystallization (as impurity)	Fisher Scientific	100%
Ferric Chloride	$FeCl_3\cdot 6H_2O$	Crystallization (as impurity)	Sigma Aldrich	98%
Nickel Chloride	$NiCl_2\cdot 6H_2O$	Crystallization (as impurity)	Fisher Scientific	MW: 237.31
Sodium Chloride	NaCl	Crystallization (as impurity)	Fisher Scientific	100%
Aluminum Chloride	$AlCl_3\cdot 6H_2O$	Crystallization (as impurity)	Fisher Scientific	MW: 241.43

3.3. Equipment and Procedure

3.3.1. Stability Tests

The experimental set-up employed in the testing of stability of $CaSO_4$ phases is shown in Figure 3.1. The tests were carried out in 250 mL Erlenmeyer flasks (1), which were sealed with rubber stoppers, containing 200 mL of known concentration of electrolyte solution ($CaCl_2$/HCl). The flasks were located in a water bath (2) heated by a thermostatic heater/circulator (3). The solution temperature was monitored by a temperature probe (4). Once the desired temperature was reached, 10 g of $CaSO_4.2H_2O$ were introduced to electrolyte solutions and magnetic stirring (5) initiated at 400 rpm. Solution and solid samples, which were withdrawn at certain time intervals, were handled carefully (refer to section 3.4) followed by the execution of required analysis (refer to section 3.5). Further details of the adopted procedure are presented in Chapter 4.

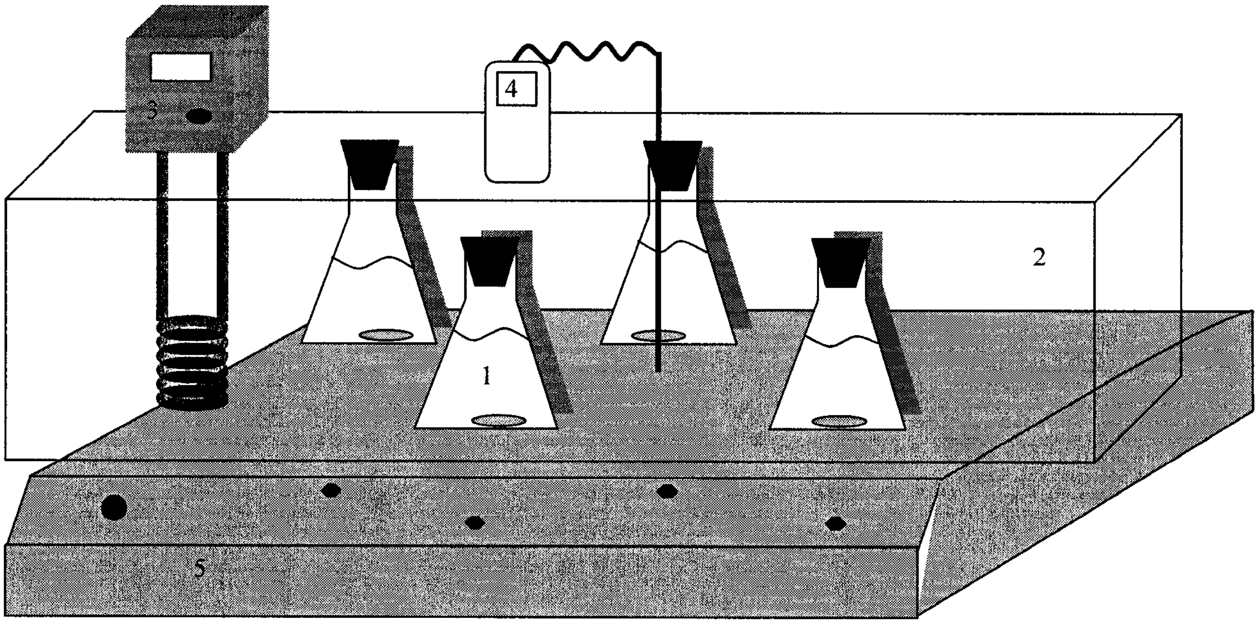

Figure 3.1. Experimental set-up used in $CaSO_4$ stability tests.

3.3.2. Reactive Crystallization Tests

Homogeneous crystallization tests: The experiments were performed in a 2-liter autoclaveable double-jacket glass reactor heated by an oil circulator (Figure 3.2). A standard volume (300 mL) of starting solution located in the reactor (1) with known $CaCl_2$/HCl concentration was heated to 80°C (for all crystallization tests) with the aid of the oil circulator (2). Solution temperature was monitored with a temperature probe (3). Upon attainment of the desired temperature, addition of H_2SO_4 of known concentration was started simultaneous with the initiation of stirring at 400rpm. Stirring was provided by a motor drive (4) and a 4-blade radial impeller (5) was used. The location of the impeller provided uniform mixing. All internal parts were made of glass (reactor, stirring rod) or PVC (reactor top cover) or teflon (impeller) to avoid corrosion problems from the hot and concentrated HCl (solution and vapour).

During $CaCl_2$-H_2SO_4 reaction, H_2SO_4 addition by titration was done using a standardized burette (6) while stepwise addition of acid was made using a graduated cylinder.

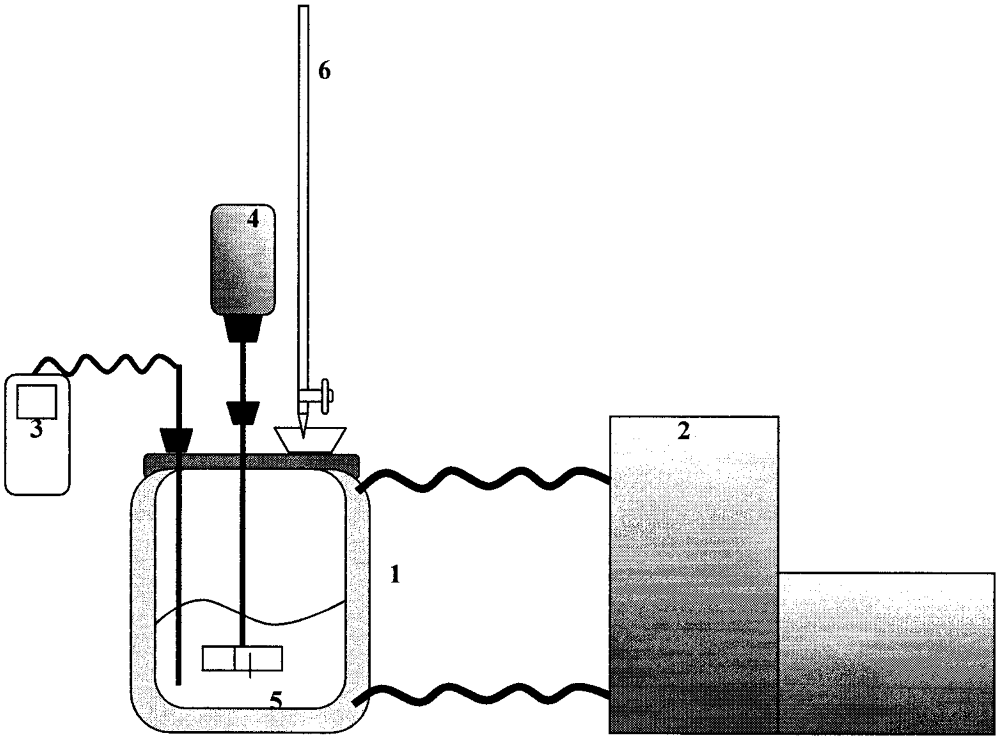

Figure 3.2. Experimental set-up used in crystallization tests.

Most of the reactive crystallization tests involved an equilibration time following the $CaCl_2$-H_2SO_4 reaction period (acid addition period). Aqueous and solid samples taken during reaction and/or equilibration period were carefully handled and subjected to required analysis and filtration rate measurements if required.

Seeding/recycling and metal chloride tests: The basic procedure followed during seeding and recycling tests, which is presented in Chapter 6, was similar to that of the homogeneous tests. In this part of the study H_2SO_4 was added in steps (8 or 4) and the fresh seed (50 or 100g/L) was added in the pre-heated electrolyte solution at the beginning (prior to the addition of H_2SO_4). Each test was run for 4 hours. Lab-made alpha-HH and Omega alpha-HH were used as the fresh seed material.

At the end of each cycle the slurry was divided into two parts. One part was filtered, washed, and dried. A small sample from the dried product was subjected to solid analysis, while the appropriate amount of the rest (approximately 50 or 100g/L) was used as seed material for the next cycle. For each cycle, fresh electrolyte solution was used.

The other part of the solid material produced at the end of each recycle was used for the filtration rate determinations. The solid and solution samples taken during and after each recycling were handled carefully and characterized.

Same crystallization test procedure was followed during the tests where the effect of metal chlorides was investigated. Metal chloride of salts, i.e. $FeCl_2$, $FeCl_3$, $MgCl_2$, $NiCl_2$, NaCl, $AlCl_3$ were added in initial 3M $CaCl_2$ solution to give 0.1M or 1M metal concentration. The impurity-containing $CaCl_2$ solution was reacted with H_2SO_4 at 80°C via 8 addition stages for 4 hours. No equilibration time was allowed.

Measurement of filtration rate: Filtration rate of the resultant crystal suspension was measured immediately following the crystallization test to avoid any property change due to cooling. Filtration was carried out using a press filter under 20 psi pressure and a Whatman filter paper (No. 1, >11μm) of 0.142m diameter. The hot slurry was placed in the filter and immediately sealed tight. 20 psi pressure introduced in the filter and liquid discharge and timer started at the same time. The moment when the pressurized flow of liquid stopped, filtration time recorded. The volume of the collected solution was measured by a graduated cylinder and the filter cake was weighed immediately. The filtration rate reported as the mass of wet filter cake (75-83% solid) deposited on the filter paper per unit area per time in hours.

Stability and crystallization tests were randomly repeated in order to check the reproducibility of the tests. Duplicate data were clearly indicated on presented graphs.

3.4. Material Handling

Handling of produced $CaSO_4$ crystals is critical due to the possibility of phase transformation. This is especially true from the drying point of view, since it may lead to crystallization water loss [3]. On the other hand, washing the crystals with cold water may lead to the transformation of HH to DH. Therefore, washing, filtration, drying and storage should be done properly to avoid phase changes. For this purpose, the temperature of washing water, filtration and drying were tested in order to find the optimum material handling conditions. After performing tests with AH, HH and DH crystals, it was clearly seen that there was no measurable effect of water and filtration temperature on crystal modification, however crystal morphology deteriorated with decreasing washing water temperature [Figure 3.3].

Original HH crystals

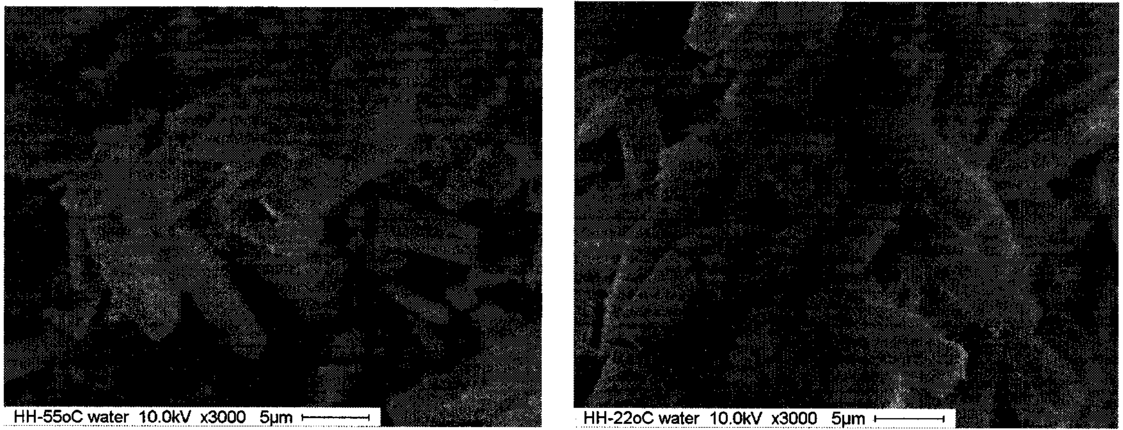

55°C

25°C

Figure 3.3. Deterioration of HH crystals as a function of washing water temperature.

The drying temperature is another important parameter and the tests conducted at 60, 80 and 100°C on DH and HH crystals showed that, drying DH crystals at 100°C promoted the conversion of DH crystals to HH in less than 3 hours (Figure 3.4). However, no conversion was observed on DH at 60 and 80°C after 10 hours drying (Figure 3.5). On the other hand drying HH at 60, 80 and 100°C showed no signs of conversion to AH after 24 hours (Figure 3.6).

As a result of these material-handling tests, the following standard procedure was adopted in the present study. The produced crystals were filtered while hot and then washed with boiling water first and then with acetone to avoid HH to DH conversion and to maintain fast removal of surface water, respectively. Drying was done at 60°C until the constant weight is reached.

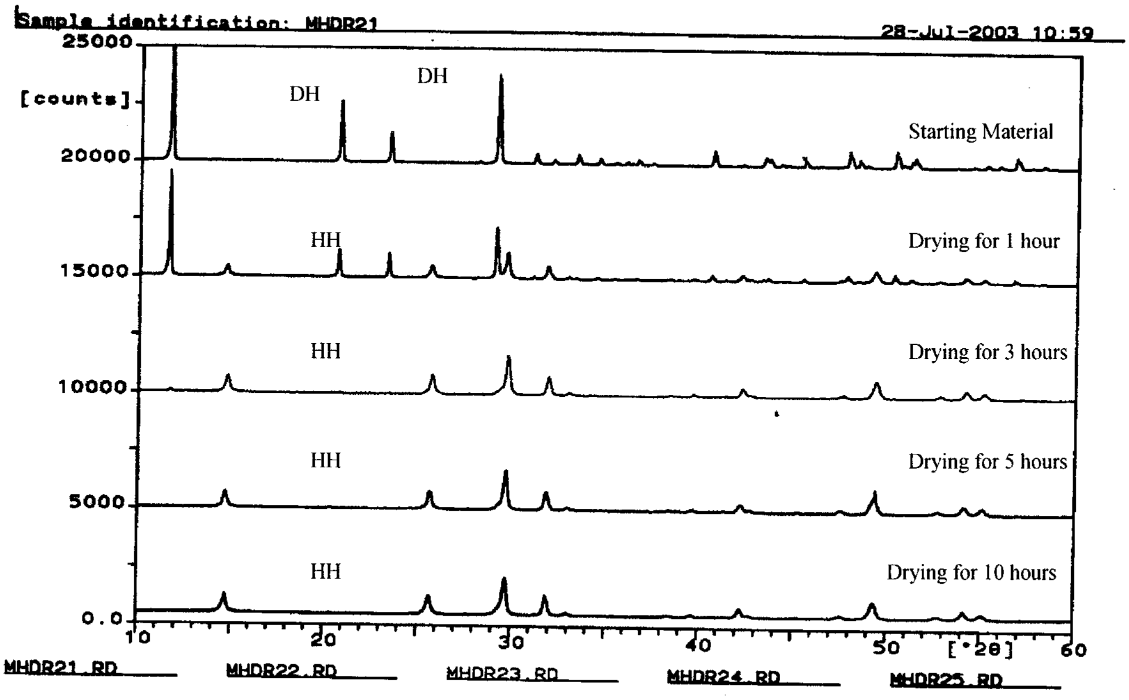

Figure 3.4. Transformation of DH to HH during drying at 100°C.

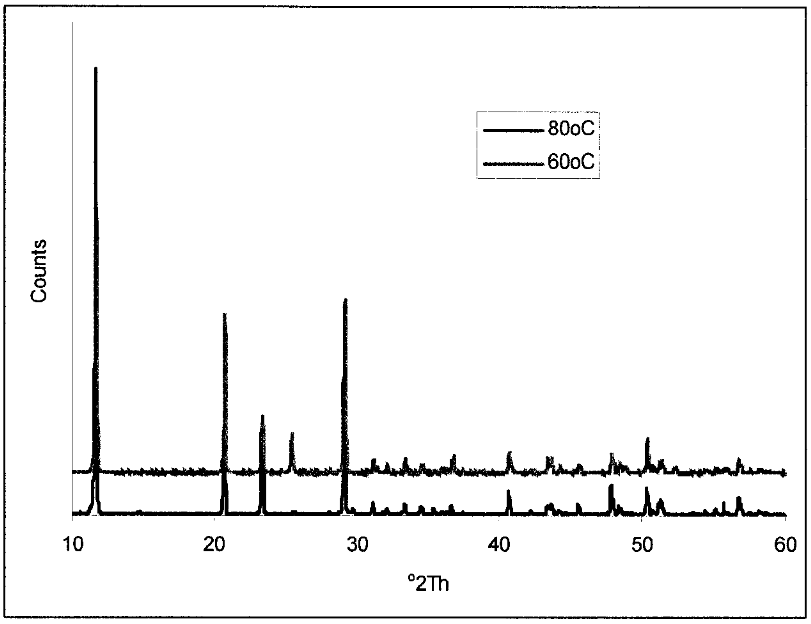

Figure 3.5. Drying DH crystals at 60 and 80°C.

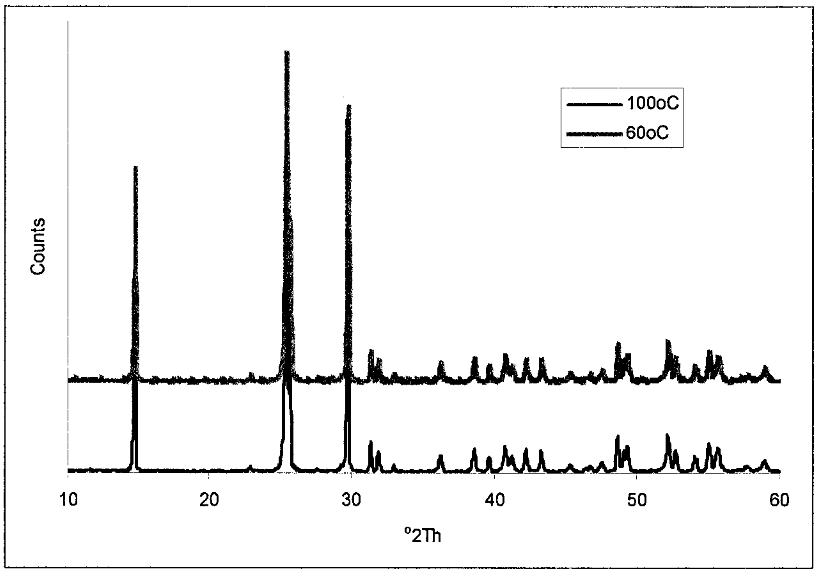

Figure 3.6. Drying HH crystals at 60 and 100°C.

3.5. Analytical Methods

3.5.1. Solution Composition

Solution samples from stability and crystallization tests were analysed by Inductively Coupled Plasma Atomic Emission Spectroscopy (ICP-AES) for calcium and sulphur. ICP was selected due to its lower detection limit, lower inter-element interference and speed [4]. A Thermo Jarrell Ash ICP-AES model instrument was used for the measurements. The calibration was done by using 0, 50 and 100ppm Ca and S standards, which were prepared from 1000ppm certified ICP standard solutions (Fisher Scientific). The $CaSO_4$ content of the solution was calculated assuming all S content (as total SO_4) is present as $CaSO_4$. In some instances HCl concentration was determined by using acid titration method, where titration was done by a certified standard solution of NaOH (0.1N) and phenolphthalein as indicator.

3.5.2. Characterization of Solid Products

The solid samples from stability and crystallization tests were characterized by a number of methods.

X-ray Powder Diffraction analysis (XRD), employed to identify the $CaSO_4$ phases, was performed using a Phillips PW1710 X-ray diffractometer. The X-ray source was Cu-$K\alpha$ and the general scanning angle (2θ) was between 10° and 60°.

The produced XRD patterns were used for the quantitative determination of hemihydrate. The dihydrate-hemihydrate mass ratio was calculated on the basis of the ratio of dihydrate peak intensity to hemihydrate peak intensity between the 2θ angle range of 10° and 30°. The calibration of the method was made using 0, 20, 40, 60, 80 and 100% hemihydrate-dihydrate standards (refer to Figure 3.7). The standards were prepared by using lab-made alpha-hemihydrate and synthetic dihydrate.

Scanning electron microscopy was used for the examination of crystal morphology and phase transformations. A JEOL 840A model SEM was used for this purpose. The samples were exposed to carbon coating prior to imaging to avoid the noise generation due to non-conductive nature of $CaSO_4$ phases.

For the determination of the impurity uptake by the α-$CaSO_4 \cdot 0.5H_2O$ crystals, EDS microanalysis was performed using a VP-SEM (Hitachi S-3000N) employing high vacuum.

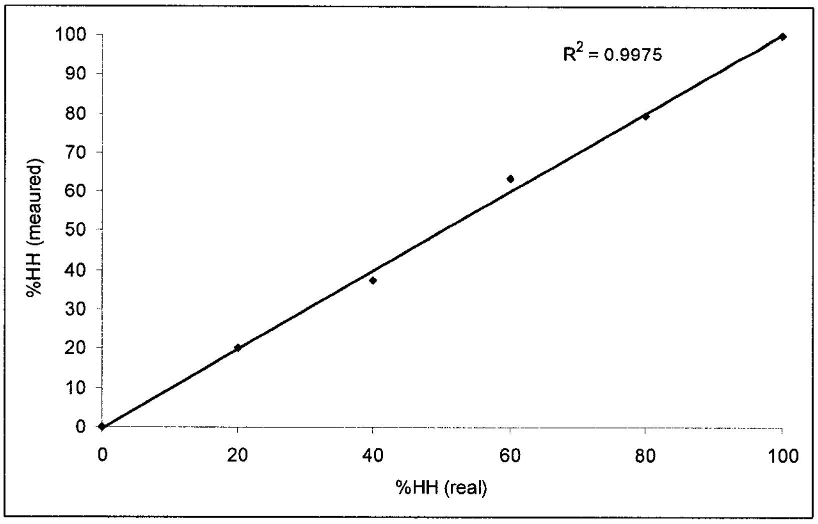

Figure 3.7. Calibration of standards for quantitative HH determination in HH and DH containing samples.

The crystal size distribution and volume-based equivalent mean diameter of the produced crystals were determined with the Horiba LA 920 laser scattering particle size analyzer. Measurements were done in iso-propanol medium to ensure the stability of the $CaSO_4$ hemihydrate phase. Once the sample was introduced to the device it was subjected to 2 minutes high speed circulation and centrifuging to provide good dispersion. The centrifuge function was on during the measurement stage as well.

Differential scanning calorimeter was the method used to distinguish between the alpha and beta forms of hemihydrate. These two forms of hemihydrate can be distinguished by the characteristic exothermic peak around 210°C for alpha and 410°C for beta hemihydrate, respectively [5, 6].

The number of crystallization water moles was determined in few instances by the Thermo-Gravimetric Analysis method (TGA) using a Perkin-Elmer TGA7 Thermogravimetric Analyzer. Figure 3.8 presents the thermo-gravimetric analysis of standard materials used in this study. Beta hemihydrate (Fisher) yielded 6.13% weight loss corresponding to 0.5 water moles while alpha hemihydrate (Omega) exhibited 6.52% weight loss, which is equivalent to 0.53 water moles. On the other hand gypsum sample provided from Fisher Scientific yielded 1.7 water moles with 18.4% weight loss.

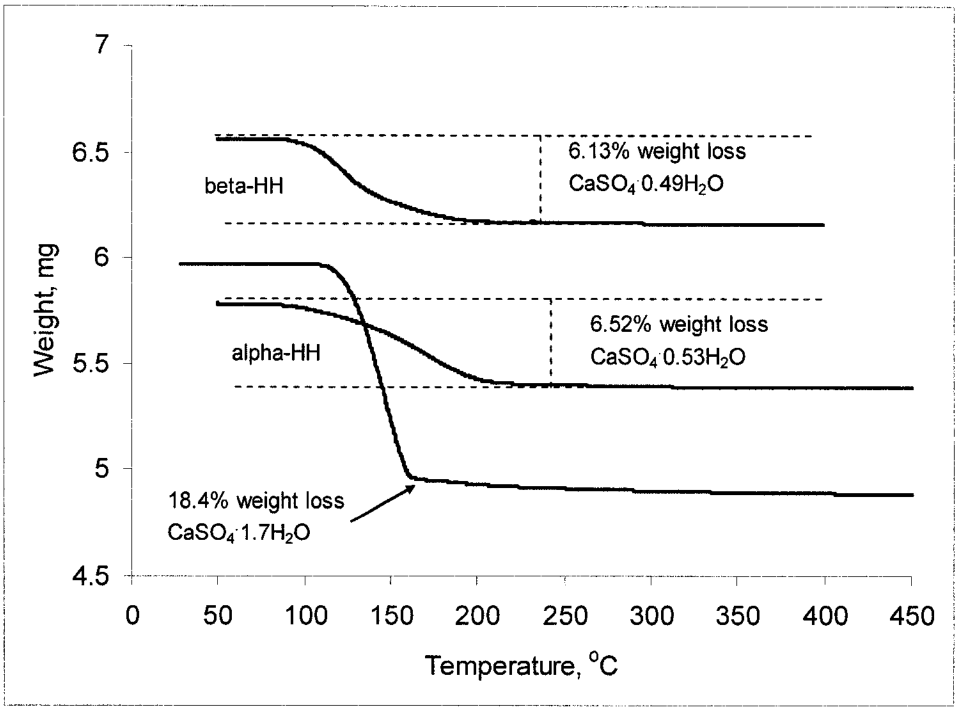

Figure 3.8. TGA of commercial gypsum, β-HH and Omega α-HH.

Metal impurity (i.e. Fe, Ni, Al, Mg and Na) and chloride uptake of produced crystals were determined by Atomic Absorption (AA) and Ion Chromatography (IC) techniques respectively. For this purpose crystals were dissolved in 10% HNO_3 solution and diluted to required concentration in accordance with the detection limit and standard requirements. In the case of IC, crystal dissolution and dilutions were done by using deionised water in order to avoid the interference of Cl^-, which may be present in distilled water. The Dionex brand DX-100 model IC and Perkin Elmer brand 3110 model AA spectrometer were the equipments used for these analyses.

3.6. OLI Stream Analyser

The solubility of CaSO4 phases (i.e. $CaSO_4 \cdot 2H_2O$, $CaSO_4 \cdot 0.5H_2O$ and $CaSO_4$) in HCl-$CaCl_2$-H_2O solution and water activity were estimated with the aid of the OLI thermodynamic software, Stream Analyser [7] after the latter was modified by Li [8, 9] at McGill. Li regressed the solubility data he produced in the lab and produced new model parameters. With the aid of these new model parameters (Bromley-Zemaitis parameters), the inclusion of $CaSO_4 \cdot 0.5H_2O$ and correction of the dissociation equilibrium constant of bisulphate ion (HSO_4^-) he established a private databank, which proved superior to the commercial one.

References

[1] College, J.W., "Sulphur dioxide removal from sulfur dioxide-containing hot gaseous streams under formation of α-hemihydrate gypsum", USA patent, No: 5,312,609, 1994.

[2] College, J.W., "The Omega Process: Direct conversion of calcium sulphite to alpha hemihydrate", in 6th International Conference on Natural and Synthetic Gypsum, Process Research Ortech, Toronto, ON, 2000, 25-1 to 25-11.

[3] Chan, T. K. -C., Darvell, B. W., "Effect of storage conditions on calcium sulphate hemihydrate-containing products", Dental Materials, 17 (2), 2001, 134-141.

[4] Moldoveanu, G.A., "Crystallisation of Inorganic compounds with Alcohols", Ph.D. Thesis, McGill University, Montréal, QC, 2005.

[5] Ling, Y., "Direct production of alpha-calcium sulphate hemihydrate from sulphuric acid", Ph.D. Thesis, McGill University, Montréal, QC, 2004.

[6] Ling, Y., Demopoulos, G.P., Giove, A., Filippou, D., "Technical evaluation and characterization of alpha calcium sulphate materials", in 7th Science and Technology Conference on Gypsum and Fly Ash, Toronto, Ontario, 2002, 6-1 to 6-14.

[7] http://www.olisystems.com/stream10.htm.

[8] Li, Z., "Measurement and chemical modelling of $CaSO_4$ solubilities in concentrated chloride media", Ph.D. Thesis, McGill University, Montréal, QC, 2006.

[9] Li, Z., Demopoulos, G.P., "Development of an improved chemical model for the estimation of $CaSO_4$ solubilities in the HCl-$CaCl_2$-H_2O system up to 100°C", Industrial Engineering and Chemistry Research, 45, 2006, 2914-2922.

CHAPTER 4

Stability of $CaSO_4$ Phases

4.1. Introduction

In order to design and control the $CaSO_4$ hemihydrate production process it is crucial to know the phase transition behaviour of $CaSO_4$ phases. Thermodynamic and kinetic factors impact the phase transformation mechanism hence the need to consider the solubility and stability of $CaSO_4$ hydrates, namely dihydrate (DH), hemihydrate (HH) and anhydrite (AH). In particular, solubility measurements make possible the determination of the conditions (temperature, electrolyte concentration, etc.) under which different phases are in equilibrium as the pioneering work of Van't Hoff and co-workers first demonstrated [1]. Solubility studies provide useful information from a supersaturation control point of view, as well [2, 3]. On the other hand, execution of stability tests, where phase transformation is monitored as a function of time provides information on phase transformation rate and mechanism. Due to the variation of electrolyte composition in the reactive crystallization system ($CaCl_2$–H_2SO_4), it is also deemed important to determine the behaviour of $CaSO_4$ phases in single ($CaCl_2$ or HCl) and binary ($CaCl_2$ and HCl) systems.

To study the above-mentioned issues, experimental stability tests were carried out and solubilities were calculated with the aid of OLI Stream Analyser Software [4, 5]. As a result of these studies stability diagrams, which were used in the design of the hemihydrate process described in Chapters 5 and 6, were constructed.

4.2. Experimental Procedure

Stability tests were carried out by using a thermostatic water bath, flasks and magnetic stirrer. In most of the cases 10 g of reagent grade $CaSO_4 \cdot 2H_2O$ (Acros Organics, Cat No. AC31525-5000) was added in a known concentration of 200mL $CaCl_2$ and/or HCl solution, which was pre-heated to desired temperature. Technical grade α-$CaSO_4 \cdot 0{,}5H_2O$, which was provided from Omega-Eastroc-BPB, was also used in few tests. After the addition of $CaSO_4 \cdot 2H_2O$, agitation with a magnetic stirrer started. The agitation speed was kept constant at 400 rpm. Solution and slurry samples were taken at various time intervals up to 24 hours. Agitation was stopped 30 seconds prior to solution sampling to allow solids settling.

Slurry samples were taken from the flask with the help of a syringe and immediately filtered (while hot), washed and dried according to the procedure given in the material handling section (section 3.5) of Chapter 3. Dry solid samples were subjected to required analysis or characterization via XRD, SEM and Particle Size Analysis.

The withdrawn solution samples were filtered with a 0.22µm syringe-type filter cap and immediately diluted with distilled water to avoid the precipitation of calcium sulphates via cooling. Already diluted solutions were further diluted with distilled water and subjected to ICP analysis.

Solution samples and starting solutions were also titrated with a known normality standard NaOH solution in order to determine the HCl concentration of the solutions.

4.3. Phase Equilibria and Solubility of $CaSO_4$ Phases

The solubilites of different $CaSO_4$ modifications, which are necessary for the determination of phase transition conditions, can be calculated once the thermodynamic equilibrium constants (solubility products), mean activity coefficients of Ca^{2+} and $SO_4{}^{2-}$ and water activity of the solution are known [6] (eq 4.1.);

$$K_{SP} = (m_{Ca^{2+}}\gamma_{Ca^{2+}})(m_{SO_4^{2-}}\gamma_{SO_4^{2-}})(\alpha_w)^n \quad (4.1)$$

where K^0_{SP} is thermodynamic equilibrium constant, m is the molal concentration of ions (mol/kg H_2O), γ is the mean activity coefficient of ions, α_w is the activity of water and n the number of crystal waters. The respective solubility products for dihydrate (DH), hemihydrate (HH) and anhydrite (AH) can be expressed as follows;

$$K_{sp,DH} = \alpha_{Ca}^{2+}\,\alpha_{SO_4}^{2-}\,(\alpha_{H2O})^2 \quad (4.2)$$

$$K_{sp,HH} = \alpha_{Ca}^{2+}\,\alpha_{SO_4}^{2-}\,(\alpha_{H2O})^{0.5} \quad (4.3)$$

$$K_{sp,AH} = \alpha_{Ca}^{2+}\,\alpha_{SO_4}^{2-} \quad (4.4)$$

The stability of $CaSO_4$ hydrates is a function of aqueous solution composition and temperature and, therefore, can be expressed by the chemical potential of these phases [6];

$$\mu_{DH} = \mu^0 + RT\ \ln(\alpha_{Ca}^{2+}\,\alpha_{SO_4}^{2-}\,(\alpha_{H2O})^2) \quad (4.5)$$

$$\mu_{HH} = \mu^0 + RT\ \ln(\alpha_{Ca}^{2+}\,\alpha_{SO_4}^{2-}\,(\alpha_{H2O})^{0.5}) \quad (4.6)$$

$$\mu_{AH} = \mu^0 + RT\ \ln(\alpha_{Ca}^{2+}\,\alpha_{SO_4}^{2-}) \quad (4.7)$$

where μ^0 is the standard chemical potential under 25°C temperature and 1 bar pressure conditions. At equilibrium the solid phase and solution chemical potentials are equal [7];

$$\mu_{DH,s} = \mu_{DH,l} \quad (4.8a)$$

$$\mu_{HH,s} = \mu_{HH,l} \quad (4.8b)$$

$$\mu_{AH,s} = \mu_{AH,l} \quad (4.8c)$$

By substituting equations 4.5 to 4.7 in 4.8 (a, b and c) we get;

$$\mu^0 + RT\ \ln(K_{sp,DH}) = \mu^0 + RT\ \ln(\alpha_{Ca}^{2+}\,\alpha_{SO_4}^{2-}\,(\alpha_{H2O})^2) \quad (4.9)$$

$$\mu^0 + RT\ \ln(K_{sp,HH}) = \mu^0 + RT\ \ln(\alpha_{Ca}^{2+}\,\alpha_{SO_4}^{2-}\,(\alpha_{H2O})^{0.5}) \quad (4.10)$$

$$\mu^0 + RT\ln(K_{sp,AH}) = \mu^0 + RT\ln(\alpha_{Ca}{}^{2+}\,\alpha_{SO_4}{}^{2-}) \quad (4.11)$$

Since the solubilities, C, or better activities, i.e. $\alpha_{Ca}{}^{2+}\,\alpha_{SO4}{}^{2-}$, of the two phases are equal at their transition point, the following relationships can be derived from equations 4.9-4.11;

$$K_{sp,DH}/K_{sp,HH} = (\alpha_{H2O})^{1.5} \quad (4.12)$$

$$K_{sp,DH}/K_{sp,AH} = (\alpha_{H2O})^{2} \quad (4.13)$$

Equations 4.12 and 4.13 strongly suggest that the phase transition point is a function of water activity. By calculating the K_{SP} from the solubilities of these hydrates, the phase transition point can be determined in terms of the water activity of the system [7].

Based on these thermodynamic principles, Martynowicz et al. [8] and Ling and Demopoulos [9, 10] reported that the required water activity value for dihydrate-hemihydrate phase transition is around 0.7 in H_3PO_4 and H_2SO_4 systems, respectively. The estimations involving $CaCl_2$-HCl media at 80°C are made later in this chapter by making use of OLI Stream Analyser Software recently modified and validated for this system by Li [4, 5].

4.4. Dihydrate-Hemihydrate-Anhydrite Transformations

As stated in the literature review chapter, most previous studies [11, 12] involving the equilibration of $CaSO_4$ hydrates (generally dihydrate) in chloride solutions aimed at the production of desired quality alpha-hemihydrate rather than determining in detail the underlying phase transformation phenomena. In this section, the transformation of DH to HH and AH is studied via a series of stability tests carried out in a wide range of electrolyte composition conditions.

The first set of experiments was designed with the view of simulating the $CaCl_2$-H_2SO_4 reaction system by considering the change in $CaCl_2$ (decrease) and HCl (increase) concentrations (Table 4.1). The total chloride concentration was kept constant at 6M. The data of Table 4.1 is based on XRD characterization of the starting, intermediate and final solids. Typical XRD data is shown in Figure 4.1. According to this data within 30 minutes of equilibration in 0.5M $CaCl_2$ + 5M HCl solution DH-HH conversion was completed and intermediate HH started to convert to AH as it can be deduced from the splitting of 25.5 2θ peak and the appearance of the 25.3 2θ peak of AH. In addition the HH peak at 2θ = 14.9 can be seen to constantly disappear with time.

According to the data of Table 4.1, anhydrite is the only stable phase for all concentrations tested. Decreasing $CaCl_2$ and increasing HCl concentrations accelerated the DH-HH-AH conversion sequence. In order to understand the effect of each electrolyte better, their effect on phase conversion was investigated separately in detail (section 4.4.1 and 4.4.2).

Table 4.1. Dihydrate conversion in variable $CaCl_2$-HCl concentrations at 80°C.

		FINAL PHASE					
Initial Solution $CaCl_2$ + HCl (M)	*t=0*	0.5 hour	1 hour	2.5 hours	5 hours	18 hours	24 hours
2.5 + 1.0	*D*	D	D	D(H)*	D(H)	-	A
2.0 + 2.0	*D*	-	-	H	H	A	A
1.5 + 3.0	*D*	D(H)	D(H)	D/H**	-	-	A
1.0 + 4.0	*D*	H/A	A/H	A	A	A	A
0.5 + 5.0	*D*	H/A	A(H)	A	A	A	A
0.0 + 6.0	*D*	A	A	A	A	A	A

*Phase in brackets indicates minor amount

**Phases indicated with slash (e.g. D/H) means comparable amounts of both phases

D: dihydrate, H: hemihydrate, A: anhydrite

Differential scanning calorimetry (DSC) confirmed the intermediate HH phase found to form in this series of tests to be of the alpha variety (Figure 4.2). The material of Figure 4.2 was obtained after 5 hours equilibration of DH in 2M $CaCl_2$ + 2M HCl electrolyte solution (refer to Table 4.1).

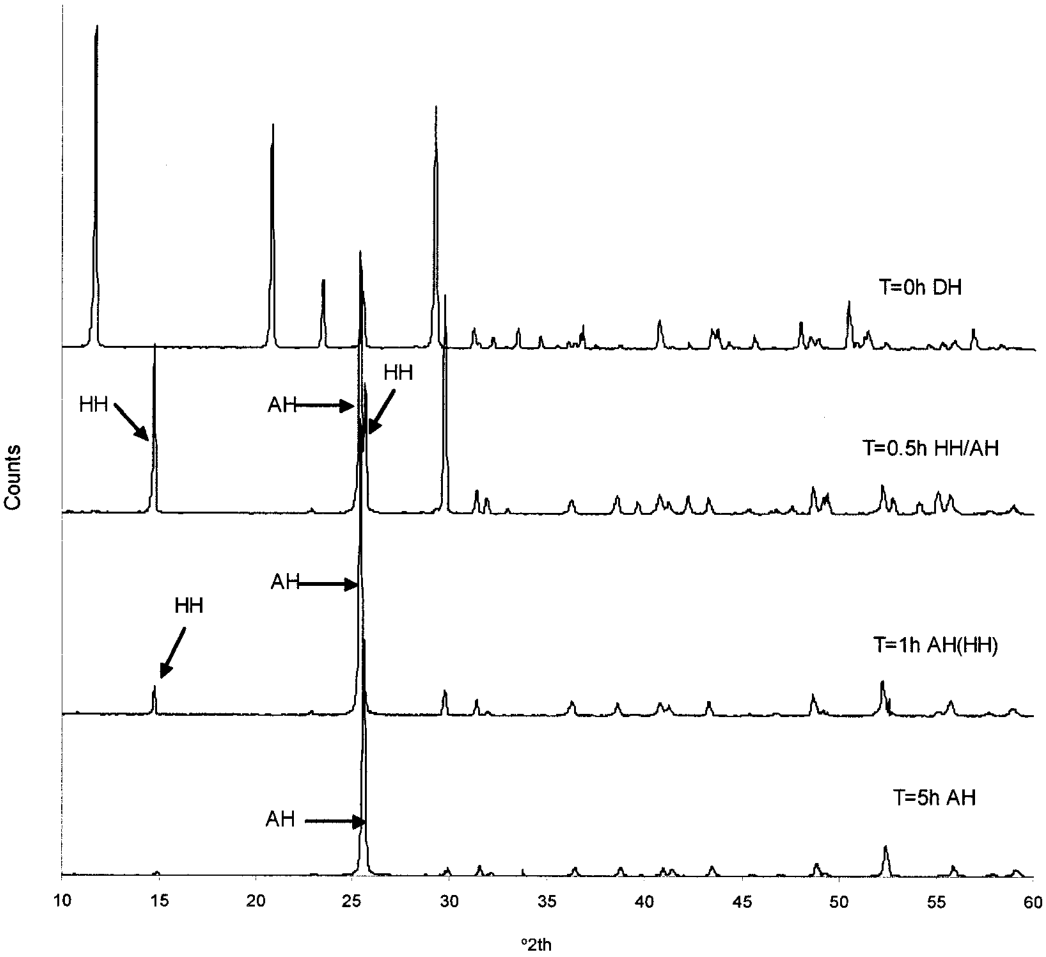

Figure 4.1. DH-HH-AH conversion with time in 0.5M $CaCl_2$ + 5M HCl solution (80°C).

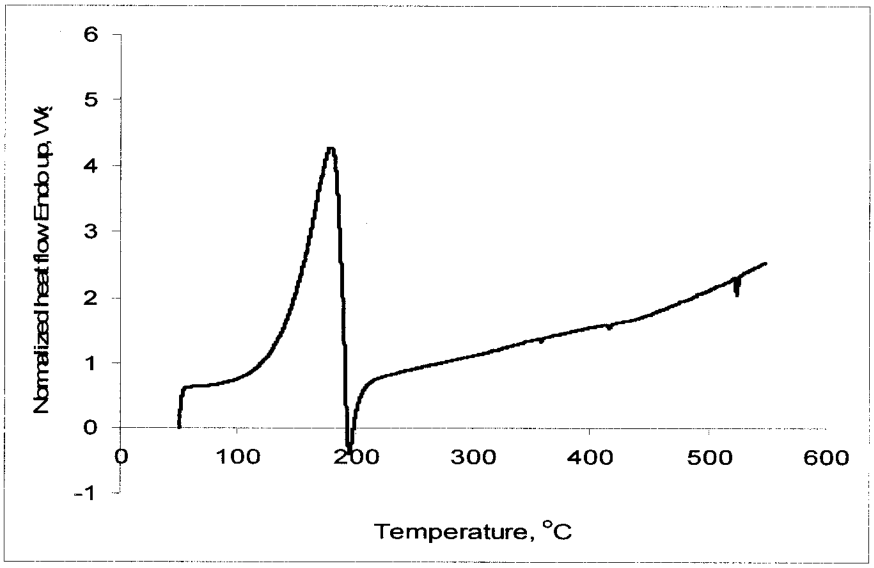

Figure 4.2. Alpha-HH pattern obtained by DSC (2M $CaCl_2$ + 2M HCl, 5 hours, 80°C).

4.4.1. Effect of HCl concentration

The effect of HCl concentration was investigated in the absence and presence of $CaCl_2$ at 80°C. The results are summarised in Tables 4.2 and 4.3. According to the data in Table 4.2, no HH was detected to any significant extent when DH was equilibrated in pure HCl solutions. In this system DH appears to be stable for a few hours at low HCl concentration but to convert completely to AH at fast rate at elevated (i.e. above 3M) HCl concentration. The accelerated DH-AH conversion kinetics corresponds to the decrease in water activity (see a_{H_2O} data –estimated with OLI- in Table 4.2)

In order to better understand the observed transformations the solubilites of the three $CaSO_4$ phases were estimated using the OLI Stream Analyser Software [4, 5]. By comparing the solubilities of the three phases the relative stability of them can be established. The estimated solubilites are shown in Figure 4.3. According to this Figure AH is the only stable phase in the 1-6M HCl concentration range at 80°C with DH being metastable at less than 3M and HH being metastable above 3M HCl. The predicted metastability of DH below 3M HCl is in agreement with the data of Table 4.2. However, HH was found not to be metastable (Table 4.2.) at >3M HCl despite the solubility predictions of Figure 4.3. This may relate to its very fast transformation kinetics. Hence the production of HH in $HCl-H_2O$ system at 80°C does not appear feasible.

Table 4.2. Phase transformation of DH as a function of HCl concentration (80°C).

Initial Solution $CaCl_2$ + HCl (M)	Water Activity	t=0	5 min	30 min	1 hour	2.5 hours	5 hours	24 hours
0 + 1	0.96	*D*	D	D	D	D	D	D(A)
0 + 2	0.91	*D*	D	D	D	D	D	
0 + 3	0.86	*D*	D	D	D	D		
0 + 4	0.79	*D*	D	D			A	A
0 + 5	0.72	*D*	D	D	D	D(A)	A	A
0 + 6	0.65	*D*	A	A	A	A	A	A

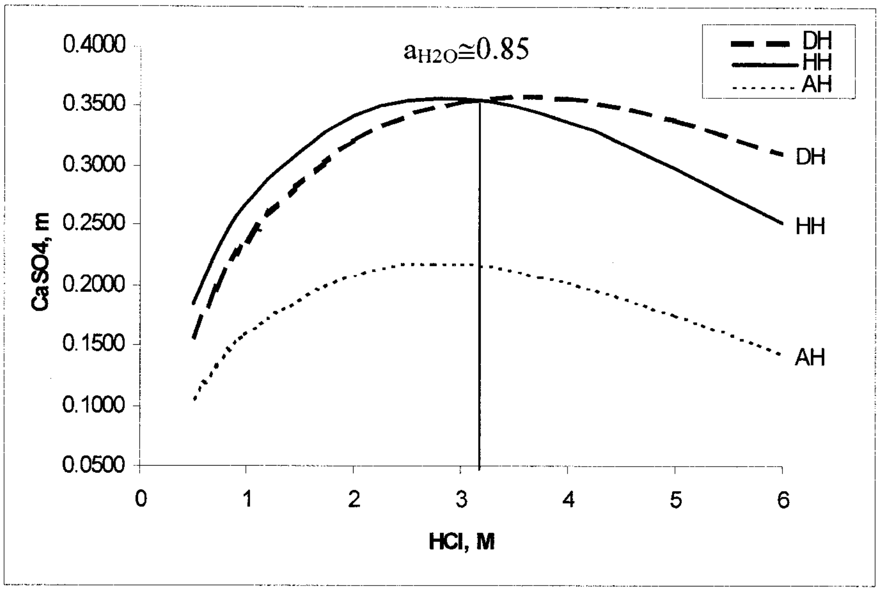

Figure 4.3. Solubility of $CaSO_4$ hydrates (DH, HH, AH) as a function of HCl concentration (80°C).

The effect of HCl in the presence of $CaCl_2$ (1.5M) yielded drastically different results (refer to Table 4.3). In this case $CaCl_2$ was found to promote the conversion of DH to HH rather than to AH. HH was metastable for at least 2 hours even when HCl concentration was as high as 6M. The presence of $CaCl_2$ resulted in a decrease in water activity as predicted by Jansz [13] but the latter did not cause the conversion of HH to AH even when it was as low as 0.5 (compare Tables 4.2 and 4.3). This implies that factors other than water activity alone control the conversion of $CaSO_4$ hydrates. The promotion of DH conversion towards HH was confirmed with the analysis of the solubility of these $CaSO_4$ phases in the $CaCl_2$ (1.5M)-HCl system (refer to Figure 4.4). It can be seen from this Figure that HH becomes metastable at >1M HCl when 1.5M $CaCl_2$ is present. In terms of water activity, this solution composition is equivalent to that of 3M HCl solution (i.e. a_{water} = 0.85) (compare Tables 4.2 and 4.3). The water activity level associated with the transformation of DH to HH found in this work is higher (0.85 vs. 0.7) than the work calculated for the H_3PO_4 [8] and H_2SO_4 [9, 10] electrolyte systems. It is not clear at this point why the conversion of DH to HH (or AH) is catalysed in the chloride system.

Table 4.3. Transformation of DH as a function of HCl concentration in the presence of $CaCl_2$ (80°C, 1.5M $CaCl_2$).

Initial Solution $CaCl_2$ + HCl (M)	Water Activity	*t=0*	10 min	20 min	30 min	1 hour	2.5 hours	5 hours
1.5 + 0	0.90	*D*	D	D	D	D	D(H)	D(H)
1.5 + 1	0.84	*D*	D	D	D	D	D(H)	D(H)
1.5 + 2	0.78	*D*	D	D	D(H)	D(H)	D(H)	D(H)
1.5 + 3	0.70	*D*	D	D	D(H)	D(H)	D/H	H
1.5 + 4	0.62	*D*	D(H)	D(H)	D(H)	H	H	H
1.5 + 5	0.54	*D*	H	H	H	H	H	H(A)
1.5 + 6	0.46	*D*			H	H	H	

The kinetics of DH-HH conversion were determined in terms of HH ratio in the final product (determined by XRD analysis-refer to section 3.5.2 of Chapter 3) and is presented in Figure 4.5. 100% conversion was achieved in less than an hour in the presence of 4M HCl while in 1M and 2M HCl solutions the HH ratio in the final product after 5 hours conversion was found to be 22.7 and 43.6%, respectively. In the latter 2 cases, the conversion process was observed to slow down considerably (i.e. after 60 minute for 2M and 150 minutes for 1 M HCl) after an initial (relatively) fast conversion stage.

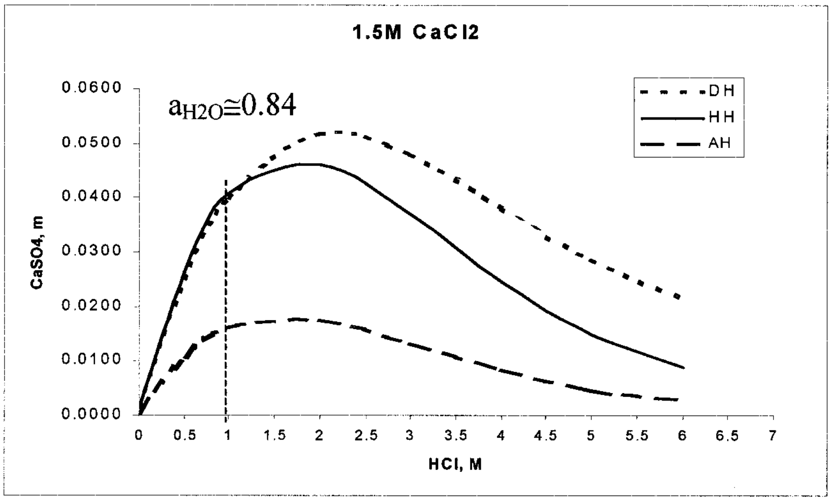

Figure 4.4. Solubility of $CaSO_4$ hydrates (DH, HH, AH) as a function of HCl concentration presence of 1.5M $CaCl_2$ (80°C).

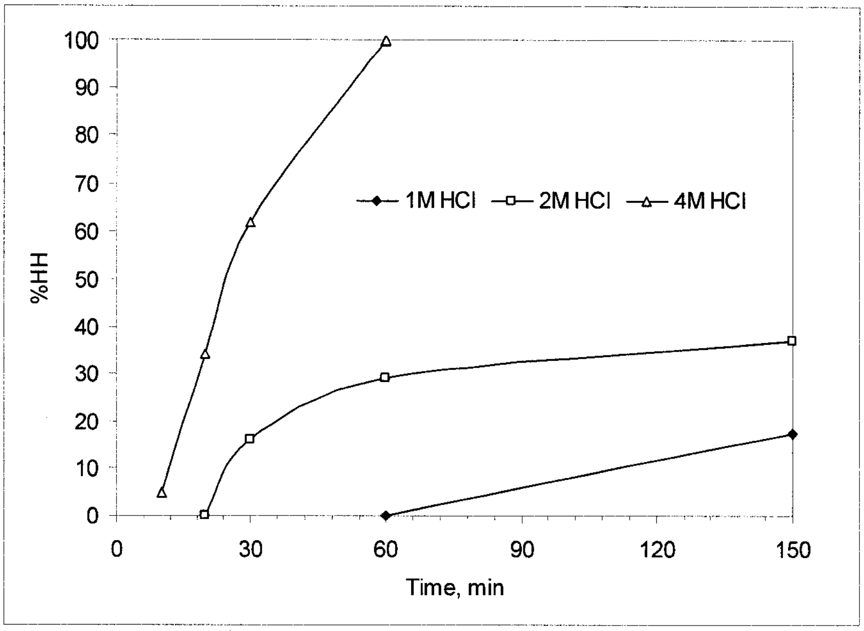

Figure 4.5. HH fraction in final product as a function of time and HCl concentration ($1.5M\ CaCl_2$, 80°C).

4.4.2. Effect of $CaCl_2$ Concentration

The effect of $CaCl_2$ concentration on dihydrate conversion was investigated at various constant HCl strengths (0, 3, 6M HCl). In the first set of experiments, the effect of $CaCl_2$ was tested at 80°C in the absence of HCl. The results are summarised in Table 4.4. It can be deduced from this data that elevated $CaCl_2$ concentrations improve the conversion kinetics of DH to HH. Complete conversion was observed at 4M $CaCl_2$ and 5 hours retention time.

Table 4.4. Phase transformation of DH as a function of $CaCl_2$ concentration (80°C).

Initial Solution $CaCl_2$ + HCl (M)	Water Activity	*t=0*	1 hour	2.5 hours	5 hours	7.5 hours
1.0 + 0	0.90	*D*	D	D	D	
1.5 + 0	0.90	*D*	D	D(H)	D(H)	D(H)
2.0 + 0	0.86	*D*	D(H)	D(H)	D(H)	D(H)
2.5 + 0	0.80	*D*	D(H)	D(H)	D(H)	D(H)
3.0 + 0	0.73	*D*	D(H)	D(H)	D(H)	D(H)
3.5 + 0	0.66	*D*	D(H)	D(H)	D/H	D/H
4.0 + 0	0.58	*D*	D(H)	D(H)	H	H

The transformation of DH to HH is exemplified with the XRD data presented in Figure 4.6. After 1 hour of equilibration of DH in 1.5M $CaCl_2$ + 0M HCl electrolyte solution at 80°C, only the DH pattern is present. With the progress of equilibration test (i.e. 2.5 hours), a significant HH peak at $2\theta = 14.9Å$ is clearly observed. However, the conversion is rather slow with DH peaks still been present even after 7.5 hours retention. The transformation kinetics of DH to HH in 4M is presented in Figure 4.7 in the form of % fraction of HH in final product as a function of time.

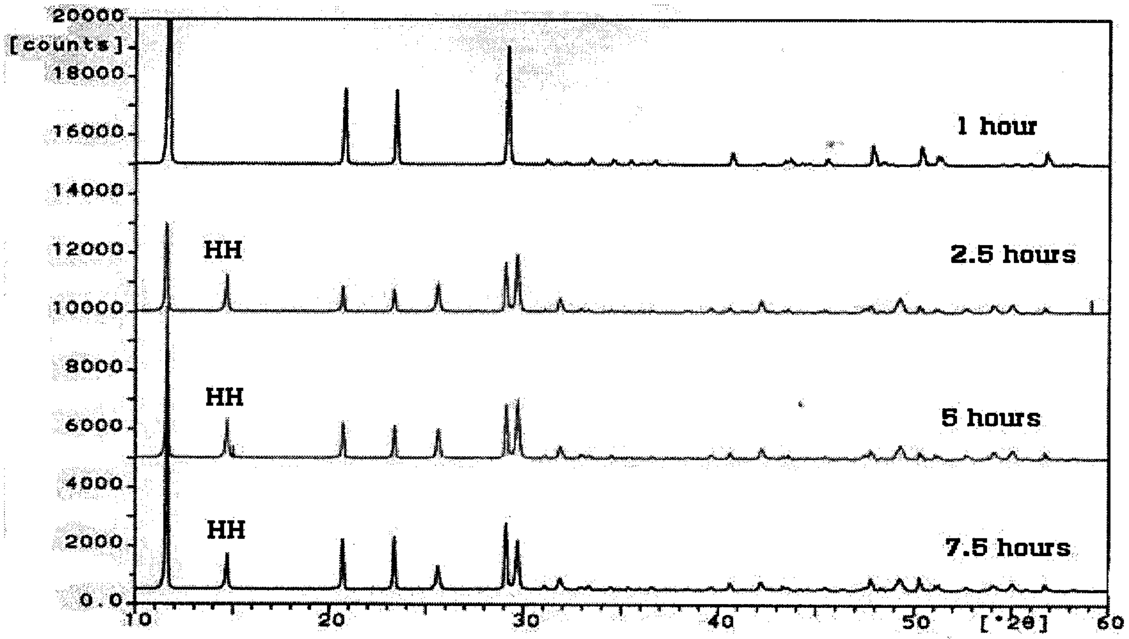

Figure 4.6. DH-HH conversion with time in 1.5M $CaCl_2$ + 0M HCl solution (80°C).

Analysis of the solubilities (estimated with the aid of OLI) of the 3 phases (refer to Figure 4.8) revealed that the transition from DH to HH is predicted at ≈ 2.75M $CaCl_2$ or $a_{H2O} \approx 0.77$. Although this prediction is not quantitatively accurate (for example according to Table 4.4 conversion of DH to HH started at as low $CaCl_2$ concentration as 1.5M) the diagram helps to explain the favourable effect of $CaCl_2$ concentration on DH-HH conversion.

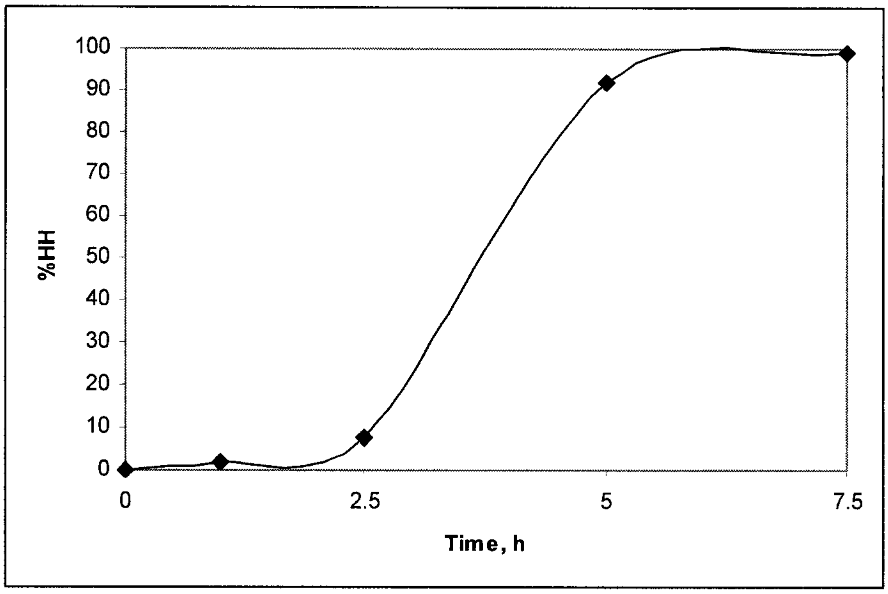

Figure 4. 7. HH fraction in final product as a function of time in 4M $CaCl_2$ solution (80°C).

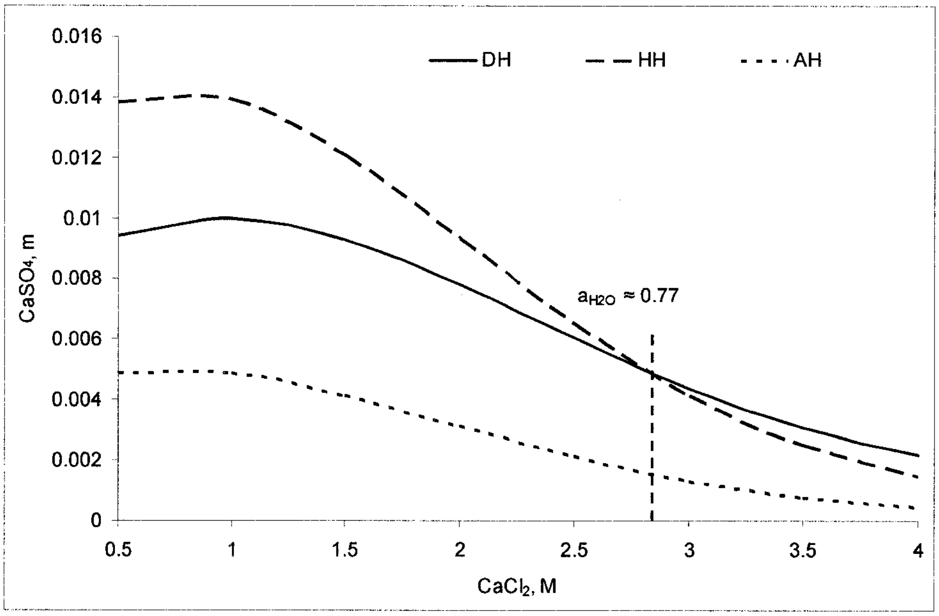

Figure 4.8. Solubility of $CaSO_4$ hydrates (DH, HH, AH) as a function of $CaCl_2$ concentration (80°C, [HCl] = 0M).

An SEM micrograph of the produced HH material in concentrated $CaCl_2$ solution (4M) by conversion of DH is shown in Figure 4.9. The produced HH material (after 5 hours equilibration of DH in 4M $CaCl_2$ + 0M HCl solution at 80°C) was confirmed once more by DSC analysis to be alpha hemihydrate (Figure 4.10).

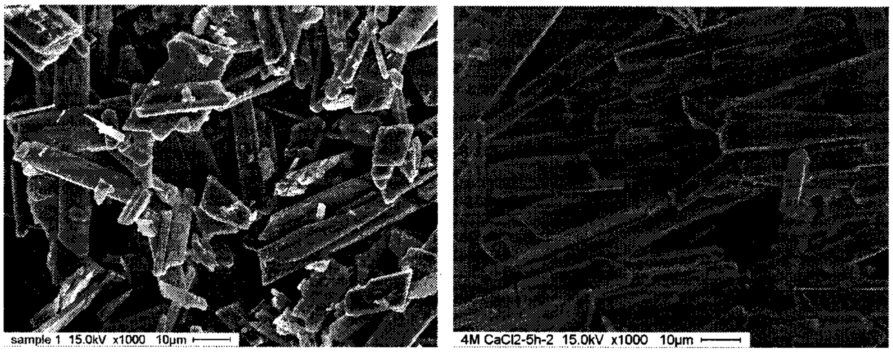

(a) (b)

Figure 4.9. SEM images of (a) starting DH and (b) produced HH material (5 hours equilibration, 4M $CaCl_2$ + 0M HCl solution, 80°C)

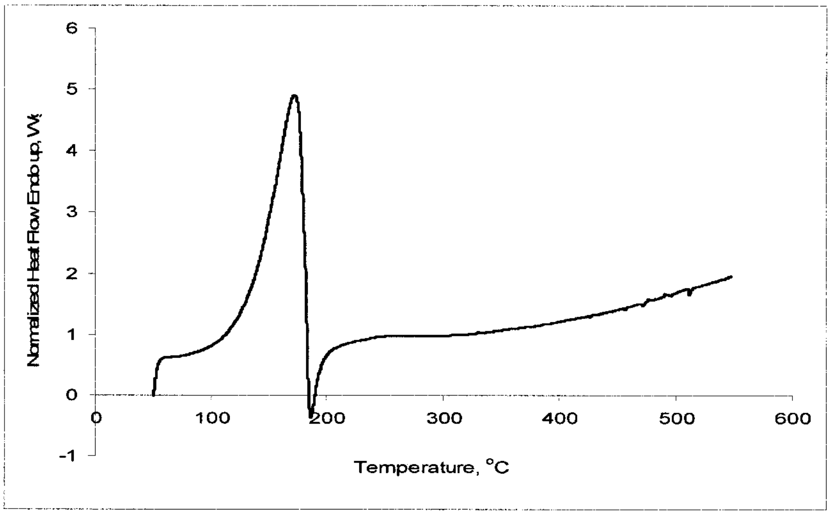

Figure 4.10. Alpha-HH pattern obtained by DSC (4M $CaCl_2$ + 0M HCl, 5 hours, 80°C).

The effect of $CaCl_2$ concentration on the conversion of DH to HH was further examined in the presence of HCl at 3M and 6M acid strength, respectively. The results are summarized in Table 4.5 along with selected data from Tables 4.2 and 4.4. It can be clearly seen that the conversion of DH to HH is promoted as HCl concentration increases at the same $CaCl_2$ level (see for example row no 3) or as $CaCl_2$ concentration increases at fixed HCl concentration (see for example column no 2 (2.5 hours)). This tendency corresponds to decreasing water activity-determined with the aid of OLI (refer to Figure 4.11). On the same Figure water activity line (a_{H2O} = 0.85) corresponding to the transition from DH to HH (refer to Figures 4.3, 4.4) is included, as well. The observed correspondence between water activity and conversion of DH to HH breaks when no $CaCl_2$ is present. On the other hand, water activity cannot explain why $CaCl_2$ provides stability to HH.

Table 4.5. DH phase transformation at variable $CaCl_2$ and HCl concentrations at 80°C.

Column→		1			2			3		
HCl, M→		0			3			6		
Time, hours→		1	2.5	5	1	2.5	5	1	2.5	5
Row↓	$CaCl_2$, M↓									
1	0.0	-	-	-	D	D		A	A	A
2	0.5	-	-	-	D	D	D	H	H	A
3	1.0	D	D	D	D	D(H)	D(H)	H	H	H(A)
4	2.0	D(H)	D(H)	D(H)	H	H	H	H	H	H
5	3.0	D(H)	D(H)	D(H)	H	H	H	H	H	H

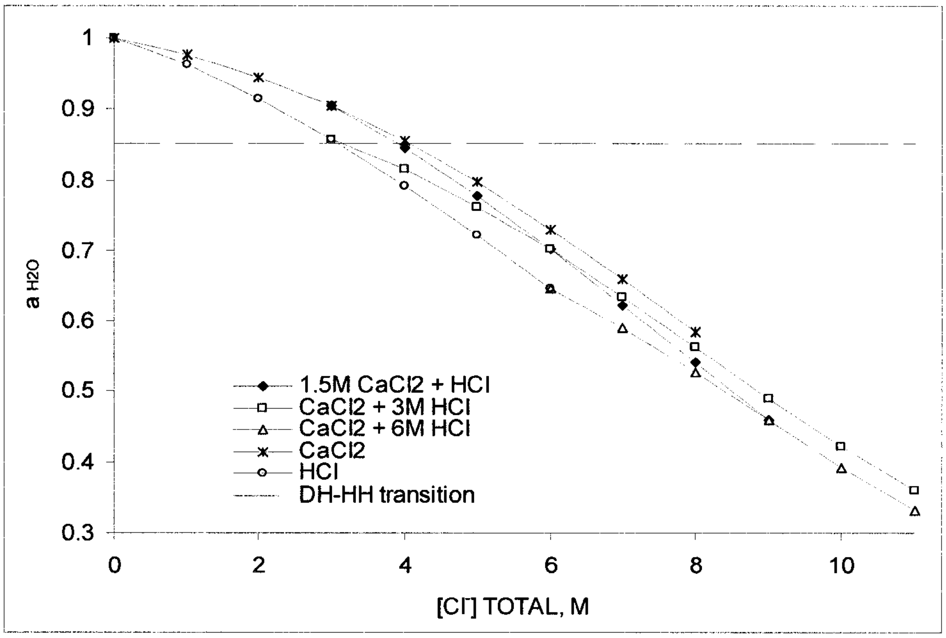

Figure 4.11. Variation of a_{H2O} as function of total chloride concentration at 80°C.

In addition to affecting the stability of HH, increased $CaCl_2$ concentration was found to have another significant effect. $CaCl_2$ interfered with crystal growth as can be judged from the SEM micrographs of Figure 4.12. According to these images, the HH crystals obtained in 0.5M $CaCl_2$ – 6M HCl solution are well grown in length (typically ≈ 100μm) with relatively high aspect ratio (L/D ≅ 11.5) ,while those produced at 3M $CaCl_2$ – 6M HCl are shorter with aspect ratio (L/D) around 6.5. The effect of $CaCl_2$ concentration on mean crystal length is further illustrated with the crystal size data of Figure 4.13.

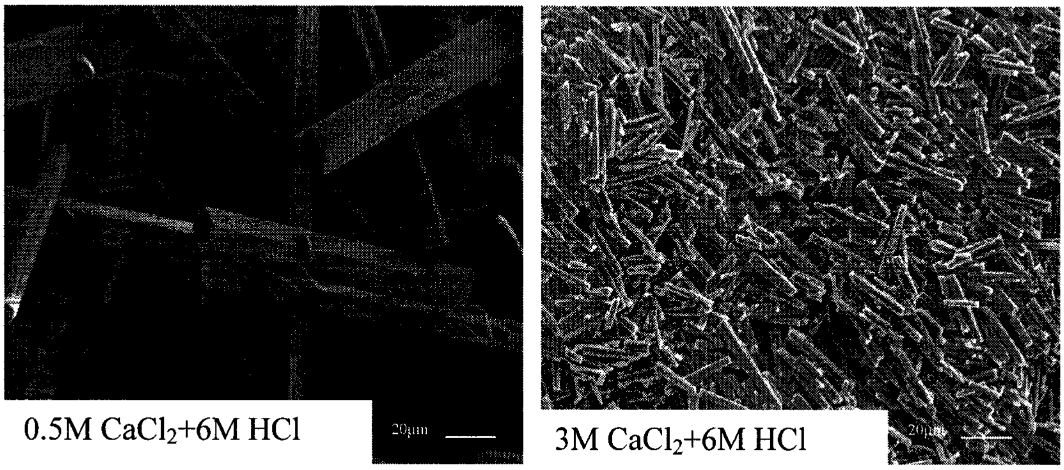

0.5M $CaCl_2$+6M HCl

3M $CaCl_2$+6M HCl

Figure 4.12. Effect of $CaCl_2$ concentration on hemihydrate morphology (80°C, 6M HCl, 5 hours).

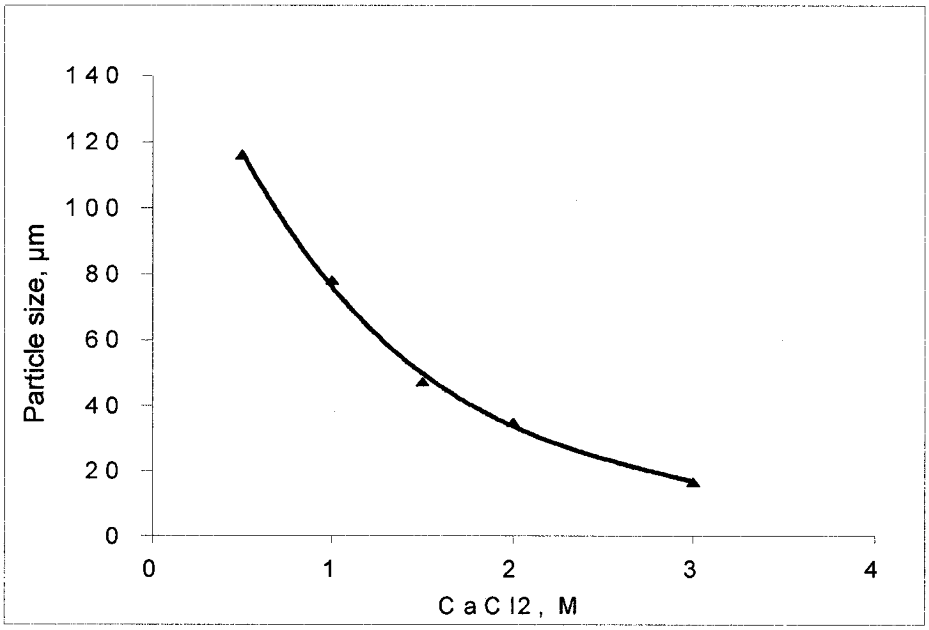

Figure 4.13. Effect of $CaCl_2$ concentration on mean particle diameter (80°C, 6M HCl, 5 hours).

4.4.3. Effect of Temperature

Lowering the temperature from 80°C to 70°C and further down to 60°C was found to slow down significantly the conversion kinetics of DH to HH (and AH). A typical sample of conversion data collected at different temperatures by equilibrating DH in 0.5M $CaCl_2$ + 6M HCl solution at various times is given in Table 4.6.

Table 4.6. Phase transformation of DH as a function of temperature (0.5M $CaCl_2$ + 6M HCl).

Temperature, °C	T=0	30 min	1 hour	2.5 hours	5 hours
60	D	D	D	D(H)	H
70	D	D/H	H(D)	H	H(A)
80	D	H	H	H	A

4.5. Kinetics-Based Stability Diagrams

The experimental findings from all stability tests run at 80°C were used to construct dihydrate-hemihydrate-anhydrite kinetics-based stability diagrams (Figure 4.14). There are 4 main regions in the diagram, namely dihydrate, hemihydrate and anhydrite regions and finally mixed hydrates (phase transition) region, which evolve with time. At the initial stage of equilibration time (i.e. 1 hour retention time), the DH region was wide but due to DH-AH or DH-HH transition with the progress of time, this region reduced in size. In the case of HH stability, HH-AH conversion is seen to take place at low [$CaCl_2$], high [HCl] region (e.g. 0.5M $CaCl_2$ and 5-6M HCl).

Figure 4.15 illustrates the kinetic evolution of phases in more detail by indicating the phase transition regions in 1, 2.5 and 5 hours. Direct transformation of DH to AH in the absence of $CaCl_2$ (4, 5 and 6M HCl) is also indicated on this diagram.

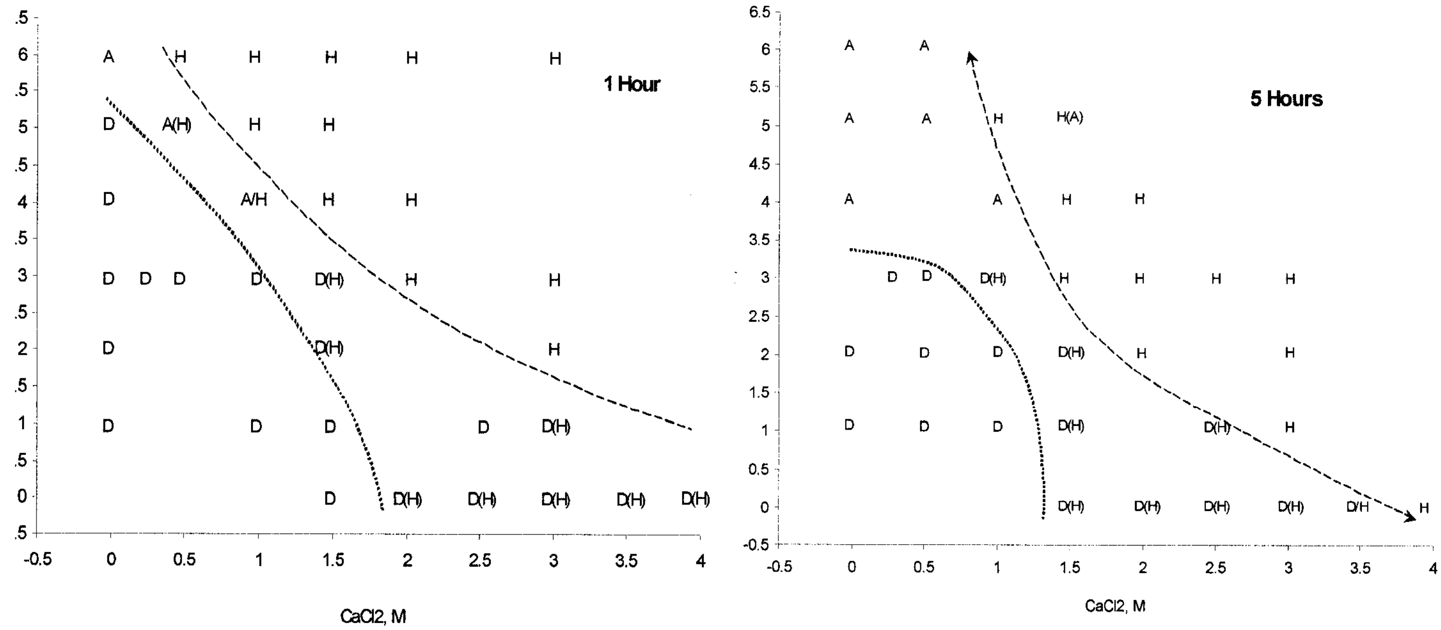

Figure 4.14.Experimental stability data of $CaSO_4$ hydrates as a function of [HCl] and [$CaCl_2$] in 1 hour and 5 hours (80°C).

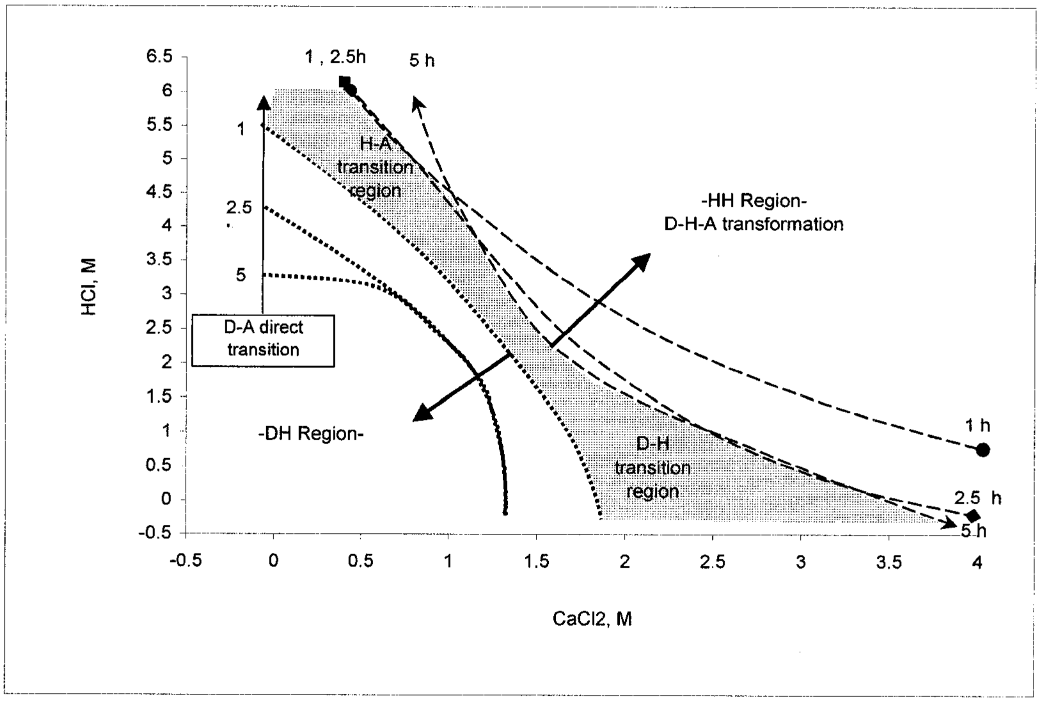

Figure 4.15. Kinetic stability regions of $CaSO_4$ hydrates in HCl-$CaCl_2$ solution at 80°C.

As mentioned in section 4.3, phase transition is driven by water activity change. Thermodynamically speaking, 80°C in pure water ($a_w = 1$) satisfies the condition for DH to AH transformation, but kinetics are not favourable. Moreover, HH is not metastable hence its formation-production is not feasible [11]. By lowering, however, the water activity with an increase in electrolyte concentration, conversion of DH to HH or AH is promoted. According to the solubility curves reported in Figures 4.3 and 4.4, the water activity level signifying the onset of the DH-HH transition is around 0.85.

In an effort to reconcile the experimental stability data generated in this work with the water activity and solubility equilibria of the $CaSO_4$-HCl-$CaCl_2$-H_2O system the diagram of Figure 4.16 was constructed. In this diagram water activity lines as a function of electrolyte concentration, experimental stability data after 5 hours equilibration and the theoretical DH/HH transition line are plotted. The theoretical transition line was determined by following the points at which DH and HH have the same solubility (refer for example to Figures 4.3, 4.4 and 4.7). There is satisfactory agreement between the experimental stability region of DH and the theoretical DH stability region defined by DH/HH transition line. However there is no agreement between theory and experiments at high HCl concentration (>3M) in the absence of $CaCl_2$. As already mentioned the origin of this disagreement is not known.

4.6. Crystal Phase Transformation Mechanism

There are three possible crystal transformation mechanisms by which DH converts to HH and/or AH; (a) recrystallization, involving the dissolution of one phase followed by nucleation of a new phase in solution; (b) topochemical, involving nucleation of the new phase on the surface of the old one; and (c) solid-state conversion, involving nucleation of the new phase inside the body of the old phase. Till recently recrystallization was thought to be the main DH→HH conversion mechanism. However, Sirota et al. [14] established by SEM that DH-HH conversion may occur via the solid-state mechanism. In this part of the study, the mechanism of phase transitions between the 3 $CaSO_4$ hydrates is discussed by examining crystal morphological changes with SEM and analyzing solution composition changes.

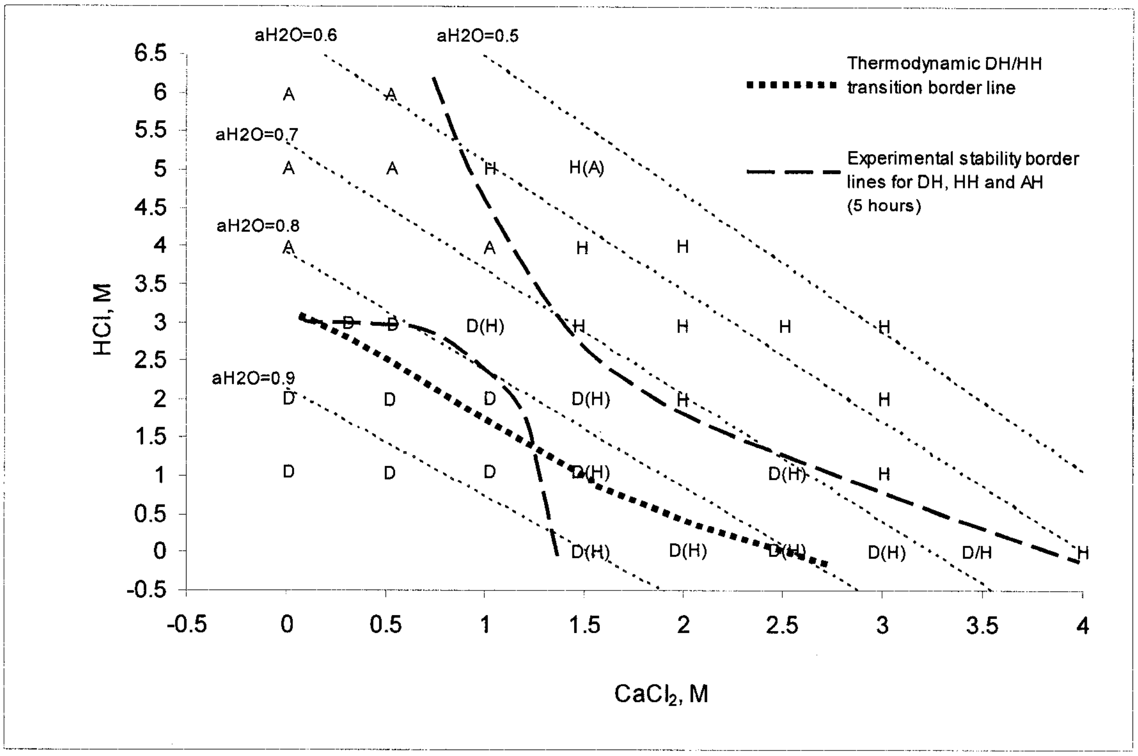

Figure 4.16. Experimental and theoretical stability regions for $CaSO_4$ hydrates and water activities in HCl-$CaCl_2$ solutions at 80°C.

According to examination of several SEM images of partially reacted DH crystals, evidence was found for the DH→HH conversion to have followed most likely the topochemical mechanism. This is exemplified with the selected images presented in Figure 4.17. The presented images represent partially reacted DH crystals at different extents of conversion. There appears that HH nuclei form and grow (unaxial growth) on the surface rendering support to the topochemical mechanism (Figure 4.17 a). With the progress of the conversion process the new born HH crystals grows at the expense of the mother DH crystal (Figure 4.17 b) ultimately leading to the production of needle-shaped HH crystals out of the columnar DH crystals (Figure 4.17 c).

The conversion of DH to HH was also monitored in terms of solution composition changes. A typical C vs. Time profile is shown in Figure 4.18 for the system DH→HH in 1.5M $CaCl_2$ + 3M HCl at 80°C (refer to Table 4.3). On the same Figure the solubility lines of DH and HH are shown, too (these were calculated with the aid of OLI-refer to Figure 4.4). The solubilities are shown to be constant simply because the bulk composition of the electrolyte solution was essentially constant during the conversion test (i.e. 1.5M $CaCl_2$ + 3M HCl) as ICP and acid titration analysis showed. As it can be seen, dissolution of the DH crystals occurred first reaching saturation in less than 30 minutes. Similar observations were made by Li [4]. The $CaSO_4$ concentration remained near the solubility of DH up to 2.5 hours and subsequently decreased below this level. The early stage concentration fluctuations are thought to be due to dissolution-recrystallization behaviour. After 5 hours equilibration all DH had been converted to HH but the solution had not yet reached equilibrium, in other words the solution is supersaturated reflecting the slow crystallization rate of HH at low supersaturation.

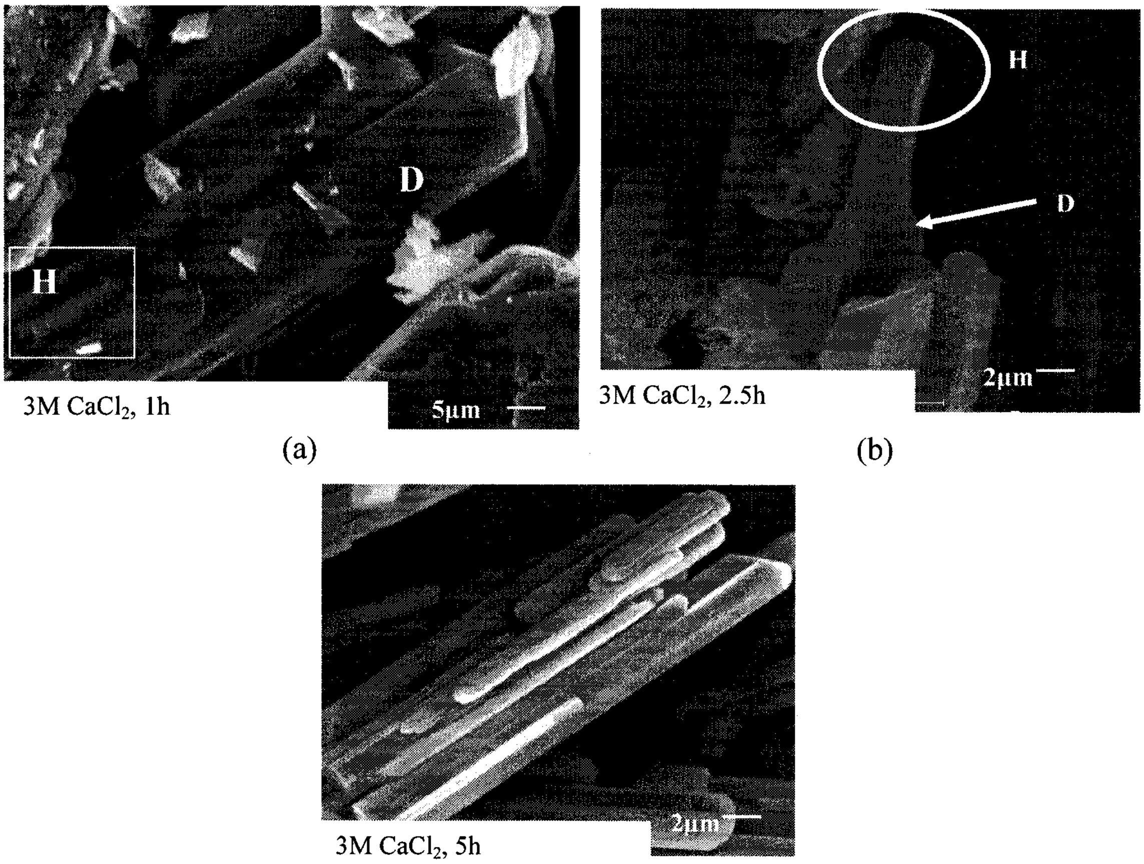

(a) (b)

(c)

Figure 4.17. HH formation and growth out of DH crystals.

In the case of HH to AH conversion, the SEM evidence seems to support the solid-state transformation mechanism. As it can be seen from Figure 4.19, decomposition of HH is prevalent throughout the crystal body leading to *in-situ* formation of fibre-like AH crystallites. The monitoring of $CaSO_4$ concentration with time during HH-AH transformation in 0.5M $CaCl_2$ + 6M HCl solution is shown in Figure 4.20. The solubilities of DH, HH and AH are also indicated. The crystal transformation from DH to HH was very fast apparently in this case (30 min) with the solution reaching equilibrium with the HH phase after 2.5 hours. The subsequent conversion of HH to AH (after 5 hours) did not result in lower $CaSO_4$ concentration in the bulk of solution. This implies that solution crystallization of AH is not kinetically favoured. This observation further supports, therefore, the conclusion that the conversion of HH to AH takes place *in-situ* via the solid-state transformation mechanism.

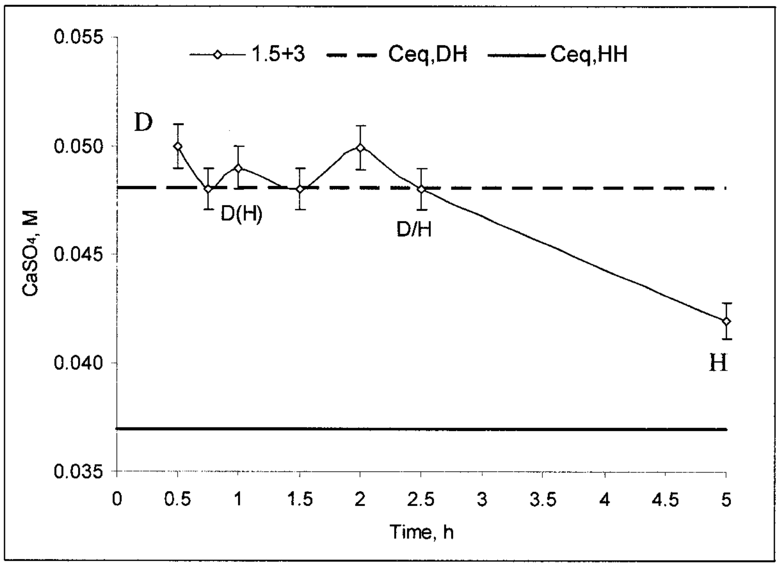

Figure 4.18. $CaSO_4$ concentration change during phase transformation (1.5M $CaCl_2$+3M HCl, 80°C) (Φ = experimental error range).

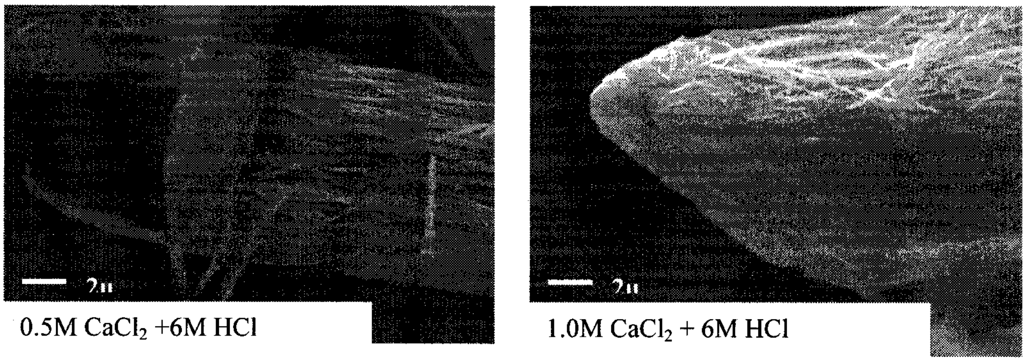

0.5M $CaCl_2$ +6M HCl

1.0M $CaCl_2$ + 6M HCl

Figure 4.19. HH-AH transformation in the volume of HH crystal at 80°C (5 hours).

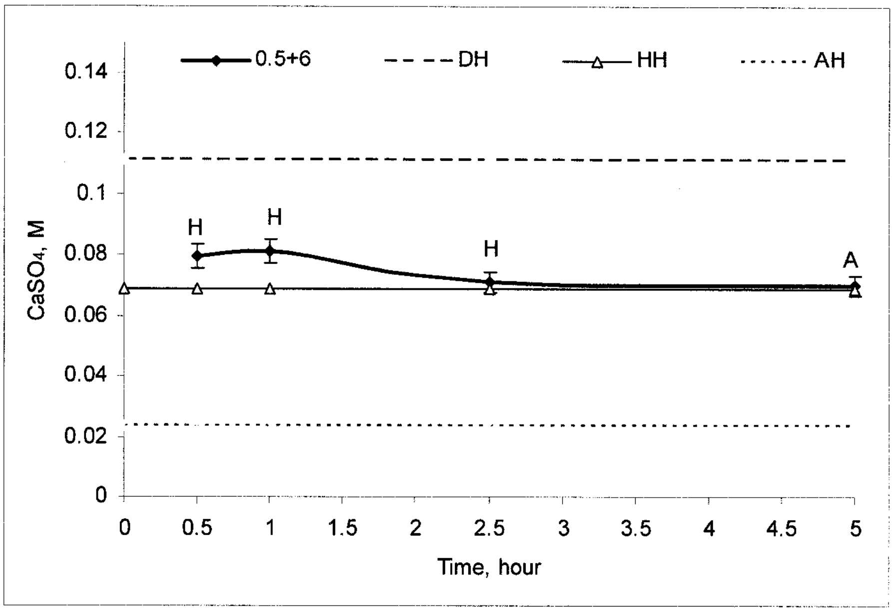

Figure 4.20. $CaSO_4$ concentration change during HH-AH phase transformation (0.5M $CaCl_2$+6M HCl, 80°C) (Φ = range of experimental error).

Finally the direct conversion of DH to AH was monitored in 5M HCl solution. SEM images presented in Figure 4.21 provide evidence to the formation of AH flakes on the surface of initial DH crystal similar to the case of HH-AH conversion via the solid-state mechanism. On the other hand, as the images of Figure 4.22 suggest, if the amount of DH ($mass_{DH}$) added in the electrolyte solution corresponds to a concentration lower than the solubility of DH but higher than AH solubility (i.e .0.34M>X>0.175M), DH completely dissolves (in 30 minutes) and AH recrystallizes in this case in solution (at time > 40 min) suggesting that dissolution-recrystallization mechanism operates.

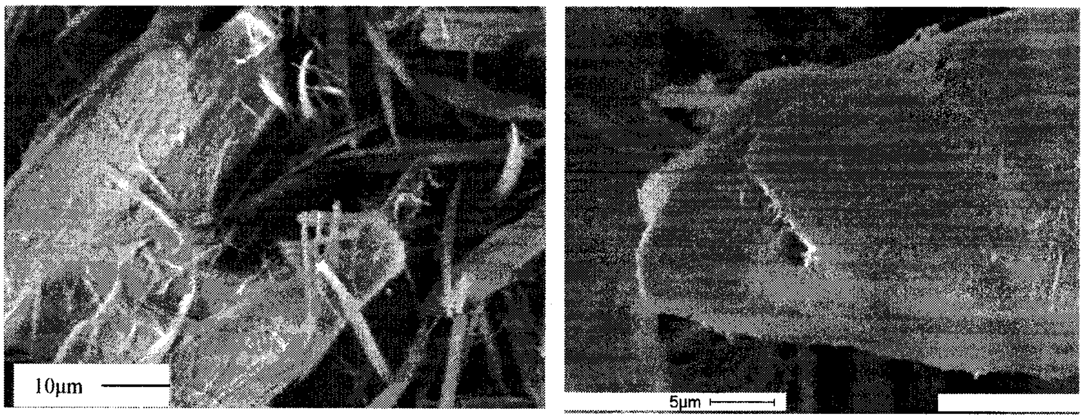

Figure 4.21. DH-AH transformation in the volume of DH crystal at 80°C (5M HCl, 2.5h).

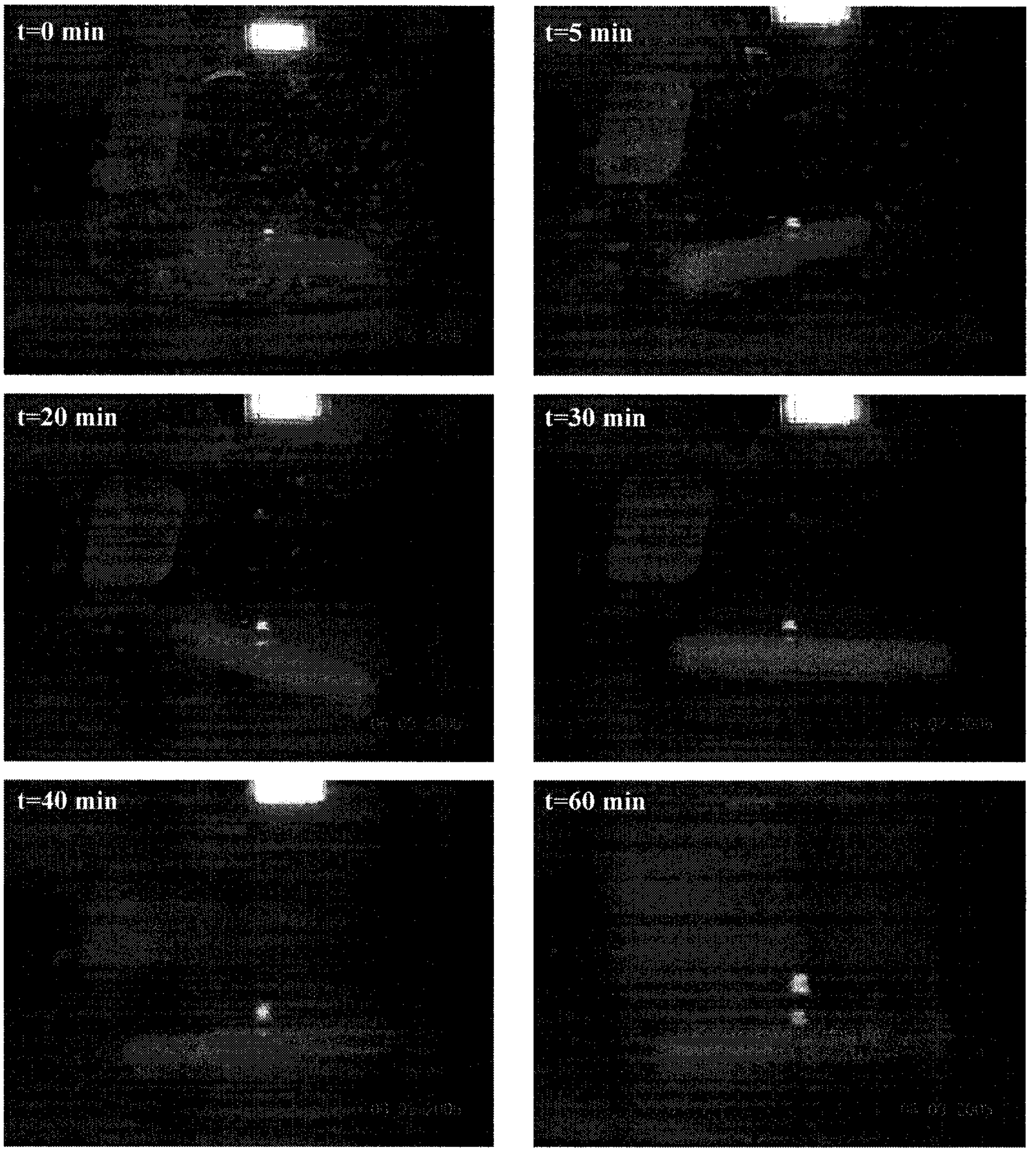

Figure 4.22. Demonstration of DH dissolution-AH recrystallization during equilibration (5M HCl, 80°C).

4.7. Conclusions

1. Anhydrite was found to be the only thermodynamically stable phase at 80°C.
2. Dihydrate was found to be metastable at low HCl (<3M) and $CaCl_2$ (<1.5M) concentration range.

3. Hemihydrate was unstable in HCl solutions being metastable only in the presence of $CaCl_2$.
4. Elevation of HCl concentration was found to speed up DH to HH and HH to AH conversion. On the other hand increasing the $CaCl_2$ concentration of the solution was found to render kinetic stability to HH by delaying HH to AH conversion.
5. Direct transformation of DH to AH is observed in the absence of $CaCl_2$ and in the presence of more than 3M HCl in the solution.
6. Elevated $CaCl_2$ concentrations found to interfere with the growth of elongated, column shaped HH crystals.
7. Solubility determinations suggested that a threshold water activity (around 0.85) exists for DH-HH transition in the $CaCl_2$-HCl system at 80°C.
8. Theoretical estimations of the DH/HH transition with OLI Stream Analyser software were in reasonable agreement with experimental findings.
9. The transition from DH to HH appears to be governed by the topochemical mechanism while that of DH to AH or HH to AH by the solid-state conversion mechanism.

References

[1] Van't Hoff, J.H., Amstrong, E.F., Hinrichsen, W., Weigert, F., Just, G., "Gypsum and anhydrite", Zeitschrift fur Physikalische Chemie, 45, 1903, 257-306.

[2] Demopoulos, G.P., "Precipitation in aqueous processing of inorganic materials: a unified colloid-crystallization approach to the production of powders with controlled properties", in Processing Materials for Properties, Eds: H. Henein and T. Oki, TMS, Warrendale, PA, 199, 3, 537-540.

[3] Mullin, J.W., "Crystallization", 3rd Edition, Butterworth-Heinemann, Oxford, UK, 1993.

[4] Li, Z., "Measurement and chemical modelling of $CaSO_4$ solubilities in concentrated chloride media", Ph.D. Thesis, McGill University, Montreal, QC, 2006.

[5] Li, Z., Demopoulos, G.P., "Development of an improved chemical model for the estimation of $CaSO_4$ solubilities in the HCl-$CaCl_2$-H_2O system up to 100°C", Industrial Engineering and Chemistry Research, 45, 2006, 2914-2922.

[6] Marshall, W.L. and Slusher, R., "Thermodynamics of calcium sulphate dihydrate in aqueous sodium chloride solutions, 0-110°C", Journal of Physical Chemistry, 70, 1966, 4015-4027.

[7] Martynowicz, E.T.M.J., "Impurity uptake in calcium sulphate during phosphoric acid processing", Ph.D. Thesis, Delft University Press, Delft, NL, 1994.

[8] E.T.M.J. Martynowicz, G. Witkamp, G.M. Rosmalen, "The effect of aluminum fluoride on the formation of calcium sulphate hydrates", Hydrometallurgy, 41, 1996, 171-186.

[9] Ling, Y., Demopoulos, G.P., "Phase transformation relationships in the $CaSO_4$-H_2SO_4-H_2O system", in EPD Congress 2004, Ed: M.E. Schlesinger, TMS, Warrendale, Pa, 2004, 477-487.

[10] Ling, Y., "Direct production of alpha-calcium sulphate hemihydrate from sulphuric acid", Ph.D. Thesis, McGill University, Montreal, QC, 2004.

[11] Hina, A., G.H. Nancollas, "Alpha calcium sulphate hemihydrate and a method of making alpha calcium sulphate hemihydrate", World Patent no. WO0179116, 2001.

[12] Zurz, A., I. Odler, F. Thiemann, K. Berghofer, "Autoclave-free formation of α-Hemihydrate gypsum", Journal of the American Ceramic Society, 74 (5), 1991, pp. 1117-1124.

[13] Jansz, J. J. C., "Estimation of ionic activities in chloride systems at ambient and elevated temperatures", Hydrometallurgy, 11 (1), 1983, 13-31.

[14] Sirota, I.S., Dorozhkin, S.V., Kuruchinina, M.V., Melikhov, I.V., "Phase transformation and dehydration of calcium sulphate dihydrate in solution studied by SEM", Scanning, 14, 1992, 269-275.

CHAPTER 5

Homogeneous Crystallization

5.1. Introduction

As mentioned earlier (in Chapter 2), information available in literature on α-$CaSO_4$ hemihydrate (HH) production in chloride media is limited to studies involving the conversion of gypsum (DH) to HH. No studies have been reported on the direct production of α-HH from $CaCl_2$ solution apart from an early patent (ICI) by Berrie and Wooley [1] and a paper by Yasue et al [2]. On the other hand, the nucleation and growth of HH crystals in a batch reactive crystallization environment (i.e., $CaCl_2$ and H_2SO_4 reaction) is rather complicated due to the fact that the activities of solution components (water and solutes) are not constant during the progress of precipitation hence the solubility and supersaturation are not constant either. In this chapter the homogeneous crystallization of α-$CaSO_4$ hemihydrate is investigated in a semi-batch reactor configuration. As per the objectives of this thesis outlined earlier (in Chapter 1), this chapter is not only about the production of HH but also about the underlying crystallization chemistry and, in particular, the role supersaturation plays in final HH crystal quality. Since crystallinity, crystal size and crystal morphology are the major indicators of crystal quality [3], a great attention is paid to monitoring these properties.

5.2. Experimental Procedure

All tests presented in this chapter were performed at 80°C following the general experimental techniques described in Chapter 3. In particular, three types of investigations were undertaken, which are described here. The first one aimed to elucidate the reactive crystallization chemistry; the second one aimed to determine the operating window in terms of [$CaCl_2$], [HCl] and time dimensions; and the third one aimed to optimize the method of acid addition.

5.2.1. Operating Window Determination Tests

The experiments were performed in a 2-liter autoclaveable glass reactor as described in Chapter 3. The starting $CaCl_2$/HCl solution with a known concentration (1-3M $CaCl_2$, 0-4M HCl) and volume (300mL) was preheated to 80°C and as soon as the target temperature was reached, H_2SO_4 of known concentration (2.66-5.32M) was added into it by titration using a burette while agitating with a speed of 400rpm. Following titration (this generally lasted 2-4 hours) the resultant slurry was equilibrated for typically 2-4 hours. During titration and equilibration, samples withdrawn by a syringe from the reactor, were subjected to solid (XRD, DSC, SEM, TGA, PSA) and solution (ICP) analysis for Ca and S content and titration for acid concentration. The final $CaCl_2$ / HCl solution concentration was further calculated on the basis of reaction stoichiometry. In all calculations or solution analyses the effect of dilution as a result of H_2SO_4 addition into the $CaCl_2$ solution was taken into account.

The determination of critical supersaturation (associated with the onset of homogeneous nucleation) involved the addition of very small doses of H_2SO_4 solution (typically 0.02 mL) using a micropipette into preheated (80°C) $CaCl_2$/HCl solution. After each H_2SO_4 dose added, enough time (30-60minutes) was allowed (to compensate for any induction time) before adding a new dose. The concentration, at which the first nuclei (cloud formation) were observed, signalled the attainment of the critical homogeneous nucleation concentration (critical supersaturation).

5.2.2. Acid Addition Optimization Tests

The same procedure as per 5.2.1 was employed. In this case though, in addition to adding H_2SO_4 by titration, a stepwise addition method was investigated, as well. Each step was

30 or 60 minutes long. Sulphuric acid (5.32-10M) in the latter case was added in $CaCl_2$ solution (3.5M) with a graduated cylinder.

5.3. Reactive Crystallization Chemistry

According to classical nucleation theory, the concentration of the solute should exceed a certain value for the formation of stable solute crystals [4]. Therefore, the mixing of reactants in a reaction crystallization system should produce sufficiently high concentration (supersaturation) of the solute to exceed the critical level for homogeneous nucleation to occur:

$$CaCl_2 + H_2SO_4 \rightarrow CaSO_{4(aq,\,s)} + 2HCl \qquad (5.1)$$
$$C_{CaSO4} \geq C_{CaSO4,cr} > C_{CaSO4,eq}$$

where C_{CaSO4} is the actual concentration measured by S analysis, $C_{CaSO4,cr}$ is the experimentally determined critical concentration (concentration of $CaSO_4$ at the point where first crystals were visually observed) and finally $C_{CaSO4,eq}$ is the equilibrium $CaSO_4$ concentration at given electrolyte concentration.

The present semi-batch reactive crystallization procedure may be analyzed with the aid of LaMer diagram concept (Chapter 2). Figure 5.1 depicts the variation of $CaSO_4$ with time during a typical titration test. On the same figure the variation of solubility with time is plotted. This was estimated using data generated by Li [5, 6]. The solubility increases with time because the reaction generates HCl (at least up to 3M), which elevates $CaSO_4$ solubility [6, 7]. In addition, the solubility increases because $CaCl_2$ concentration decreases with time. This is better seen with the results plotted in Figure 5.2. These results refer to the titration of 1.0M $CaCl_2$ + 4M HCl solution with 2.66M H_2SO_4 at 1.25mL/min H_2SO_4 addition rate. Returning to Figure 5.1, it is seen that after the peak is reached (signifying the critical nucleation concentration), $CaSO_4$ concentration drops for a certain time; however, a continuous increase follows due to continuous addition of H_2SO_4 and the accompanied increase in $CaSO_4$ solubility. Using the data of Figure 5.1, S_{cr} (signifying the onset of homogeneous crystallization) and S_{gr} corresponding to growth period were determined to be respectively 4.85 and 3.2.

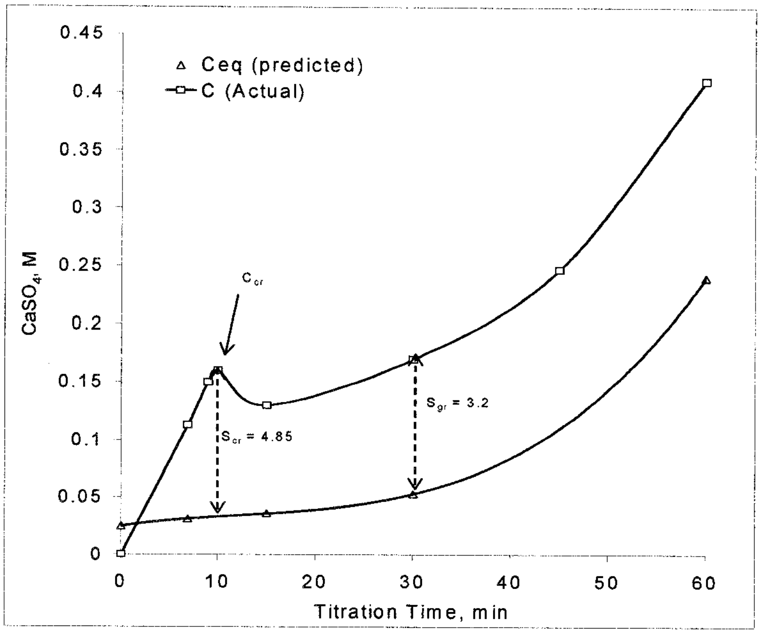

Figure 5.1. Actual $CaSO_4$ concentration variation and predicted solubility during the course of titration (conditions; $[CaCl_2]_o$=1M , $[HCl]_o$= 4M, $[H_2SO_4]_{titr}$= 2.66M, $Q_{H2SO4\ addition}$=1.25mL/min).

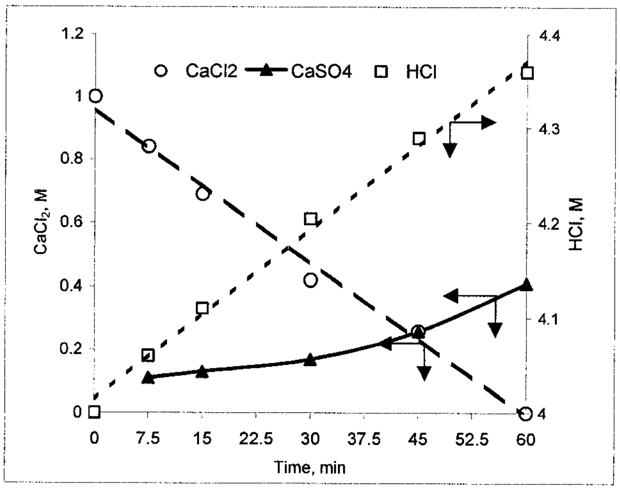

Figure 5.2. Variation of $CaCl_2$-HCl concentration during titration (conditions; $[CaCl_2]_o$=1M , $[HCl]_o$= 4M, $[H_2SO_4]_{titr}$= 2.66M, $Q_{H2SO4\ addition}$=1.25mL/min).

Another means of representation of the reactive crystallization (i.e. titration) test is given in Figure 5.3. In this case two types of $CaSO_4$ concentrations are reported; the 'actual', based on the solution analysis and 'added', estimated by assuming no precipitation. The difference between the two indicates the amount of $CaSO_4$ precipitated and the point, at which the 'added' and 'actual' curves separate, signifies the onset of precipitation. The particular conditions for this test were; 1.0M $CaCl_2$ + 4M HCl starting solution, 2.66M H_2SO_4; 1.25mL/min H_2SO_4 addition rate giving total molar ratio of SO_4/Ca =1.0 and 60 minutes total titration time.

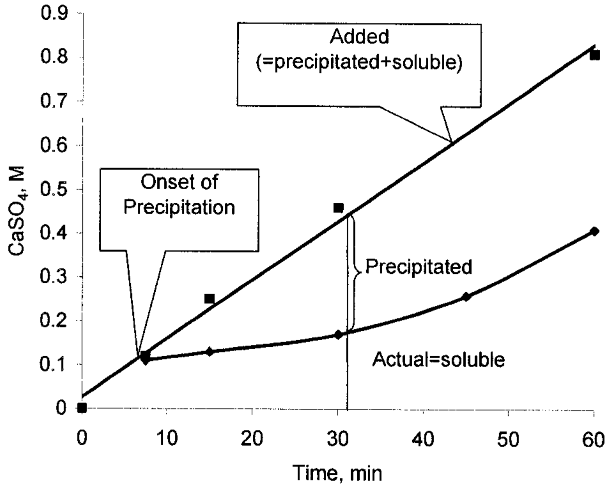

Figure 5.3. Profile of a titration-crystallization test at 80°C: 1.0M $CaCl_2$ + 4M HCl solution titrated with 2.66M H_2SO_4 at 1.25mL/min addition rate.

5.4. Determination of Operating Window

In addition to the stability tests described in Chapter 4, reactive crystallization tests were performed in this section, where the kinetics of HH formation and kinetic stability of formed HH crystals were monitored, in order to determine the operating window for the production of α-HH.

5.4.1. Solution Composition and Time Effects

A series of preliminary tests (always at 80°C) were conducted at various initial and final $CaCl_2$/HCl (total [Cl^-] kept constant at 6M) and H_2SO_4 concentrations in order to understand the behaviour of $CaSO_4$ phase formation and transformation before a detailed investigation was performed. Table 5.1 summarizes the experimental conditions and the nature of produced $CaSO_4$ material. Taking into account the reported data in literature [5, 8, 9, 10, 11] and the findings of Chapter 4, it was expected AH to be the only stable phase under the applied experimental conditions (at 80°C). This means that the produced DH and HH are metastable in nature.

Table 5.1. Summary of preliminary tests (initial solution volume = 300mL).

Test No.	Initial Solution $CaCl_2$ + HCl, M	Final Solution (Estimated*) $CaCl_2$ + HCl, M	Titrant H_2SO_4, M	Titrant Volume, mL	Titration/Equilibration Time, hour	SO_4/Ca Ratio	Phase After Equilibration
1	3.0+0.0	1.45+1.45	2.66	75	1/6	0.33	DH
2	3.0+0.0	0.72+2.90	5.32	75	2/4	0.66	α-HH
3	2.5+1.0	0.36+3.63	5.32	75	2/4	0.80	α-HH
4	2.0+2.0	0.84+3.37	5.32	37.5	1/4	0.50	α-HH
5	1.5+3.0	0.36+3.63	2.66	75	1/4	0.66	α-HH
6	1.5+3.0	0.42+4.21	5.32	37.5	1/4	0.66	α-HH
7	1.0+4.0	0.00+4.36	2.66	75	1/4	1.00	AH
8	1.0+4.0	0.00+5.05	5.32	37.5	1/4	1.00	AH
9	2.0+2.0	0.00+4.36	5.32	75	2/4	1.00	AH

*The estimation assumed 100% conversion of added H_2SO_4 to $CaSO_4$ (aq or s) and HCl

The solution composition after titration (reaction) in which the crystals were equilibrated for 4-6 hours was found to be critical on the type of $CaSO_4$ phase produced. Thus, as the case of Tests No 7, 8 and 9 indicates, independent of H_2SO_4 strength, the absence of $CaCl_2$ at sufficiently high final HCl concentration leads to the formation of the stable phase anhydrite (AH) after 5 to 6 hours processing (titration + equilibration).

On the other hand, the strength and the volume of H_2SO_4 reacted with $CaCl_2$, was found to directly influence the strength of generated HCl solution as well as the final $CaCl_2$ concentration, which in turn determine the phase of produced crystal. These phenomena are exemplified by comparing Tests No 1 and 2. Thus, in the former one, 2.66M H_2SO_4 generated low strength HCl (1.45M) and due to this fact, even after 6 hours of equilibration, initially formed DH crystals remained unchanged (Figure 5.4). However, when the DH crystals were subjected to SEM examination, it was observed that DH had undergone ripening upon prolonged equilibration (Figure 5.5).

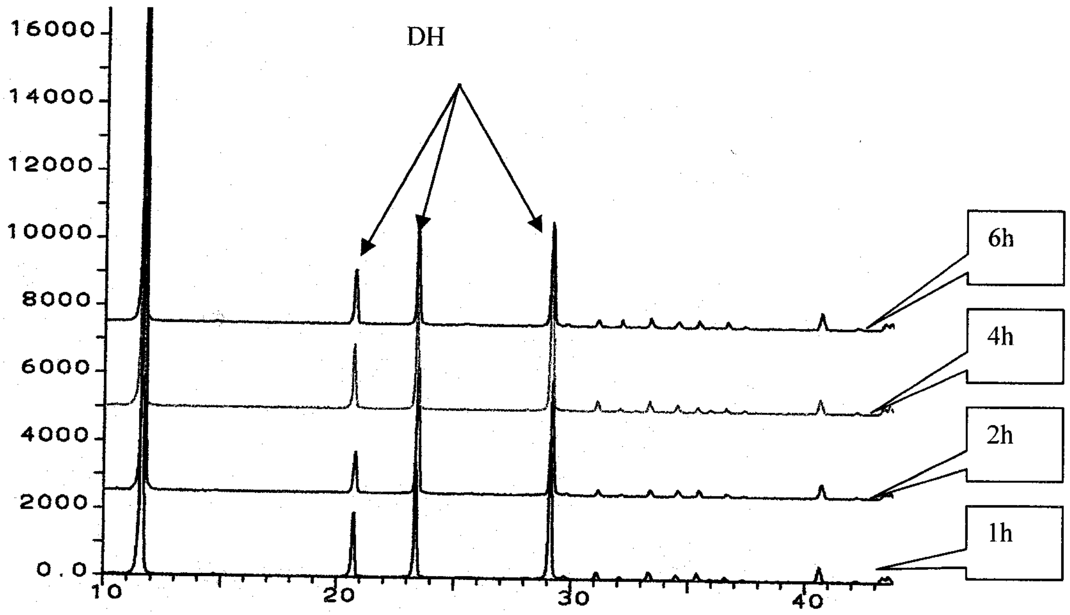

Figure 5.4. X-Ray examination of solids obtained by the titration of 3M $CaCl_2$ with 2.66M H_2SO_4 at 80°C ($SO_4/Ca=0.33$) as a function of equilibration time.

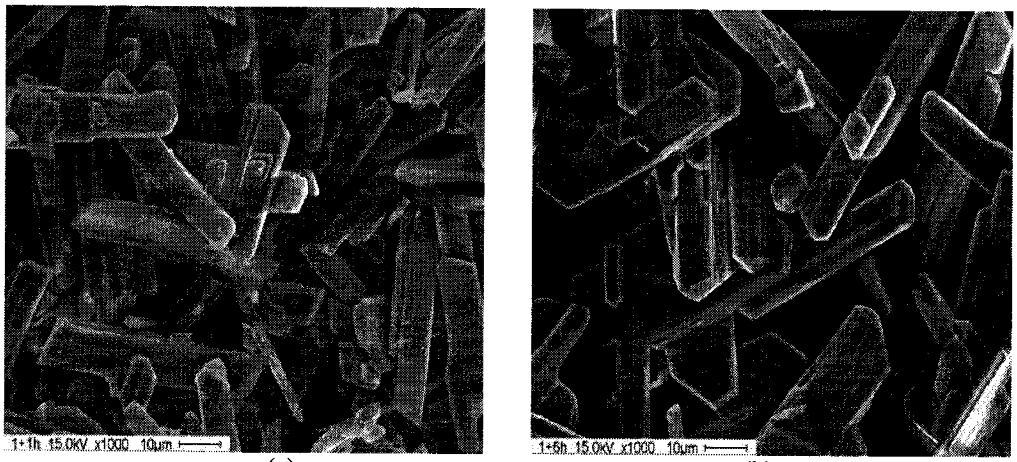

(a) (b)

Figure 5.5. SEM images of DH crystals obtained after (a) 1 hour titration and (b) 1 hour titration and 6 hours equilibration (titration of 3M $CaCl_2$ with 2.66M H_2SO_4 at 80°C ($SO_4/Ca=0.33$).

When the SO_4/Ca ratio increased to 0.66 by using 5.32M H_2SO_4 (i.e. titration time was extended to 2 hours in order to keep sulphate addition rate constant) as the precipitating agent (Test no 2), the final HCl concentration increased to 2.9M, enabling the complete conversion of DH to HH after 4 hours equilibration (Figure 5.6). The conversion of DH to HH was associated with significant morphological changes (Figure 5.7), while DSC (see section 3.4.4 for distinction of α and β forms by DSC) proved the produced HH to be of the alpha variety (Figure 5.8). Samples exhibited an exothermic peak at around 190°C, which is characteristic of the α-phase [12].

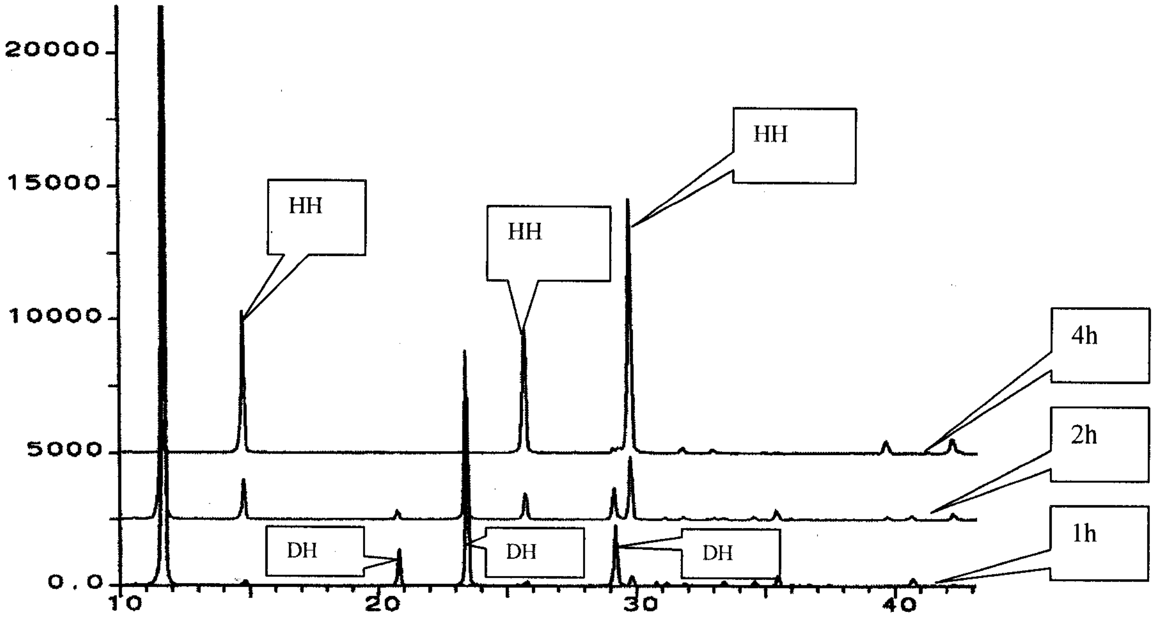

Figure 5.6. Conversion of DH to HH after 4 hours equilibration following the titration of 3M $CaCl_2$ solution with 5.32M H_2SO_4 at 80°C.


(a) DH (b)DH+HH (c)HH

Figure 5.7. SEM images of equilibrated solids following the 2 hours titration of 3M $CaCl_2$ solution with 5.32M H_2SO_4 at 80°C after (a) 1 h, (b) 2 h and (c)4 h equilibration.

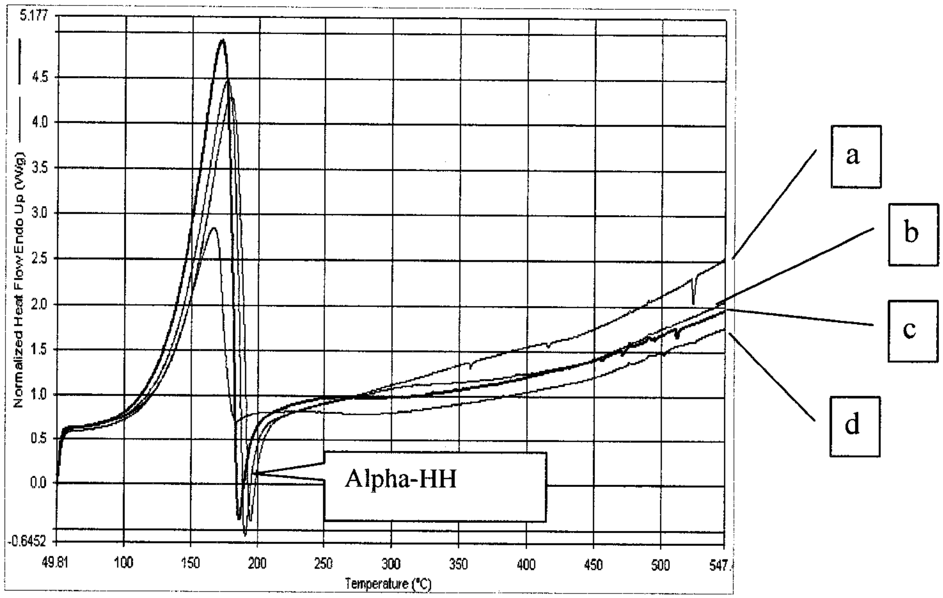

Figure 5.8. DSC examination of produced $CaSO_4$ hemihydrate crystals; a) Table 5.1, Test no. 2, b) Test no. 3, c) Test no. 4, d) Test no. 5.

5.4.2. Effect of Final HCl Concentration

Having determined in the preliminary precipitation tests that the final electrolyte ($CaCl_2$ / HCl) concentration plays a critical role in the production of α-HH, it was decided to conduct a detailed investigation on this effect. For this purpose, initially the effect of HCl was tested in two series of experiments in which the initial electrolyte concentration was systematically changed so to produce final solutions of varying HCl strength.

Table 5.2 summarizes the conditions and reports the form of produced crystal phase for the first series of experiments. The data show that upon elevation of the final HCl concentration, the conversion of DH to HH is catalyzed. However, the conversion did not stop there but continued towards the formation of AH (Figure 5.9). In other words, the elevation of HCl concentration alone accelerates HH formation but at the same time accelerates the conversion of the latter to AH. The phase transformations among the three $CaSO_4$ phases were also confirmed by SEM examination (Figure 5.10). Thus, the elongated hexagonal HH crystals are shown to transform into very fine AH crystals with fibre- and flake-like morphology.

Table 5.2. Results of HCl-effect-investigation tests (5.32M H_2SO_4, final $CaCl_2$ ≅0.47M).

Test No.	Initial Solution $CaCl_2$ + HCl, M	Final Solution (Estimated) $CaCl_2$ + HCl, M	Titration Time (min)	SO_4/Ca Ratio	Phase after Equilibration for			
					0h	1h	2h	4h
10	1.0 + 3.0	0.46+ 3.66	60	0.50	DH	DH	DH	DH
11	1.5 + 3.0	0.47 + 4.15	60	0.66	DH(HH)*	HH	HH	HH(AH)
12	2.0 + 3.0	0.48 + 4.59	120	0.70	-	HH	HH	HH(AH)
13	3.0 + 3.0	0.46 + 5.30	120	0.78	HH	HH	HH	HH/AH**

*: ( ) indicates the minor phase,**:/ indicates approximately the same amount for both phases

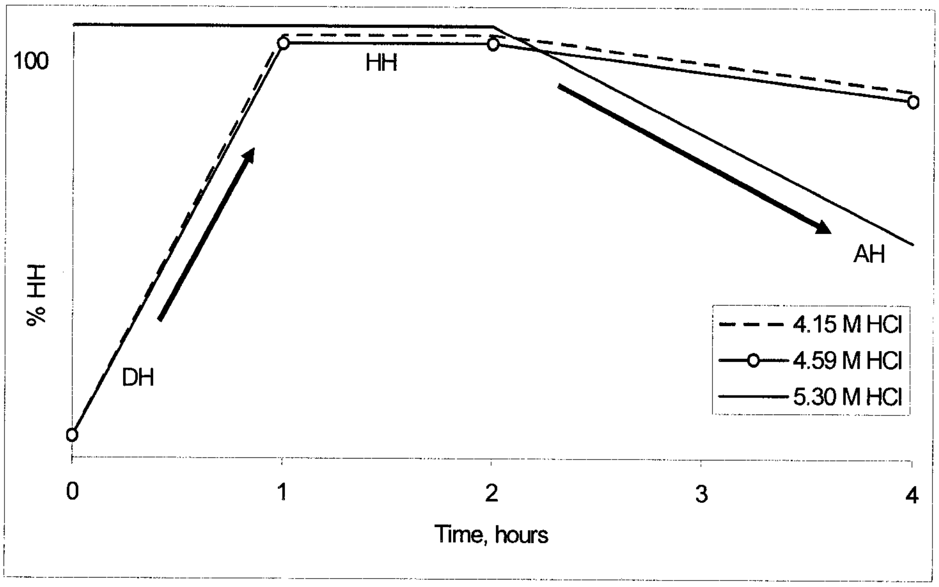

Figure 5.9. HH kinetic stability as a function of equilibration time and final HCl concentration (for complete set of conditions refer to Table 5.2).

The second series of tests was realized at fixed initial (2.5M) and final (0.36M) $CaCl_2$ concentration. The effect of increasing final HCl strength was found to be consistent with the results presented in Table 5.2, i.e. that HCl kinetically promotes the conversion of DH to HH and HH to AH (Table 5.3). Decreasing the residual $CaCl_2$ concentration down to 0.36M did not compromise intermediate HH formation. It is reminded here that as per the findings of the stability tests reported in Chapter 4 in the absence of $CaCl_2$ no HH formation occurs.

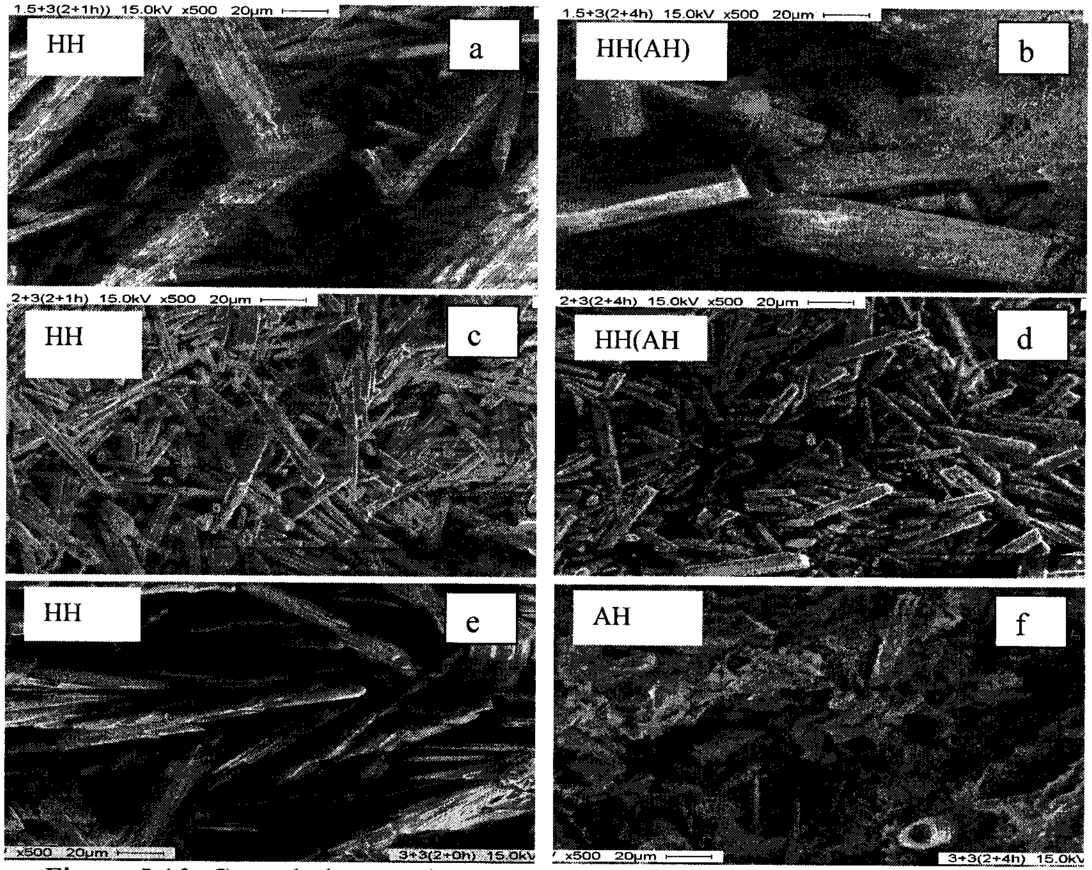

Figure 5.10. Crystal phase and morphology changes as a function of final HCl concentration: a) 4.15M final HCl, 1h equilibration, b) 4.15M final HCl, 4h equilibration, c) 4.59M final HCl, 1h equilibration, d) 4.59M final HCl, 4h equilibration, e) 5.30M final HCl, 1h equilibration, f) 5.30M final HCl, 4h equilibration.

Table 5.3. Results of HCl-effect-investigation tests (5.32M H_2SO_4, final $CaCl_2$ $\cong$0.36M).

Test No	Initial Solution $CaCl_2$ + HCl (M)	Final Solution (Estimated) $CaCl_2$ + HCl (M)	Titrant Volume (mL)	Titration Time (min)	SO_4/Ca Ratio	Phase after Equilibration for			
						0h	1h	2h	4h
14	2.5 + 0.0	0.36 + 2.90	75	120	0.80	-	DH(HH)	DH(HH)	DH(HH)
3	2.5 + 1.0	0.36 + 3.64	75	120	0.80	DH/HH	HH	HH	HH
15	2.5 + 2.0	0.36 + 4.36	75	120	0.80	-	HH	HH	HH
16	2.5 + 4.0	0.36 + 5.80	75	120	0.80	-	HH	HH(AH)	AH

The results of Tables 5.2 and 5.3 clearly show that depending on the time and HCl concentration, the reaction of $CaCl_2$ with H_2SO_4 at 80°C yields initially dihydrate crystals which gradually convert to HH (confirmed by DSC to be α-HH) and ultimately to AH upon prolonged equilibration.

The observed phase change sequence (DH→HH→AH) is in agreement with the order of the stability (or solubility) of these phases as can be seen from Figure 5.11. Solubilites were estimated with the aid of OLI Stream Analyzer 1.2-McGill Databank [5, 13, 14]. Finally the transformation of HH to AH during equilibration at 5.8M final HCl concentration (Test No. 16) was found to correspond to solution composition changes. Thus, it can be seen in Figure 5.12 the solution to be initially supersaturated in terms of HH, but becoming after 2 hours undersaturated (but supersaturated in terms of AH) hence, setting in motion the conversion of HH to AH. All these phase changes obey the Ostwald Rule of Stages [15].

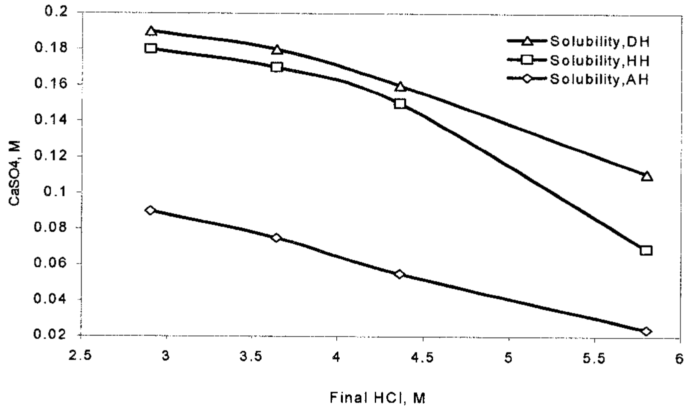

Figure 5.11. The solubility curves of DH, HH and AH as a function of HCl concentration at 80°C calculated with the aid of OLI Stream Analyzer 1.2-McGill Databank ($[CaCl_2]=0.36M$).

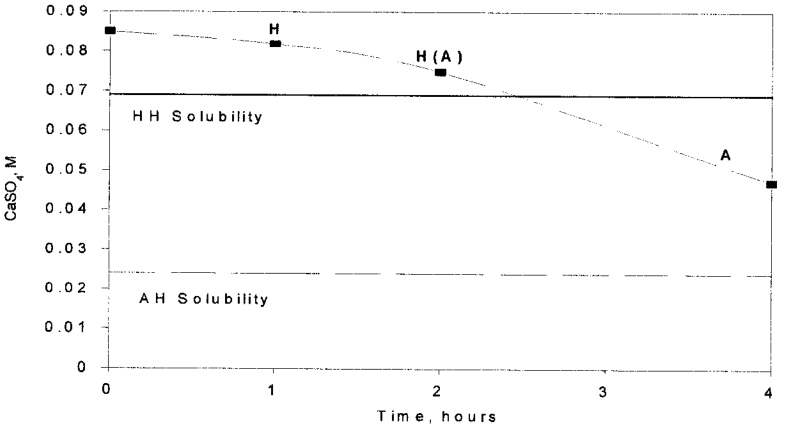

Figure 5.12. $CaSO_4$ concentration variation with equilibration time and comparison with the solubilities of HH and AH (Test no 16-refer to Table 5.3).

5.4.3. Effect of Final $CaCl_2$ Concentration

The influence of $CaCl_2$ concentration on HH crystallization (DH to HH transition) kinetics and HH kinetic stability were already discussed in Section 4.4.2 and the positive effect of $CaCl_2$ on enhancing the kinetic stability of HH was established. Here a series of experiments seeking to elucidate the effect of final $CaCl_2$ concentration on HH production is described. The experimental conditions and results of these tests are summarized in Table 5.4. XRD examination of the samples taken at certain time intervals during equilibration period revealed that the elevation of final $CaCl_2$ concentration accelerated DH-HH conversion but slowed down the further conversion of HH to AH (Table 5.4). Interestingly enough, in the absence of $CaCl_2$ it was not possible to detect HH at all (refer to Test no 17 in Table 5.4). Hence, it is clear that the role of $CaCl_2$ is critical in stabilizing HH thus rendering the production of it feasible.

Table 5.4. Results of $CaCl_2$-effect-investigation tests (5.32M H_2SO_4, final HCl $\cong$3.64M)

Test No	Initial Solution $CaCl_2$ + HCl, M	Final Solution (Estimated) $CaCl_2$ + HCl, M	Titrant Volume (mL)	Titration Time (min)	SO_4/Ca Ratio	Phase after Equilibration for			
						0h	1h	2h	4h
17	2.5 + 0.34	0.00 + 3.64	141	120	1.00	DH	DH(AH)	DH(AH)	DH/AH
3	2.5 + 1.00	0.36 + 3.64	113	120	0.80	DH/HH	HH	HH	HH(AH)
18	2.5 + 1.41	0.60 + 3.64	95.3	120	0.68	HH	HH	HH	HH
19	2.5 + 1.75	0.84 + 3.64	80.8	120	0.57	HH	HH	HH	HH

In a search of finding an explanation (refer to section 4.5) of the cause behind the different conversion sequence in Test no 17 (DH to AH rather than DH-HH-AH) the solubility of DH and HH during the progress of 2 hours reaction (Figure 5.13) for the systems with or without intermediate HH formation (Test nos 17, 3 and 19) was estimated. The solubility curves for all conditions indicate that DH has higher solubility than HH under the given conditions. The major difference among the systems is that in the case of 0.0 M final $CaCl_2$ concentration, the solubilities of DH and HH are closer than in the cases of 0.36 and 0.84M $CaCl_2$ concentrations. This closeness in the solubility of

DH and HH at 0.0M $CaCl_2$ appears to imply that direct conversion of DH to AH is now energetically favoured as per the Ostwald Rule of Stages [15].

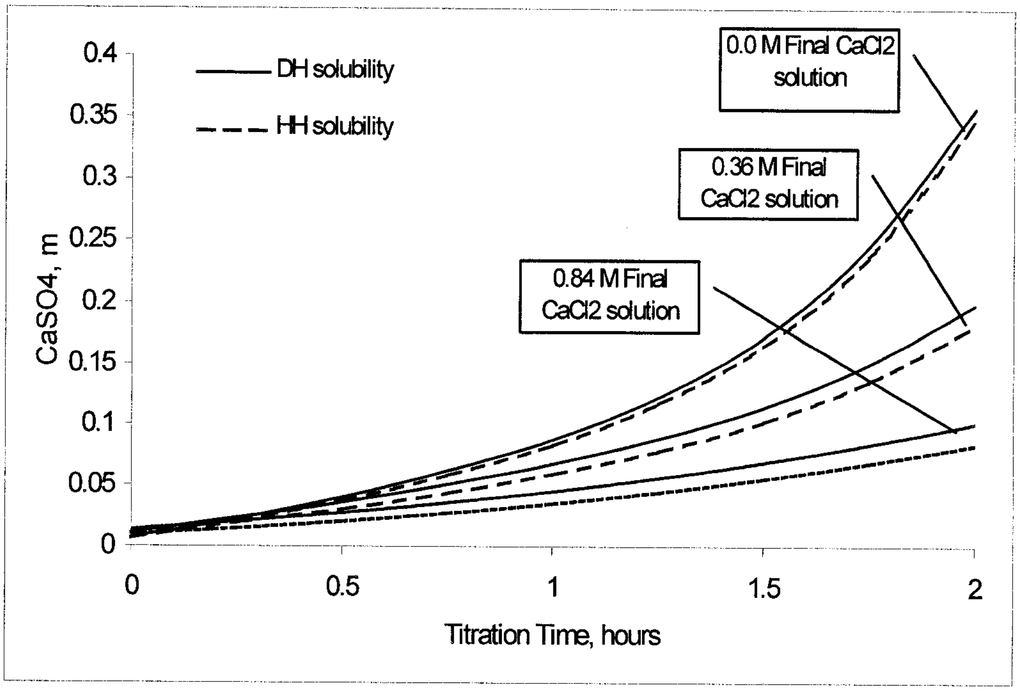

Figure 5.13. DH and HH solubility as a function of final $CaCl_2$ concentration estimated with the aid of OLI Stream Analyzer Version 1.2-McGill Databank [5] (refer to Table 5.4. for all conditions).

SEM images presented in Figure 5.14 also confirm the crystal phase transformations. Direct conversion of DH to AH is associated with the destruction of plate-like DH crystals and formation of AH fibers on DH surface and in the bulk solution after 4 hours equilibration (Figure 5.14a). On the other hand, as it can be seen in Figure 5.14b only HH crystals are present in the presence of $CaCl_2$ (Test no 19).

5.4.4. Transition Diagram

The results obtained from the tests reported in sections 5.4.1 to 5.4.3 were used to construct a time-dependent stability diagram for HH. The nature of $CaSO_4$ obtained after

1 and 4 hour equilibration was located on $CaCl_2$ vs. HCl plots (Figure 5.15). All borders (approximate) were drawn in order to delineate the region of metastability of HH.

The major difference between 1 and 4 hours is the region where HH transforms into AH. This region was bordered with minimum 4M HCl and maximum 0.5M $CaCl_2$ concentration. The HH metastability is time-sensitive; thus all HH detected in this region after the 1st hour of equilibration, partially or completely transformed into AH after 4 hours equilibration. The positive effect of the presence of $CaCl_2$ on HH metastability is once more evident.

Figure 5.16 is a composite of the theoretical and experimentally determined stability diagrams. The theoretical stability line is defined as the intersection of solubility lines of $CaSO_4$ hydrates (DH and HH) (see also Chapter 4). The left-hand side of the continuous line represents the region where HH is unstable. The right-hand side of both the continuous and broken lines represents the region where HH is metastable from 1 to 4 hours. Since AH is the only thermodynamically stable phase at 80°C, the material produced within the range of this diagram is going to convert to AH when equilibrium is reached (≈24 hours under these conditions-refer to Table 4.2).

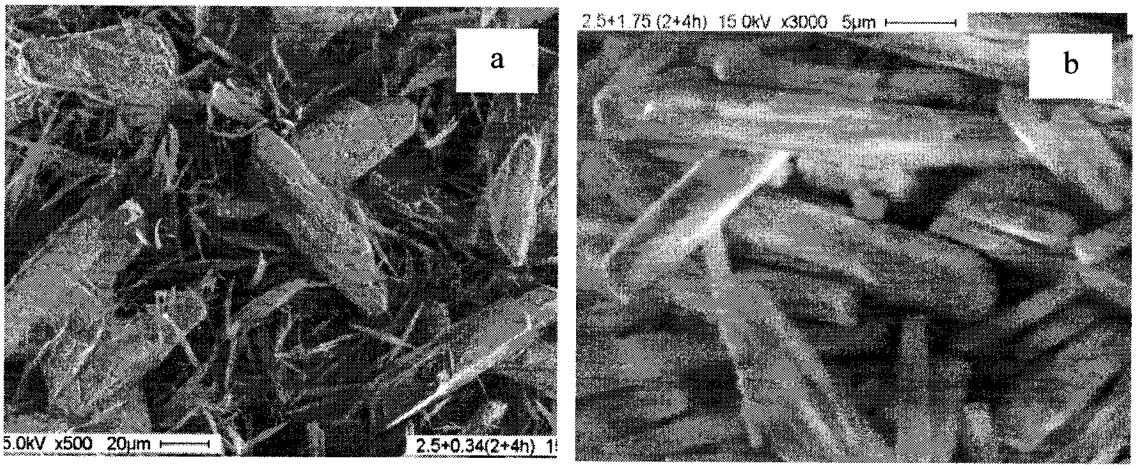

Figure 5.14. $CaSO_4$ morphologies as a function of final $CaCl_2$ concentration; a) 0.0 M $CaCl_2$, 4 hours equilibration, b) 0.84M $CaCl_2$, 4 hours equilibration.

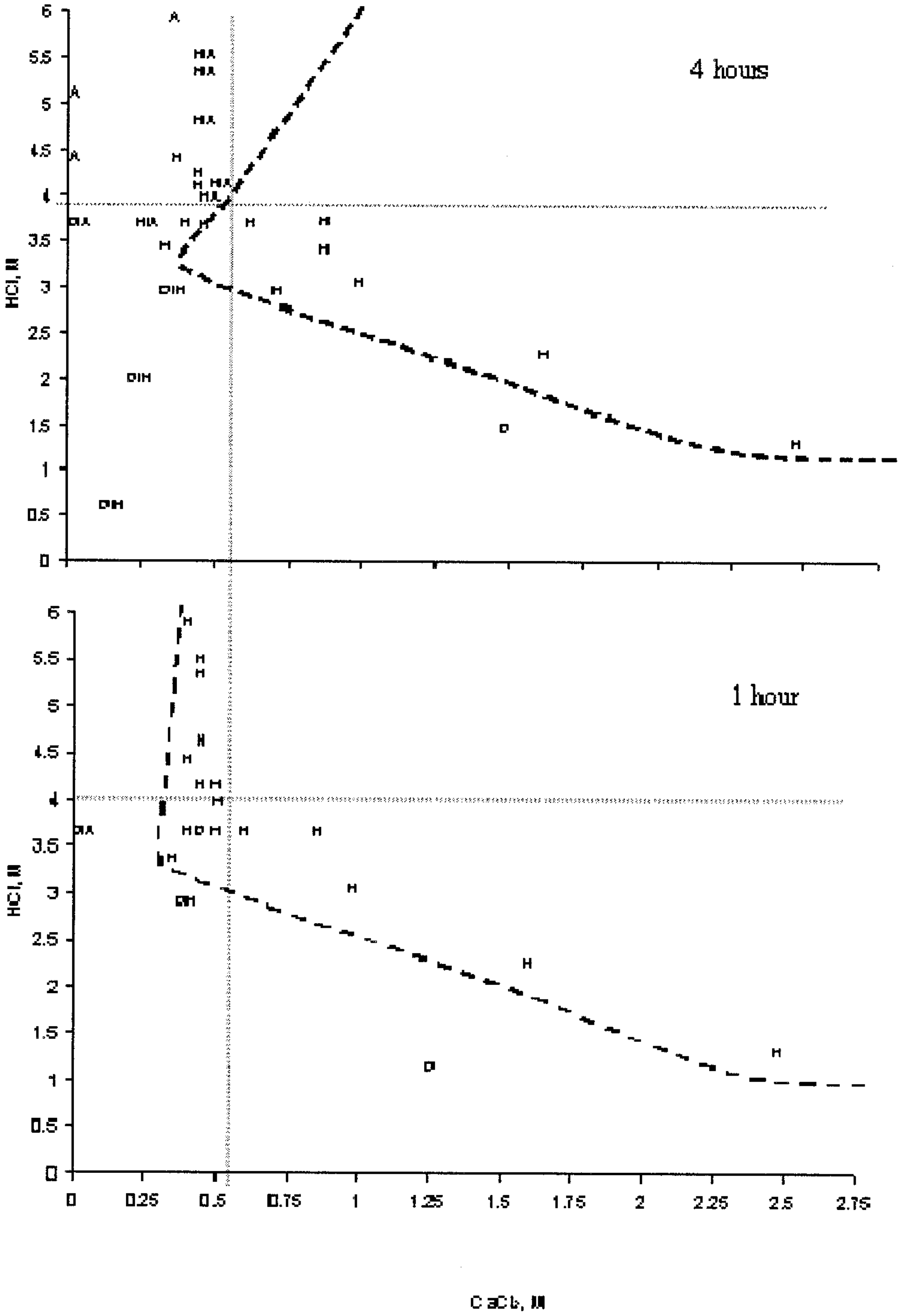

Figure 5.15. Experimentally determined stability conditions for $CaSO_4$ hydrates as a function of final electrolyte concentration and equilibration time at 80°C (2 hours titration time).

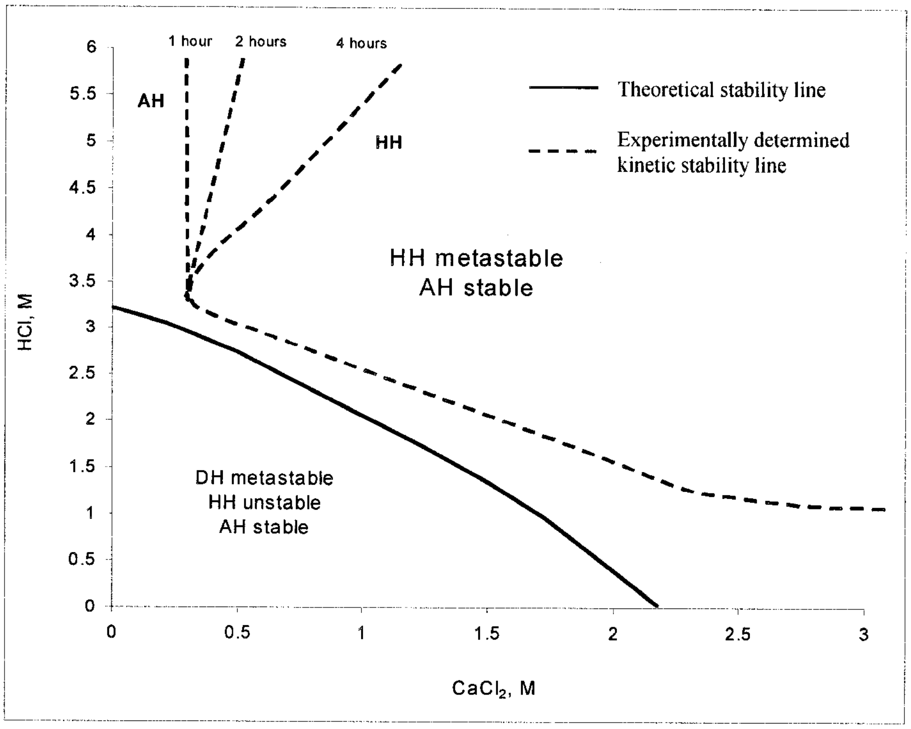

Figure 5.16. Theoretical* and time-dependent (2 hours titration+equilibration) transition diagram of HH at 80°C (*determined with the aid of OLI Stream Analyzer Version 1.2-McGill Databank [7]).

5.5. Process Analysis and Optimization

5.5.1. Effect of Reaction Extent

In the previous section the operating window in terms of final [HCl] and [$CaCl_2$] concentrations was determined at different reaction times for the production of alpha-HH at 80°C by the reaction of $CaCl_2$ and H_2SO_4. In this section the process system is further analysed by explaining and optimizing the method of H_2SO_4 addition. It becomes evident that the conditions of H_2SO_4 addition (such as acid strength, SO_4/Ca ratio addition rate and continuous vs. staged addition) would influence the supersaturation environment hence the quality of the crystals.

Homogeneous nucleation is known to occur only when a critical solute concentration (C_{cr}) or better supersaturation (S_{cr}) is reached [16]. As already examined in section 5.3 the reaction of H_2SO_4 and $CaCl_2$ solution in a semi-batch reactor configuration as the one used in this work is associated by homogeneous nucleation followed by a growth period. The relative length of the nucleation and growth periods will be a function of the method of acid addition. This is exemplified with the data of Figure 5.17. In this figure, the variation of $CaSO_4$ concentration as a function of time is monitored for a typical test and compared to the corresponding critical (C_{cr}) and equilibrium (C_{eq}) concentration levels. The test in question involved reacting a 3M $CaCl_2$ solution with 5.32M H_2SO_4 over a period of 4 hours. The acid was added in doses every 30 minutes. The HH solubility line was estimated with the aid of OLI [5] and C_{cr} was determined independently via a series of tests involving the addition of H_2SO_4 (8M) to variable $CaCl_2$/HCl composition solutions. These tests are summarized in Appendix A at the end of this chapter. It is clearly seen that during the first 45 minutes of the process, the actual concentration of $CaSO_4$ lay close to the critical concentration (C_{cr}) line, meaning that the mode of precipitation during this period was via homogeneous nucleation. The remaining precipitation, though, i.e., after the first 45 minutes, can be clearly seen to have occurred in the metastable zone via deposition on the homogeneously nucleated crystals (growth period).

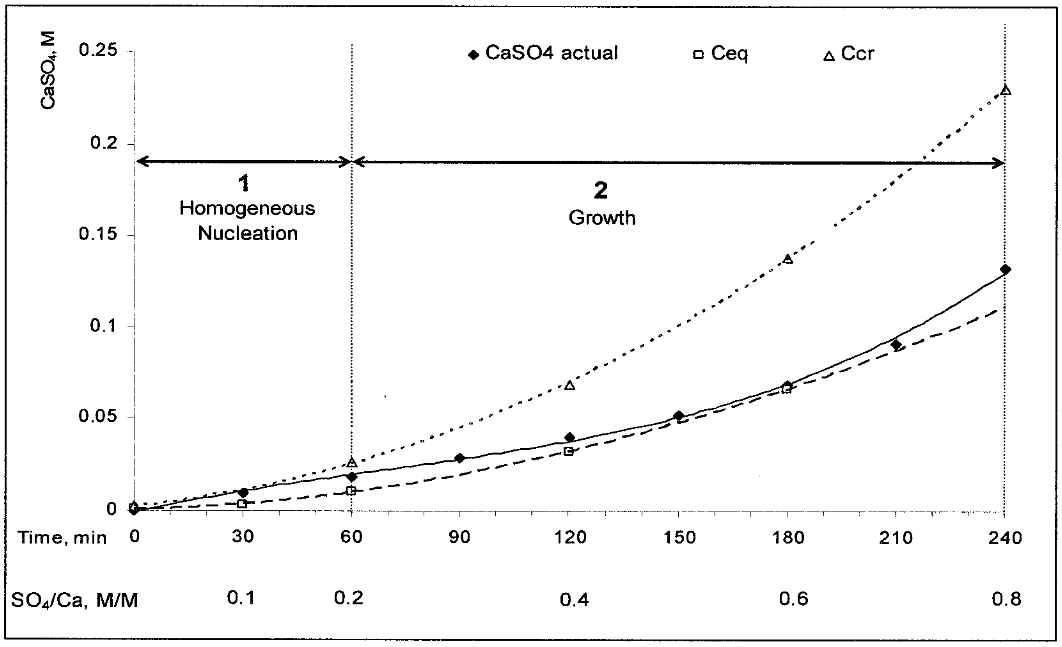

Figure 5.17. Homogeneous nucleation and growth zones in a typical reactive crystallization test (conditions: 3M $CaCl_2$, 5.32M H_2SO_4, 8-step-H_2SO_4-addition, 80°C).

The growth of the resultant crystals with the progress of reaction, i.e. the progressive addition of H_2SO_4 can be evaluated with the data of the tests summarized in Table 5.5. It can be seen that independent of the extent of reaction, i.e. SO_4/Ca ratio used, the product obtained was HH. However, particle size analysis (Figure 5.18) and SEM analysis (Figure 5.19) clearly showed the crystals to grow longer with the extent of the reaction (increasing SO_4/Ca ratio). The observed crystal growth translated to improved filtration rates; 1737 kg/m^2/h for SO_4/Ca = 0.8 vs. 869 kg/m^2/h for SO_4/Ca = 0.4.

Table 5.5. . Effect of Increasing SO_4/Ca ratio on $CaSO_4$ phase (Titration Time: 2 hours).

Test no.	Initial Solution $CaCl_2$ + HCl, M	Final Solution (Estimated) $CaCl_2$ + HCl, M	Titrant Volume -5.32M H_2SO_4- (mL)	SO_4/Ca Ratio	Phase after Equilibration for 0h	1h	2h	4h
20	3.5+0.0	2.47+1.24	39.47	0.2	HH	HH	HH	HH
21	3.5+0.0	1.66+2.21	78.94	0.4	HH	HH	HH	HH
22	3.5+0.0	1.00+3.01	118.41	0.6	HH	HH	HH	HH
23	3.5+0.0	0.46+3.66	157.88	0.8	HH	HH	HH	HH

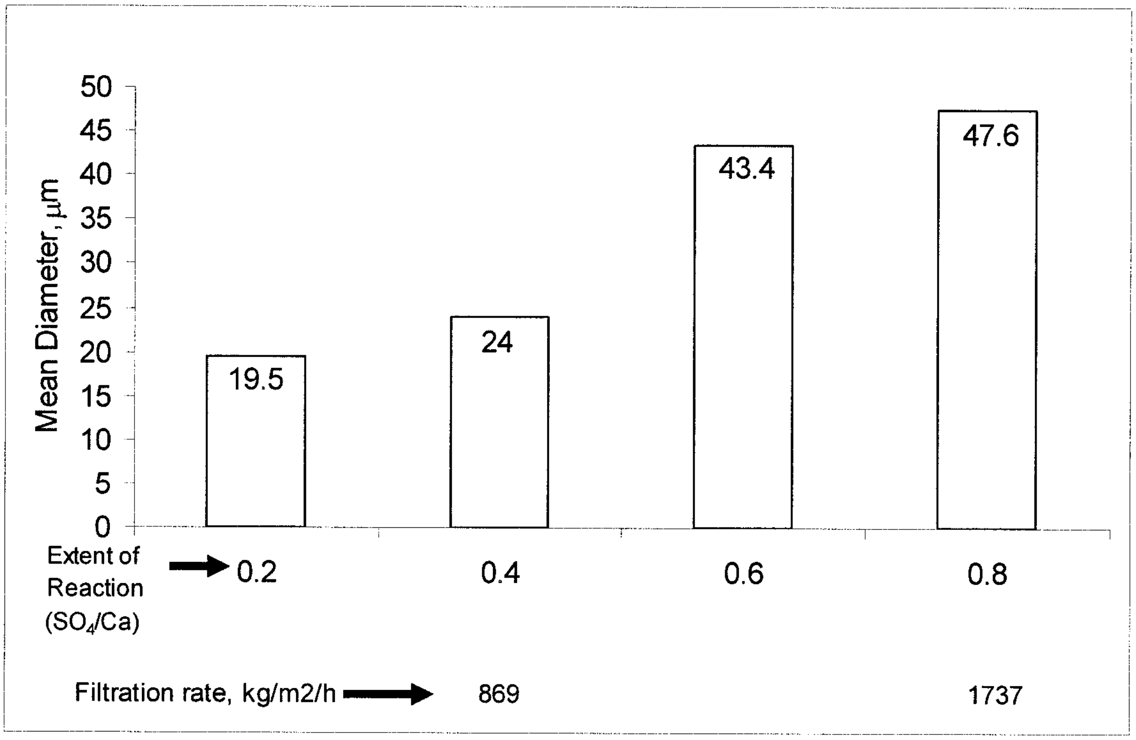

Figure 5.18 Effect of reaction extent (SO_4/Ca ratio) on mean diameter and filtration rate (refer to Table 5.5 for other conditions).

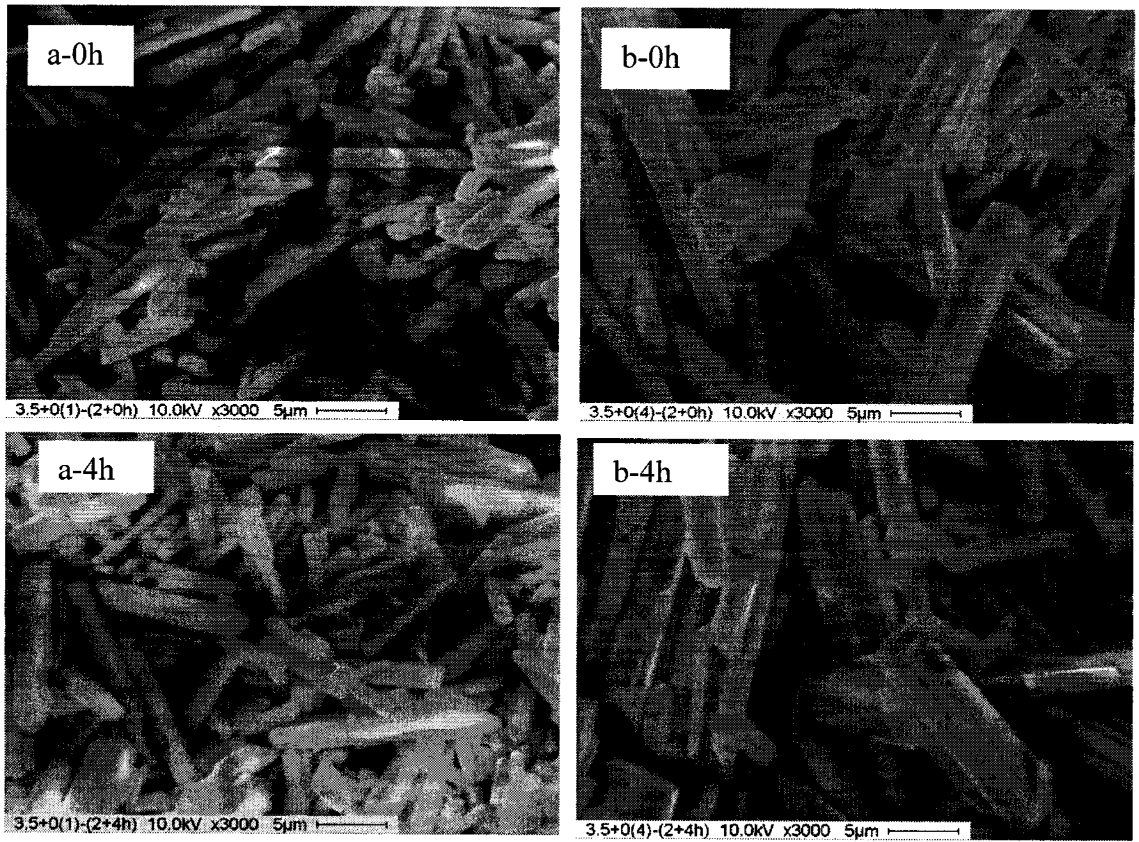

Figure 5.19 Effect of extent of reaction (SO_4/Ca molar ratio) on HH morphology at 0 and 4 hours of equilibration; a) $SO_4/Ca = 0.2$ b) $SO_4/Ca = 0.8$ (for conditions refer to Table 5.5).

Equilibration was not found (Figure 5.20) to have a noteworthy effect on growth, i.e., any crystal ripening that occurred did not measurably change the average crystal size.

5.5.2. H_2SO_4 Addition Rate and Concentration Effects

The H_2SO_4 addition rate as per previous arguments made in section 5.5.1 was confirmed to impact on crystal growth as can be deduced from the data in Figures 5.21 and 5.22. The corresponding addition rules for each titration period tested were: 78.94 mL/h, 39.47 mL/h and 26.3 mL/h for 2h, 4h and 6h titration period, respectively. These crystal property data were obtained via a series of tests run under the conditions summarized in

Table 5.6. In all cases the product was HH but the different acid addition rates resulted in different crystal sizes. Apparently the faster the addition rate the higher the supersaturation hence the more extensive was homogeneous nucleation vis-à-vis growth. This is proven with the data in Figures 5.23 and 5.24 that correspond to Tests no. 23 and 25, respectively (refer to Table 5.6). Thus, when a fast addition rate was employed (Figure 5.23) the homogeneous nucleation zone was extended to 0.5 hour that corresponds to SO_4/Ca ratio of 0.2 (obtained by multiplying time with addition rate). On the other hand in the case of slow addition rate (Figure 5.24) homogeneous nucleation was over after 0.8 hours, which corresponds to $SO_4/Ca \approx 0.1$.

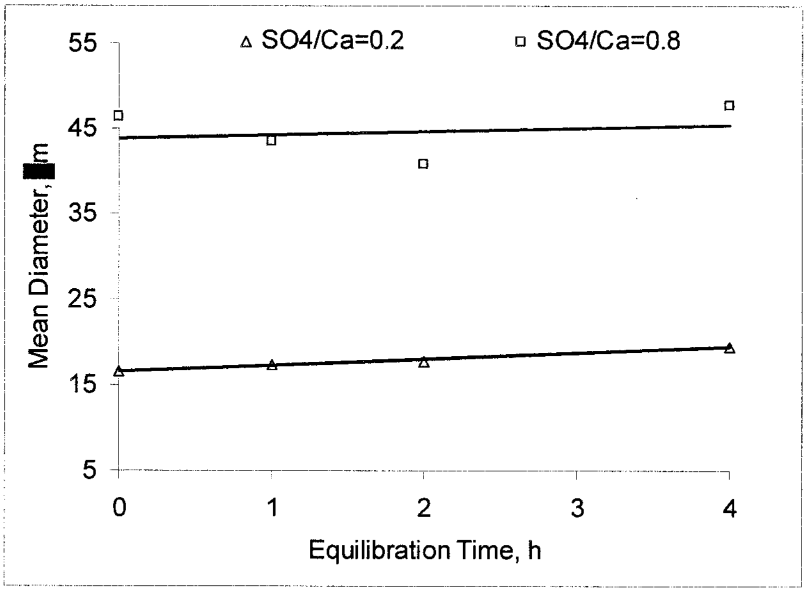

Figure 5.20. Effect of equilibration time on HH crystal size at different reaction extents (SO_4/Ca molar ratios) (for conditions refer to Table 5.5).

Table 5.6. Effect of titration/equilibration period on $CaSO_4$ modification (SO_4/Ca=0.8).

Test no.	Initial Solution $CaCl_2$ + HCl (M)	Final Solution (Estimated) $CaCl_2$ + HCl, M	Titrant Volume -5.32M H_2SO_4-(mL)	Titration/ Equilibrtion Time (hour)	Phase during residence in the reactor (titration+equilibration)		
					2h	4h	6h
23	3.5+0.0	0.46+3.66	157.88	2/4	HH	HH	HH
24	3.5+0.0	0.46+3.66	157.88	4/2	HH	HH	HH
25	3.5+0.0	0.46+3.66	157.88	6/0	HH	HH	HH

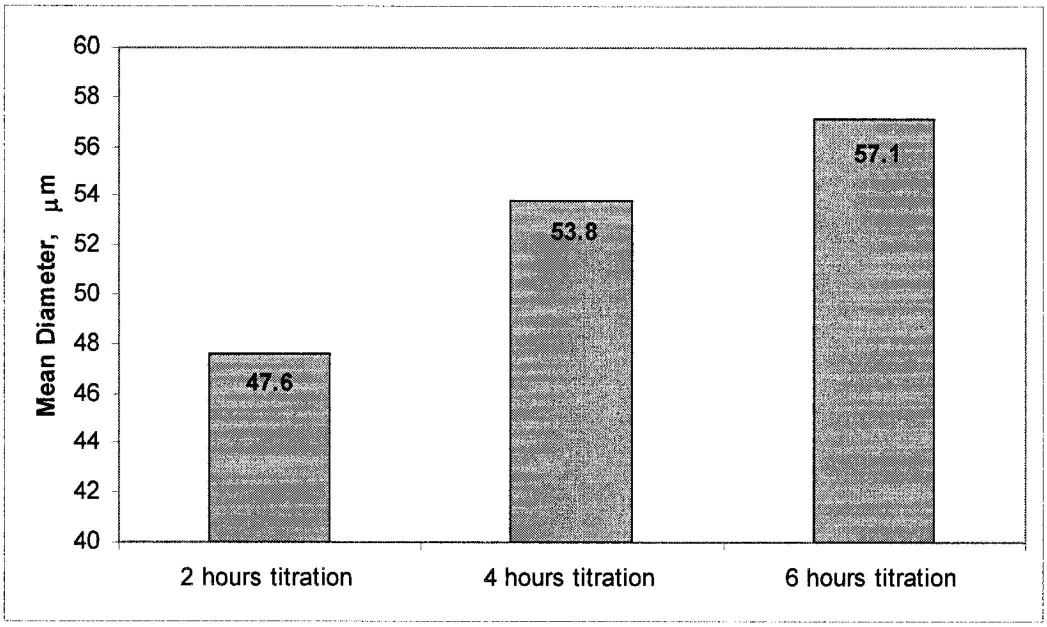

Figure 5.21. Effect of length of titration period on crystal mean diameter (for conditions refer to Table 5.6).

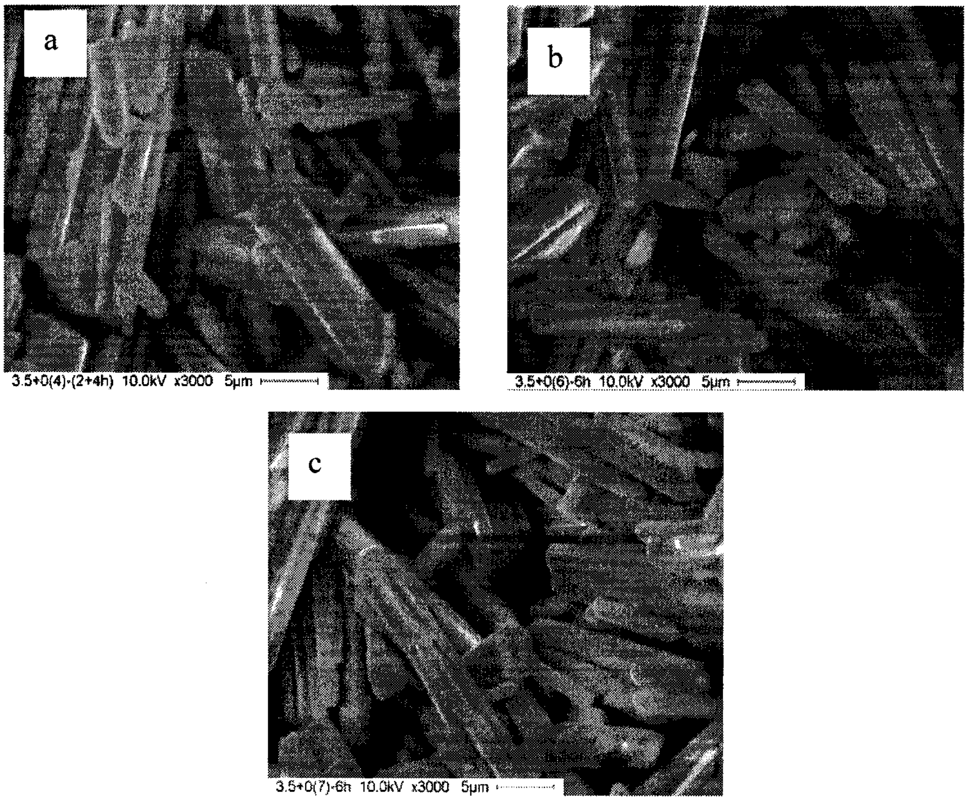

Figure 5.22. Effect of length of titration period on HH crystal morphology a) 2 hours, b) 4 hours, c) 6 hours (for conditions refer to Table 5.6).

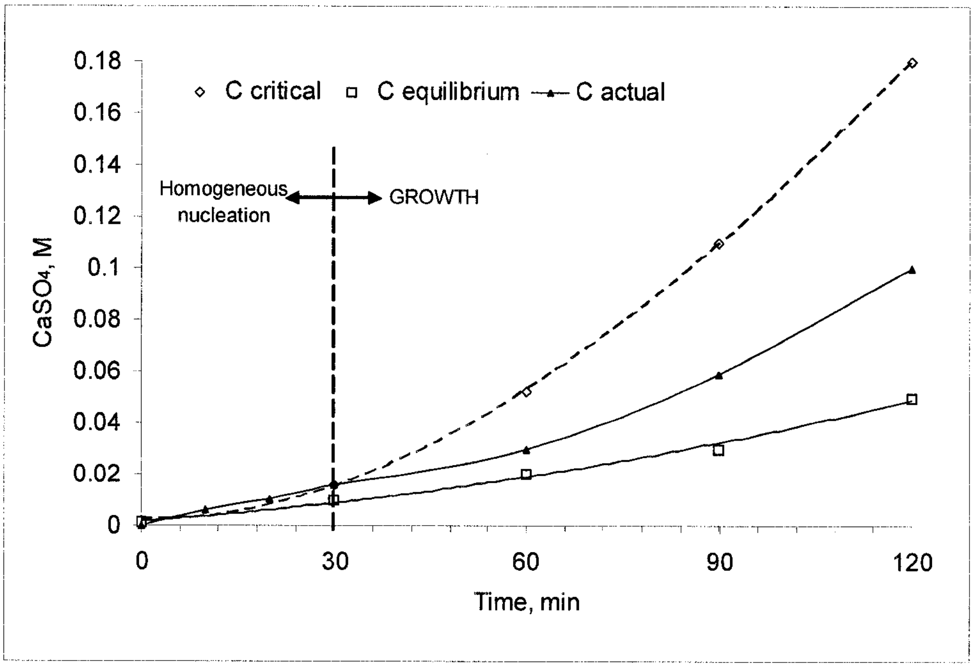

Figure 5.23. Homogeneous nucleation and growth zones in a 2-hour crystallization test (conditions: H_2SO_4 addition rate 78.94mL/h, 3.5M $CaCl_2$, 5.32M H_2SO_4, 80°C).

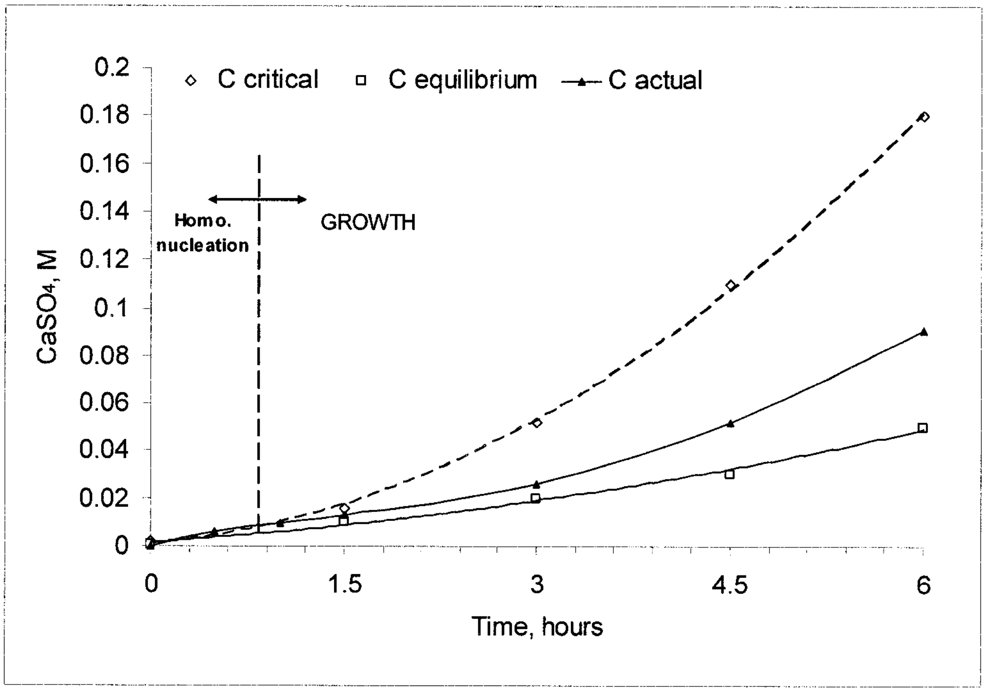

Figures 5.24. Homogeneous nucleation and growth zones in a 6-hour crystallization test (conditions: H_2SO_4 addition rate 26.3mL/h, 3.5M $CaCl_2$, 5.32M H_2SO_4, 80°C).

Since HCl regeneration is one of the objectives of this work, dilute H_2SO_4 solution, although desirable from a supersaturation control point of view, is not practically desirable as it would result in the production of weak strength HCl. Hence the H_2SO_4 concentration was chosen to be for the first tests 2.66M and later increased to 5.32M or higher. The effect of H_2SO_4 concentration on crystal properties and final HCl strength is investigated here. The data are summarized in Table 5.7. Increasing H_2SO_4 strength above 5.32M was found to promote HH decomposition and AH formation after 6 hours combined titration/equilibration time. According to the data of Table 5.7 a 4M HCl solution (containing approximately 0.5M residual $CaCl_2$ to suppress the solute fraction of $CaSO_4$) is easily achieved hence satisfying the HCl regeneration objective.

The initiation of HH crystal transformation to AH fiber-type crystals is evident with the SEM micrographs shown in Figure 5.25. Since the degree of transformation was rather limited no measurable difference in crystal size was evident nor in the filtration rate (Figures 5.26 and 5.27). It is clear, however, that if an elevated H_2SO_4 concentration is to be used shorter retention time would have to be employed ($\leq$ 4 hours) to avoid the decomposition of the HH crystals.

Table 5.7. Effect of H_2SO_4 strength on $CaSO_4$ modification (SO_4/Ca=0.8).

Test no.	Init. Conc. $CaCl_2$+HCl, M	Final Solution (Estimated) $CaCl_2$ + HCl (M)	H_2SO_4, M	Titrant Volume, mL	Titration/Equilibrtion Time, hour	Phase during residence in the reactor (titration+equilibration)		
						2h	4h	6h
24	3.5+0.0	0.46+3.66	5.32	157.9	4/2	HH	HH	HH
26	3.5+0.0	0.49+3.94	6.65	126.3	4/2	HH	HH	HH(AH)
27	3.5+0.0	0.52+4.15	8.00	105.0	4/2	HH	HH	HH(AH)

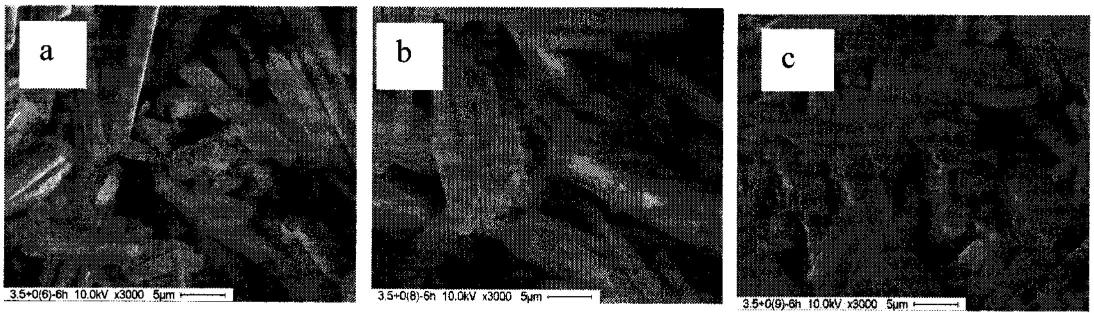

Figure 5.25. Effect of H_2SO_4 strength on HH morphology a) 5.32M, b) 6.65M, c) 8M (4 hours titration + 2 hours equilibration).

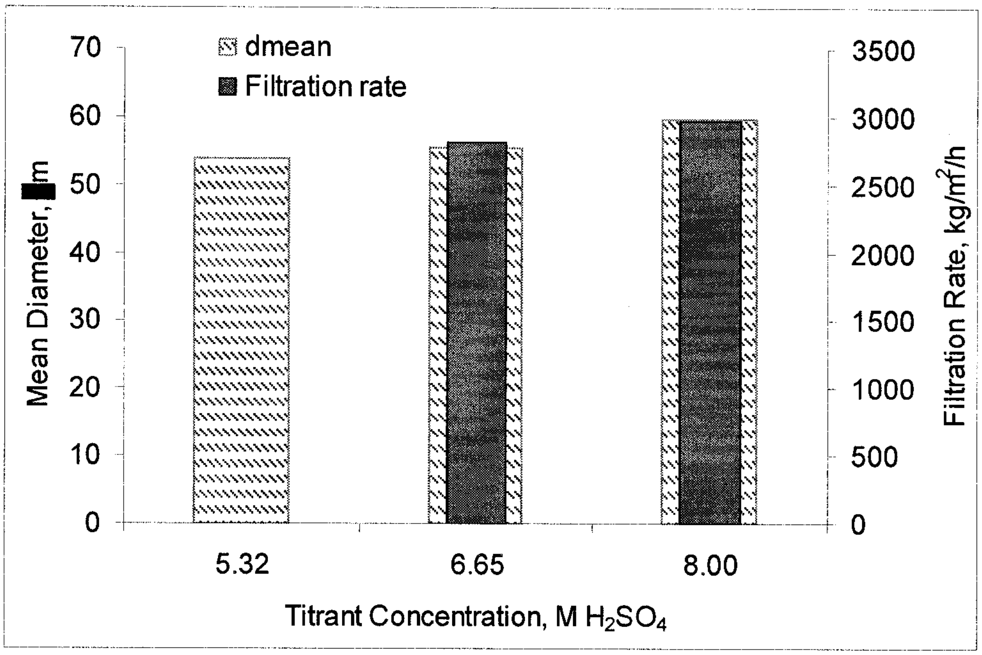

Figure 5.26. Effect of H_2SO_4 strength on the mean diameter and filtration rate of produced crystals (4 hours titration + 2 hours equilibration).

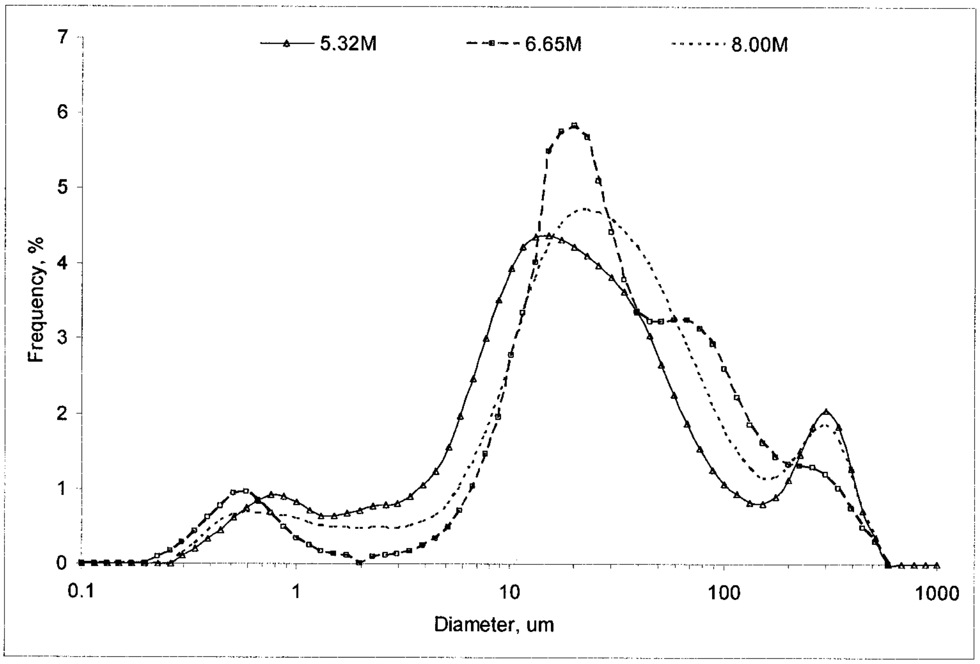

Figure 5.27. Effect of H_2SO_4 strength on the size distribution of produced crystals (4 hours titration + 2 hours equilibration).

5.5.3. Effect of Step-wise H_2SO_4 Addition

Since the titration of $CaCl_2$ solution with H_2SO_4 –as a laboratory procedure- cannot be scaled-up to real large plant operation, there arises the necessity of using a step-wise H_2SO_4 addition procedure. Each acid addition stage in this procedure will correspond to a reactor in a multi-tank precipitation circuit [17]. The step-wise precipitation tests (4 and 8 steps tried) are summarized in Table 5.8. On the same table the results of a titration test are included for comparison. In all these tests an 8M H_2SO_4 was used along a 3.5M initial $CaCl_2$ solution. The total H_2SO_4 addition time was 4 hours while all products were equilibrated for an extra 2 hours. The final SO_4/Ca ratio was 0.8. The products in all cases were found to be HH with minor AH appearing after 6 hours retention (Table 5.8). Particle size analysis however, revealed (data shown in Figure 5.28) that the 8-step procedure better approximated the titration procedure than the 4-step one. The material produced under these conditions (i.e., 8 steps-4 hours reaction + 2 hours equilibration) was subjected to further characterization to clarify the nature of the HH phase. Thermo-gravimetric and differential calorimetric analysis proved the produced material to be hemihydrate of alpha variety with the following stoichiometry: $CaSO_4 \cdot 0.55H_20$ (Figure 5.29).

The step-wise addition concept is illustrated in Figure 5.29. Each step theoretically represents an agitated crystallization reactor of mean residence time equal to 30 minutes.

Table 5.8. Comparison of H_2SO_4 addition procedure in terms of $CaSO_4$ modification (SO_4/Ca = 0.8).

Test No	Init. Conc. $CaCl_2$+HCl, M	Final Solution (Estimated) $CaCl_2$ + HCl, M	8M H_2SO_4 addition procedure	H_2SO_4 Addition + equilibration time, h	Phase after residence in the reactor 2h	4h	6h
27	3.5+0.0	0.52+4.15	Titration	4+2	HH	HH	HH(AH)
28	3.5+0.0	0.52+4.15	8 steps	4+2	HH	HH	HH(AH)
29	3.5+0.0	0.52+4.15	4 steps	4+2	HH	HH	HH(AH)

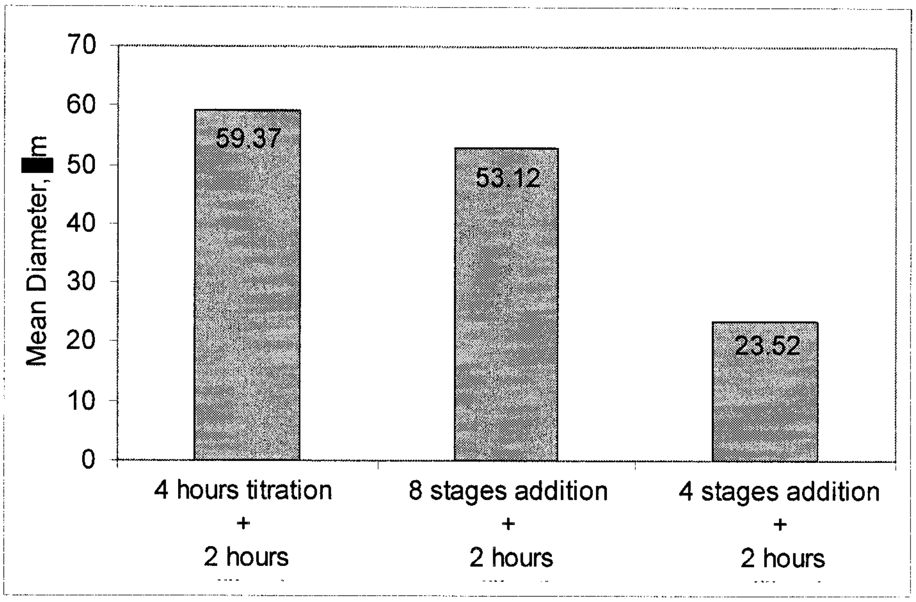

Figure 5.28. Effect of H_2SO_4 addition procedure on the mean diameter of crystals (for conditions refer to Table 5.8).

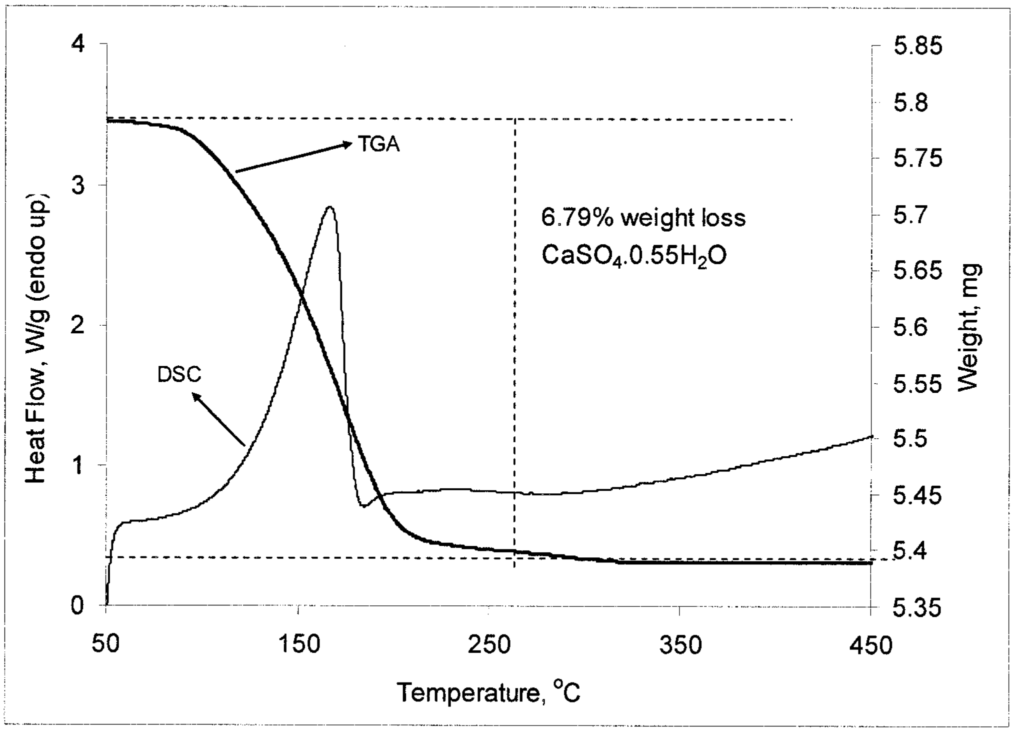

Figure 5.29. Thermal analysis (TGA&DSC) of 8 stage acid addition product (Test no 28-refer to Table 5.8 for full conditions).

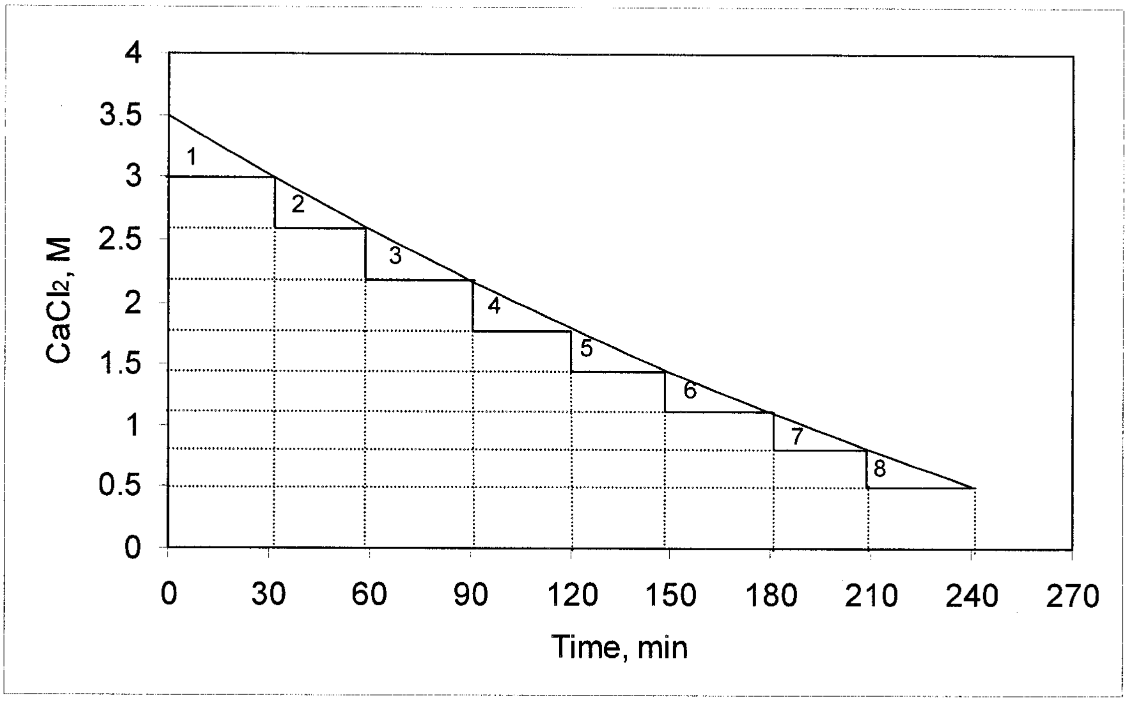

Figure 5.30. Titration vs. stepwise addition of H_2SO_4: $CaCl_2$ concentration profiles (refer to Table 5.8 for conditions).

5.6. Mechanism of HH Crystal Formation

The overall crystal formation and crystal phase transformation process can be described in simplified terms via the schematic sequence shown in Figure 5.31. The reaction of $CaCl_2$ and H_2SO_4 leads to the formation of hydrated $CaSO_4$ ion pairs, which upon supersaturation built-up to form clusters; when the latter exceed a critical size, become dihydrate nuclei and grow. Upon further reaction the DH crystals transform into hemihydrate crystals via water loss and crystal rearrangement. Finally growth of hemihydrate crystals is followed by transformation into very fine fiber-type anhydrite crystals at prolonged equilibration periods. The DH-HH-AH transformation mechanism was discussed in Chapter 4, section 4.6.

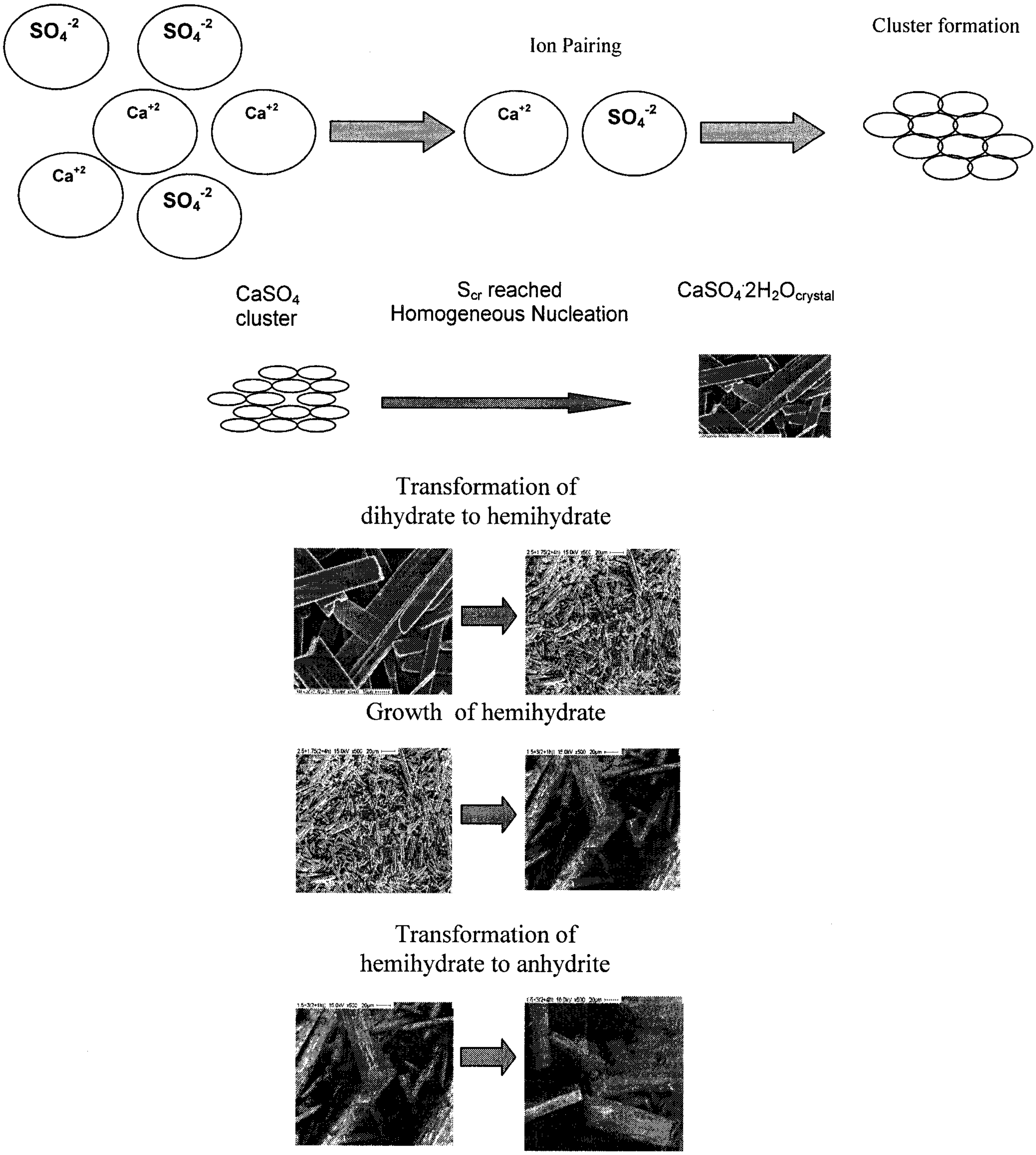

Figure 5.31. Nucleation, growth and transformation sequence of $CaSO_4$ phases.

5.7. Conclusions

1) Atmospheric production (at 80°C) of HH by direct reaction of $CaCl_2$ with H_2SO_4 was successfully demonstrated and an operating diagram for HH production was constructed. Both DH and HH are metastable under the determined HH production conditions hence the process is time sensitive.
2) The final HCl concentration was found to speed up DH to HH and HH to AH conversion. On the other hand, increasing $CaCl_2$ concentration in the final solution was found to improve the metastability of HH by delaying HH to AH conversion. The sequence of phase transformations was found to be in accordance with the Ostwald Rule of Stages.
3) Direct transformation of DH to AH was observed in the absence of $CaCl_2$ in the solution. This was attributed to the very similar solubilities of DH and HH when $CaCl_2$ is absent, a condition that permits the by-pass of HH formation.
4) Supersaturation was found to be decreasing during reaction of $CaCl_2$ with H_2SO_4 in a semi batch reactor, due to increasing $CaSO_4$ solubility. At the initial stage-high supersaturation region-homogeneous nucleation dominates while with progress of reaction, crystallization occurs within the metastable zone that favours growth.
5) Slow rate or multiple stage (at least 8-stage) addition of H_2SO_4 was found to favour crystal growth and filtration rate.
6) Elevation of H_2SO_4 strength up to 8M is possible as long as the total retention time is kept at 4 hours otherwise HH was found to convert partially to AH.
7) The general $CaSO_4$ precipitation mechanism follows the order of: a) nucleation of dihydrate, b) transformation of dihydrate to hemihydrate (nucleation and growth) and c) transformation of hemihydrate to anhydrite.

References

[1] Berrie, J.S., Wooley, G.E., "Manufacture of alpha calcium sulphate hemihydrate", U.S. Patent no. 4,120,737, 1978.

[2] Yasue, T., Kojima, Y., Kishimato, Y., Arai, Y., "Precipitation of alpha gypsum hemihydrate and control of its crystal shape under atmospheric pressure", Gypsum and Lime, No. 239, 1992.

[3] Mersmann, A., "Crystallization Technology Handbook", 2nd Edition, Marcel Dekker Inc., New York, NY, 2001.

[4] Zettlemoyer, A.C., "Nucleation", Marcel Dekker Inc, New York, NY, 1969.

[5] Z. Li, "Measurement and chemical modelling of $CaSO_4$ solubilities in concentrated chloride media", Ph.D. Thesis, McGill University, Montreal, QC, 2006.

[6] Li, Z., and Demopoulos, G.P., "Model-based construction of calcium sulphate phase transition diagrams in the $HCl-CaCl_2-H_2O$ system between 0-100°C", Industrial and Engineering Chemistry Research, 45, 2006, 4517-4524.

[7] Li, Z., Demopoulos, G.P., "$CaSO_4$ solubilities in concentrated aqueous chloride solutions", in Chloride Metallurgy 2002, Eds. E Peek, G. Van Weert, CIM, Montreal, QC, 2002, 561-574.

[8] Martynowicz, E.T.M.J., Witkamp, G., Rosmalen, G.M., "The effect of aluminum fluoride on the formation of calcium sulphate hydrates", Hydrometallurgy, 41, 1996, 171-186.

[9] Ling, Y. and Demopoulos, G.P., "Preparation of alpha-calcium sulphate hemihydrate by reaction of sulphuric acid with lime", Industrial Engineering and Chemistry Research, 44, 2005, 715-724.

[10] Langmuir, D., and Melchior, D., "The geochemistry of calcium, strontium, barium and radium sulphates in some deep brines from the Palo Duro Basin, Texas", Geochimica et Cosmochimica Acta, 49 (11), 1985, 2423-2432.

[11] Innorta, G., Rabbi, E., Tomadin, L., "The gypsum-anhydrite equilibrium by solubility measurements", Geochimica et Cosmochimica Acta, 44 (12), 1980, 1931-1936.

[12] Ling, Y., Demopoulos, G.P., Giove, A., Filippou, D., "Technical evaluation and characterization of alpha calcium sulphate materials", in Gypsum and Fly Ash 2002, 7th International Science and Technology Conference, Toronto, ON, 2002, 6-1 to 6.14

[13] http://www.olisystems.com

[14] Li, Z., Demopoulos, G.P., "Development of an improved chemical model for the estimation of CaSO4 solubilities in the HCl-$CaCl_2$-H_2O system up to 100°C", Industrial Engineering and Chemistry Research, 45, 2006, 2914-2922.

[15] Nývlt, J., "The Ostwald rule of stages", Crystal Research Technology, 30, 1995, 443-449.

[16] Sohnel, O., and Garside, J., "Precipitation, basic principals and applications", Butterworth-Heinemann Ltd, Oxford, UK, 1992.

[17] Demopoulos G.P. "Aqueous precipitation for the production of particulate materials with desired properties", Hydrometallurgy, (in Press).

APPENDIX 5.1. Determination of Critical Supersaturation (S_{cr} or C_{cr})

The critical concentration (C_{cr}) or in other words the critical supersaturation (S_{cr}) required for the onset of homogeneous nucleation (refer to Figure 5.17) was determined by a series of tests which involved the precise control of $CaCl_2$ and H_2SO_4 reaction.

100mL solution with variable composition from 3M $CaCl_2$ to 0.32M $CaCl_2$+ 4M HCl to simulate different extents of the reaction was titrated with 8M H_2SO_4 at 80°C. The H_2SO_4 solution was added in very small doses (0.02mL) via a micropipette to determine accurately the precipitation onset point. After each addition, 5-10 minutes was allowed to test the stability of the produced (if any) nuclei. If the produced nuclei dissolved back, a new dose of H_2SO_4 was added and so on. The addition sequence lasted until a stable cloud of nucei was observed to form and the cumulative amount of added H_2SO_4 to this point was recorded. The amount of sulphate added was used to estimate the "critical concentration" of $CaSO_4$. It should also be noted that the dilution of initial solution by H_2SO_4 addition was ignored due to very small amount of H_2SO_4 addition in each case (max 1-1.5mL $\approx$ 1% dilution overall).

CHAPTER 6

Seeded Crystallization

6.1. Introduction

As mentioned in Chapter 2, controlled crystal growth can be achieved with the use of seed under a low supersaturation environment. Undesired homogeneous nucleation, which produces fine and poorly crystalline solids, is avoided by seeded crystallization within the metastable zone [1, 2]. In this study supersaturation is kept low by adopting the staged acid addition method as described in the previous chapter.

Once the appropriate conditions are determined for seeded crystallization, recycling of the product under the same conditions in a continuous system should promote further crystal growth. There is limited number of studies in the area of seeded crystallization of $CaSO_4$ hydrates (α-$CaSO_4$ hemihydrate in particular). Seeding and recycling of gypsum was reported recently to improve the product handling properties (i.e. filtration and settling rate) in the $CaCl_2$-H_2SO_4 reaction system at low temperatures (<60°C) [3] or when alcohols were used as desolvating agent in the same system [4]. Ling [5] appears to be the only author who has described the effect of seeding on the crystallization of α-$CaSO_4$ hemihydrate. This was done for the system involving the reaction of H_2SO_4 with CaO at 100°C. A rather modest effect on crystal growth was noticed. Moreover, interestingly enough, Ling observed the morphology of α-HH (seed crystals originally in the form of pellets) to convert to fibre-type even in $CaSO_4$ saturated solutions. No other study mentioning the growth of α-HH crystals in the presence of seed was found in literature.

The findings of Chapter 5 (Section 5.5) provided evidence that after a certain stage of $CaCl_2$-H_2SO_4 reaction, the initially homogeneously nucleated crystals act as seed for the subsequent stages of reaction. Hence, it was decided in this part of the work to investigate further the effect of seeding on the final product quality by employing a semi-batch precipitation procedure. First tests with variable amount of seed were run followed by a series of recycling tests where the growth of α-HH was investigated.

Another objective of the work presented in this chapter was to evaluate the role of foreign metal ions on HH crystal growth and purity. Hydrometallurgical chloride solutions may contain a variety of metal chlorides in addition to $CaCl_2$. Impurities even in small doses are known to interfere with crystal growth via adsorption [6, 7]. In other instances, impurities may interfere by changing the solute's equilibrium concentration and hence the supersaturation. This in turn affects both nucleation and growth rate as well as the crystal habit. Such an effect was observed in the case of dihydrate formation instead of hemihydrate due to the shifting of the solubility line in the presence of aluminum fluoride [8]. It is commonly accepted that impurity uptake is higher at high supersaturation levels associated with homogeneous nucleation. However for systems under supersaturation-controlled crystal growth, it has been observed that the retarding effect of an impurity weakens at high supersaturation due to the shifting of the rate-limiting step of growth from surface reaction to diffusion control [9].

Impurity uptake in the case of $CaSO_4$ hemihydrate has been attributed to the incorporation of foreign cations within the long channels (around 3Å in diameter) developing parallel to z-axis [10, 11] hexagonal structure of hemihydrate.

The second part of this chapter covers the effect of foreign metal ions on hemihydrate crystal growth and purity during seeded crystallization. In particular the chloride salts of Fe^{3+}, Fe^{2+}, Ni^{2+}, Mg^{2+}, Al^{3+}, Na^{+} are investigated while both laboratory-made and commercial Omega HH crystals are used as seed materials.

6.2. Experimental Procedure

All experiments reported in this chapter were carried out at 80°C. Two types of α-$CaSO_4$ hemihydrate seed material used were; the first one was laboratory-made seed produced by the reaction of 3.5M $CaCl_2$ and 8M H_2SO_4 at 80°C after 4 hours (8 stages of acid addition-see Chapter 5, Table 5.8, Test No 28 [4 hours product]) and the other one was commercial HH material produced by the Omega Process [12].

The effect of seed concentration was examined by performing reactive crystallization tests involving the addition (in 8 stages) of 5.32M H_2SO_4 over a period of 4 hours to 300 mL of 3M $CaCl_2$ solution. Lab-made seed was added prior to acid addition at 25, 50 and 100g/L loadings.

For the recycling tests 300mL of 3M $CaCl_2$ or 1.5M $CaCl_2$ + 3M HCl starting solutions were reacted with 5.32M H_2SO_4 in 8 stages (30 minutes each) and 4 stages (60 minutes each), respectively. Fresh seed (100 g/L) was added at the beginning of each series of tests with subsequent tests involving recycling part (100 g/L for 3M $CaCl_2$, 50g/L for 1.5M $CaCl_2$ + 3M HCl) of the product. Lab-made alpha-HH and Omega alpha-HH were used as seed material. The same procedure was followed for this series of tests involving the investigation of the effect of foreign metal chlorides but in this case the solids (100g/L) were recycled only once.

In the context of this chapter, the Lab-made alpha-HH seed crystals produced by homogeneous crystallization are sometimes referred to as "0 – zero-recycle product". This is done in order to compare that product to recycling products. The material produced after the 1st recycling of seed crystals (0 – zero- recycle product) is called "1st recycle". In the same manner the commercial Omega seed is again referred to as "0 – zero- recycle product" and subsequent recycling of this seed produced the "1st recycling product".

At the end of each cycle, the slurry was divided into two parts. One part was filtered hot, washed with boiling water and acetone, and dried. A small sample from the dried product was subjected to solid analysis (i.e. SEM, XRD, PSA), while the appropriate amount of the rest was used as seed material for the next cycle. For each cycle, fresh electrolyte solution was used. In the case of the tests with metal chlorides the solids were examined with the aid of EDS to identify which of the cations were incorporated into the crystals.

The other part was used for filtration rate determination. The filtration rate was measured in a pressure filter (as described in Chapter 3) under 20-psi pressure. The volume of the solution and the mass of the cake were recorded for the filtration rate calculations, which also considered the diameter of the filter.

Solution samples were analysed following the dilution (1 mL filtrate in 100mL total volume with distilled water) by ICP-AES, Atomic Absorption or Ion.Chromatography. The impurity uptake of the produced crystals was determined after dissolving 2 g of them in 100 mL of 10% (v/v) HNO_3 solution. All the equipment (syringe, syringe filters, pipette tips, sampling hoses, glass veils etc.) used during solution sampling operation were preheated to 80°C to avoid any undesired $CaSO_4$ crystallization due to cooling.

6.3. Effect of Seed Loading

Seeding is practiced primarily for crystal growth. The amount of seed used is reported more specifically to have 2 important effects in precipitation systems: 1) variations in seed concentration (i.e. solid/liquid ratio) could influence the phase transformation kinetics; and 2) changing the seed concentration could affect the specific surface area, therefore, the number of secondary (surface) nucleation sites and the growth rate [7].

In this series of tests three seed loadings namely, 25g/L, 50g/L and 100g/L were examined using the semi-batch crystallization procedure described in section 6.2. SEM images presented in Figure 6.1 demonstrate the evolution of the seed crystal after 30 minutes and 4 hours of crystallization respectively for each of the three loadings tested. No hemihydrate-anhydrite transformation was observed. The presence of fine needles of HH was evident in the early stages of the reaction when 25g/L seed was used (Figure 6.1b). This was rather unexpected, as fragmentation (if it is assumed this to be the reason for the appearance of the fines) would have been expected to occur with the higher rather than the lower seed loading. No explanation for this behaviour can be offered. Interestingly enough the fine needles were not present in the final (4 hours) product apparently were incorporated in the larger crystals via ripening.

A quantitative appreciation of the effect of seed loading on crystal size and handling properties is possible by examining the mean crystal diameter and filtration rate data given in Figure 6.2. According to these data seeding had a profound effect on crystal growth (the volume-based diameter of the crystals increased from around 20 μm to 58-60μm) and a modest negative effect on filtration rate. For all practical purposes there was no significant difference in terms of mean crystal diameter among the three seed loadings. In terms of filtration rate the slight decrease of rate with increasing seed loading may reflect the extra resistance imposed by the larger mass of cake.

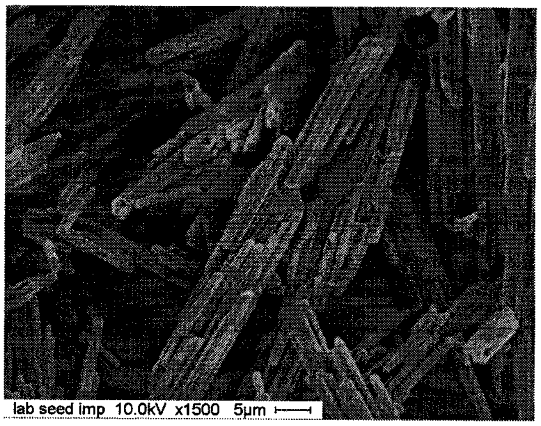

(a) Original Lab-made seed

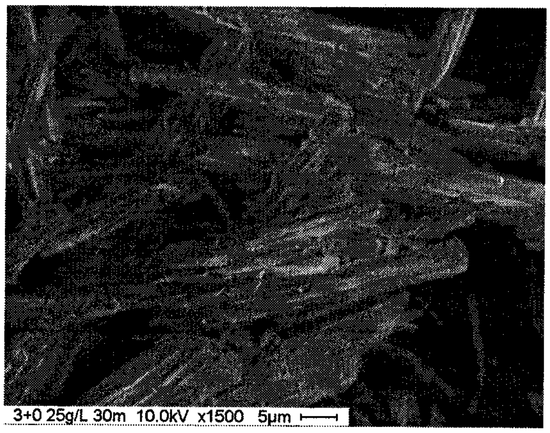

(b) 25 g/L (30 minutes)

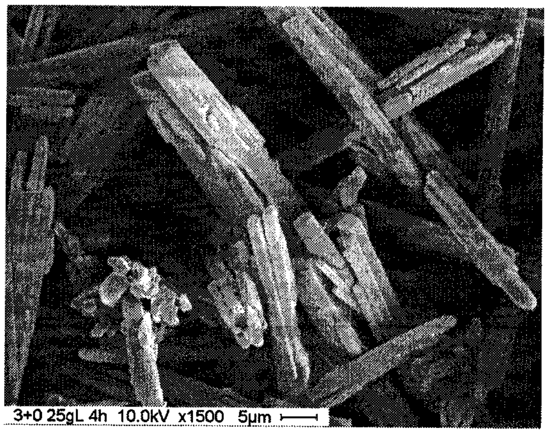

(c) 25 g/L (4 hours)

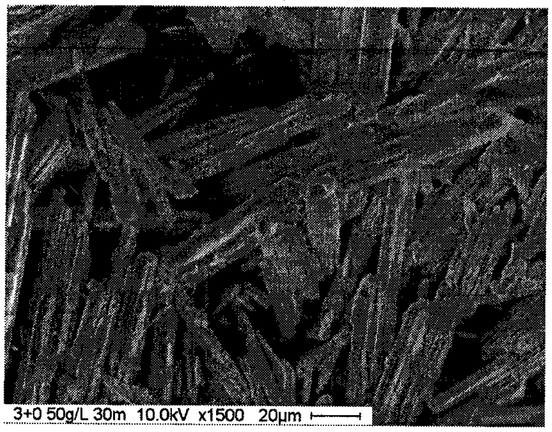

(d) 50 g/L (30 minutes)

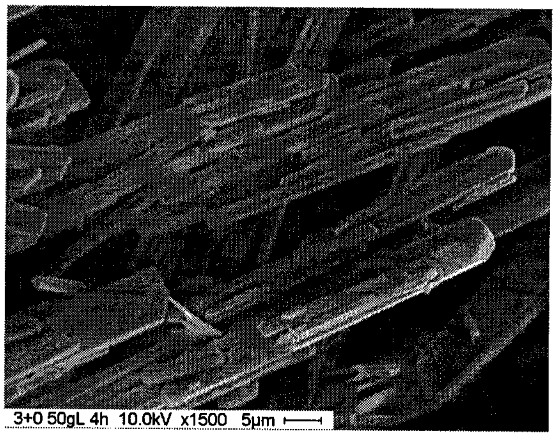

(e) 50 g/L (4 hours)

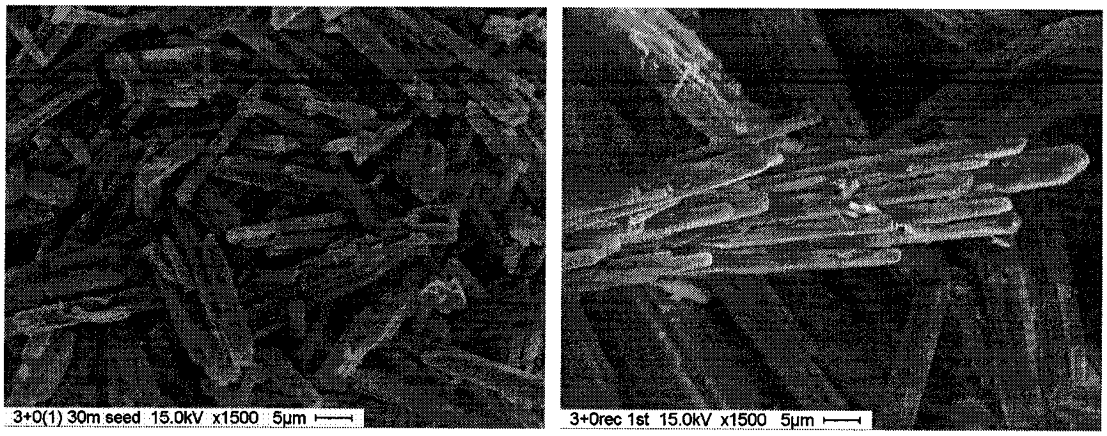

(f) 100 g/L (30 minutes) (g) 100 g/L (4 hours)

Figure 6.1. Effect of seed loading and crystallization time on crystal morphology (3M $CaCl_2$ starting solution).

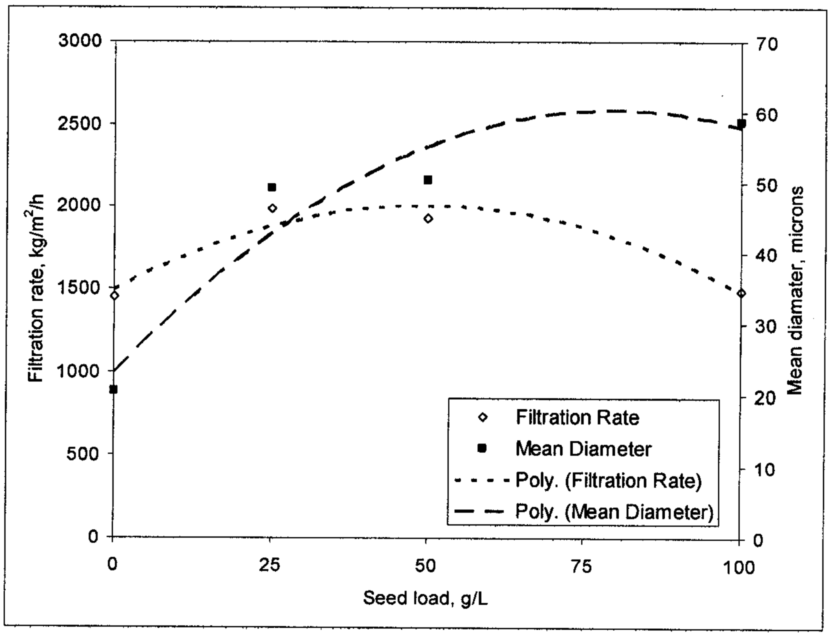

Figure 6.2. Effect of seed concentration on mean diameter and filtration rate (3M $CaCl_2$ starting solution).

6.4. Effect of Recycling

Having determined that seeding results in crystal growth, it was decided to proceed with recycling tests in order to determine the upper limit of growth that can be obtained. Recycling was investigated by using either 3M $CaCl_2$ or 1.5M $CaCl_2$+3M HCl initial solution concentrations. These solutions were reacted with 5.32M H_2SO_4 in 8 and 4 stages, respectively. The respective initial seed and recycled product loadings for 3M $CaCl_2$ and 1.5M $CaCl_2$+3M HCl were 100g/L and 50g/L (equivalent approximately to the mass of fresh crystal product per run). The semi batch crystallization procedure described in section 6.2 was followed.

Table 6.1 summarizes the conditions of the tests and $CaSO_4$ phases produced (determined by XRD) at the end of each recycle. It can be immediately seen that, both types of hemihydrate seed underwent no phase change (i.e. conversion to anhydrite) over the 5 recycles with 3M $CaCl_2$ solution, while HH-AH transformation was observed after the 2nd recycle when the mixed $CaCl_2$ (1.5M) – HCl (3M) solution was used. The difference is attributed to the increased HCl concentration, as discussed in Chapters 4 and 5, which causes HH to exhibit reduced metastability. Given the instability of alpha-HH in the 1.5M $CaCl_2$ - 3M HCl solution, it was decided not to pursue further the study of seeding/recycling in this system.

Table 6.1. Summary of conditions and $CaSO_4$ phases produced in recycling tests.

Initial Solution $CaCl_2$ + HCl, M	Original seed type	Recycled seed conc., g/L	1st recycle	2nd recycle	3rd recycle	4th recycle	5th recycle
3.0 + 0	Lab made HH	100	H	H	H	H	H
3.0 + 0	Omega HH	100	H	H	H	H	H
1.5 + 3	Lab made HH	50	H	H(A)	H/A	A(H)	A(H)

Crystal morphology-Use of needle-shaped (lab-made) seed: Alpha-hemihydrate crystallizes mainly [13, 10] in the hexagonal system (Figure 6.3). Crystals in this system mainly exhibit three different habits, namely tabular (plate-like), prismatic (thick columns) and acicular (needle-like) [2]. The homogeneously produced alpha-HH in this work was determined to be of acicular habit (refer to Chapter 5). There exists, however in the market, another form of alpha-HH (product of the Omega Process [12]) that is predominantly of the prismatic habit. Here it was decided both materials to be used as seed in order to evaluate their influence on crystal morphology and growth during recycling.

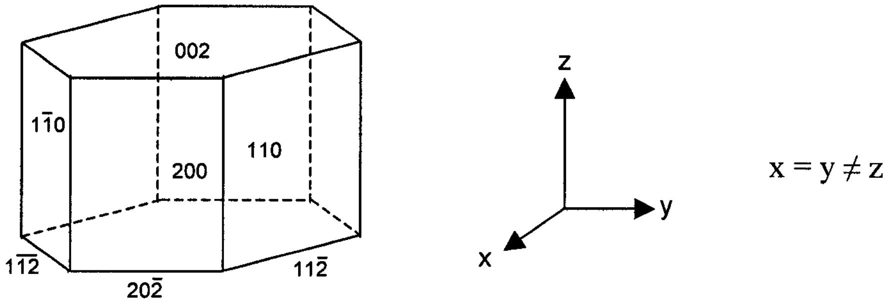

Figure 6.3. Hexagonal Crystal structure of $CaSO_4$ Hemihydrate.

SEM imaging was the primary tool used for the determination of the crystal morphology evolution as well as the visual detection of phase transformations during recycling. Figure 6.4 displays SEM images of the crystals sampled during the 1st recycle and at the end of 1st, 2nd and 4th recycle when 100g/L lab-made seed was used during crystallization of alpha-HH from a 3M $CaCl_2$ solution. It is observed from the Figure that, the initial long needle-shaped HH seed crystals have grown longer in z-direction during the 1st seeded run (1st recycle). However, with further recycling growth in all three dimensions was observed resulting in thick elongated crystals with aspect ratio of ~10/1 (refer to Figure 6.3) after 4 recycles. Growth appears to proceed initially via an agglomeration mechanism involving parallel orientation and clustering of the needle crystals (see for example the crystals of the 1st recycle-Figure 6.4a-e) followed by cementing ("fusion") and outgrowth of these agglomerates upon further recycling (see 2nd and 4th recycle crystals-Figures 6.4f, 6.4g). The occurrence of agglomeration during crystallization of calcium sulphate hemihydrate has also been described for the case of phosphoric acid solutions at 90°C [14, 15]. The fine needle-shaped crystals that are in the homogeneously nucleated (and partially aggregated) seed material may be preserved to some extent during recycling either via secondary (fragmentation) or primary (homogeneous) nucleation mechanisms. For the latter to occur, supersaturation should exceed $S_{cr,\ homo}$ or, equivalently, $CaSO_4$ concentration should exceed the critical concentration signifying the onset of homogeneous nucleation. Analysis of the solution during the first stage of the reaction did indeed reveal for the first 30 minutes $CaSO_4$ concentration to exceed C_{cr} (Figure 6.5.) The subsequent reduction of supersaturation within the metastable zone during the rest of the reaction cycle (30 min-4 hours) (see later Figure 6.9) gives apparently rise to surface nucleation and growth in all three directions (Figures 6.3 and 6.4e).

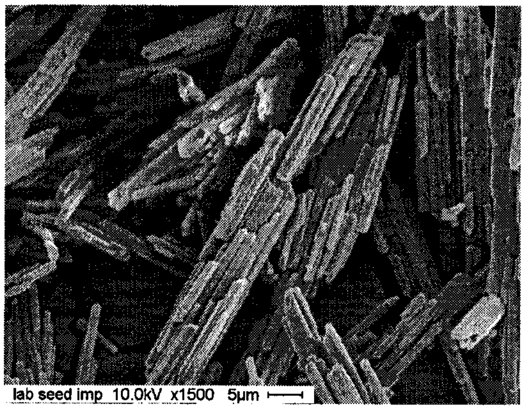

(a) Lab made seed

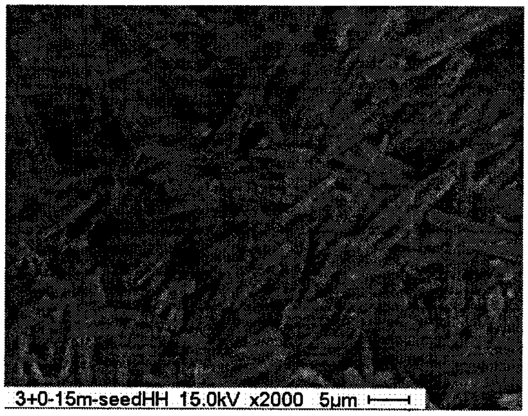

(b) 1st recycle (15 min)

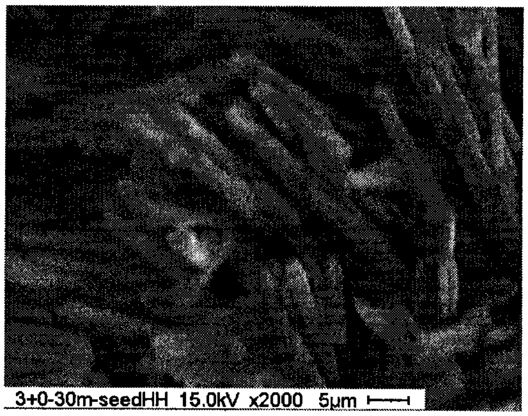

(c) 1st recycle (30 min)

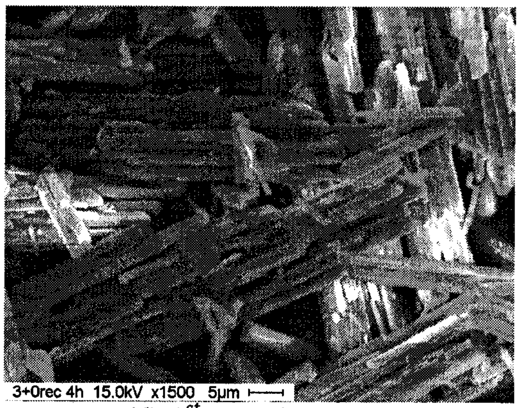

(d) 1st recycle (2 hours)

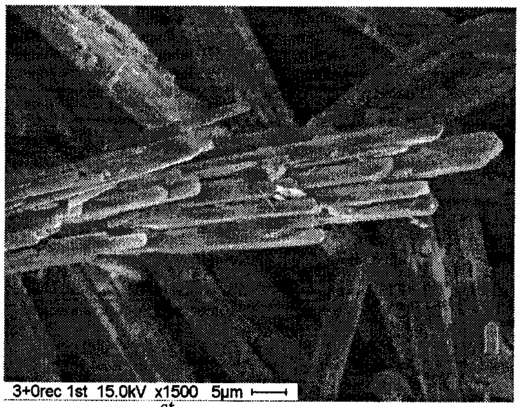

(e) 1st recycle (4 hours)

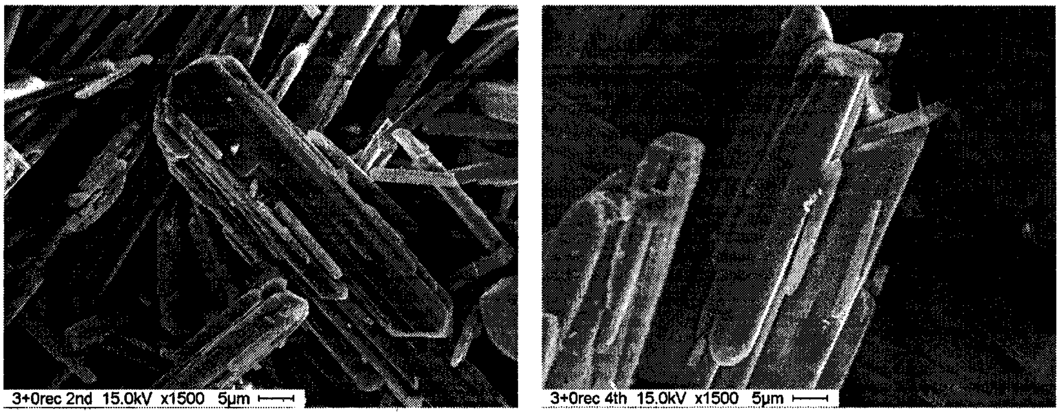

(f) 2nd recycle (4 hours) (g) 4th recycle (4 hours)

Figure 6.4. The growth of lab-made seed at different stages of recycling (3M $CaCl_2$).

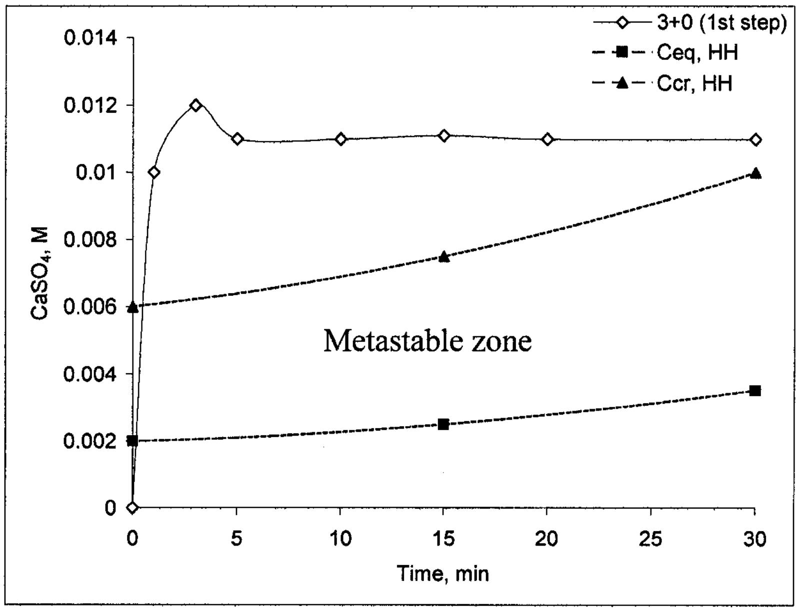

Figure 6.5. $CaSO_4$ concentration variation with reference to metastable zone of hemihydrate crystallization (3M $CaCl_2$, 1st acid addition stage of reaction)

Crystal morphology-Use of prismatic (Omega material) crystal variety as seed: Commercial alpha-HH (Omega seed) of prismatic habit (Figure 6.6a-b) was also used as seed material. SEM images of the crystals obtained from this set of recycling tests are presented in Figure 6.6. Some very dramatic changes are seen to take place with the use of Omega seed. Thus, at the initial stages of 1st recycle, there is evidence of growth of the initial prismatic crystals while at the same time very fine needle-shaped HH crystals are generated (Figures 6.6c, d and d). It looks as if the fine needles have detached from the larger prismatic crystals. One possibility for this appereance may be that once more the needle-shaped crystals were generated via homogeneous nucleation (during the first stage of the reaction, refer to Figure 6.5.) and then via agglomeration were attached to the starting seed crystals. At the end of the 1st recycle, the fine needles of HH are observed to have dissapeared (possibly due to agglomeration as discussed above and/or ripening) and large columnar-shaped crystals to have grown along the z-axis of the hexagonal system (Figures 6.3 and 6.6f). After certain growth of the columnar-shaped HH (3rd recycle-Figure 6.6g) the crystals appear to start disintegrating generating a large population of acicular HH (needle-shaped) crystals (Figures 6.6h and 6.6i). In orther words, the original prismatic morphology of Omega seed material (thick and short columns) evolved under the applied conditions (i.e., 100g/L original and recycled seed concentration, 3M $CaCl_2$ initial and 0.32M $CaCl_2$ + 3.4M HCl final electrolyte concentration, 4 hours reaction with 5.32M H_2SO_4 at 80°C) to needle-shaped crystals during the progress of recycling. This finding is in agreement with the findings of Ling [5], who studied the production of alpha-HH in concentrated H_2SO_4 solutions. This implies that in acidic environments (HCl (as in this work) or H_2SO_4 (as in Ling's work [5])) the favoured crystal morphology is that of acicular habit.

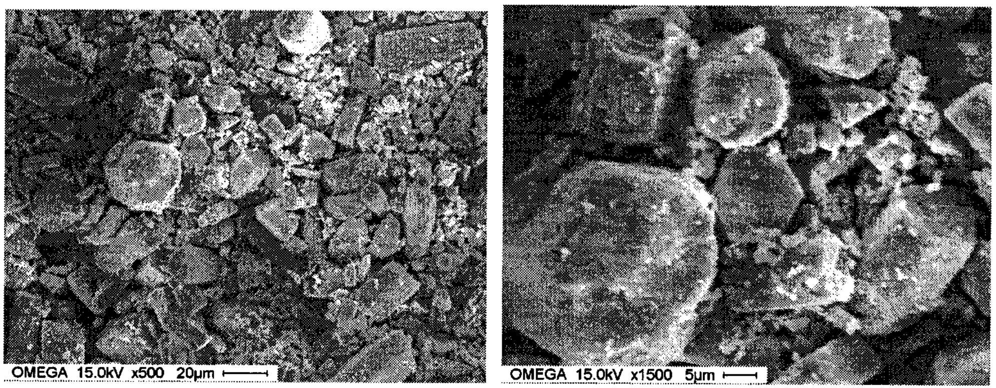

(a) Omega seed (b) Omega seed (Magnified)

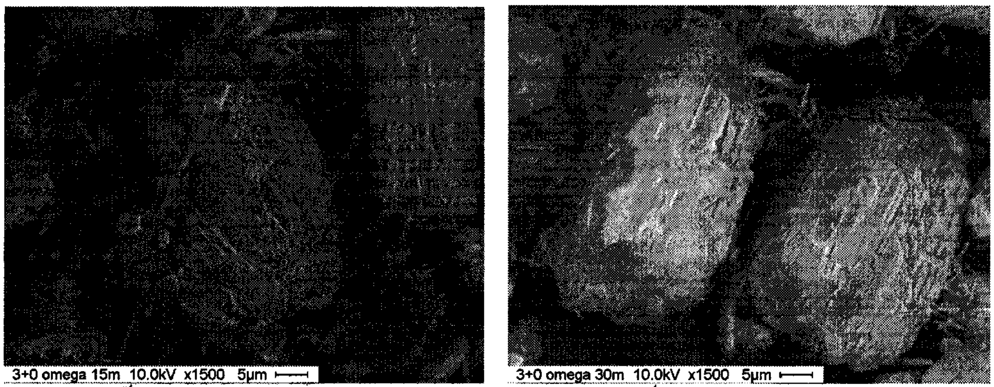

(c) 1st recycle (15 minutes) (d) 1st recycle (30 minutes)

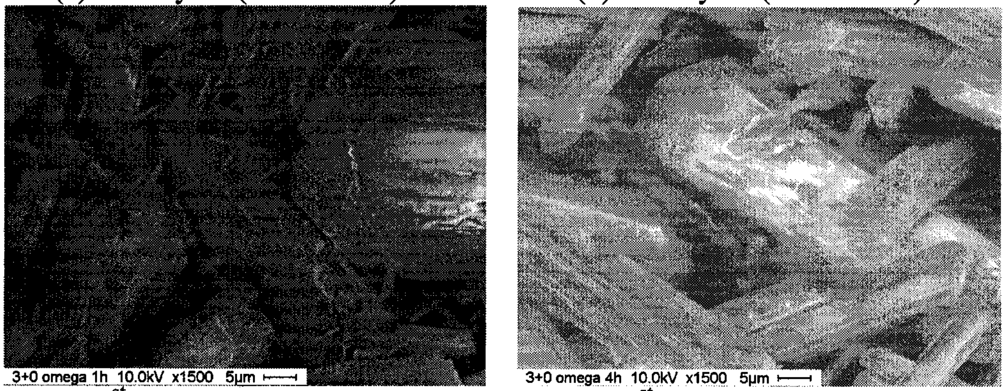

(e) 1st recycle (60 minutes) (f) 1st recycle (4 hours)

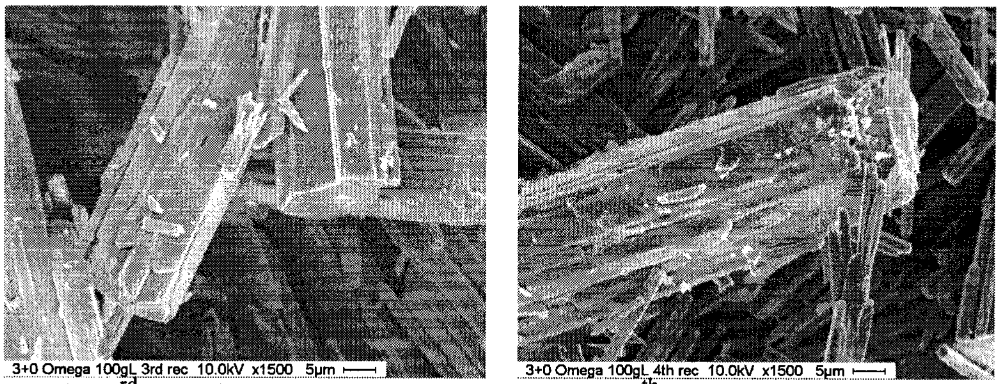

(g) 3rd recycle (4 hours) (h) 4th recycle (4 hours)

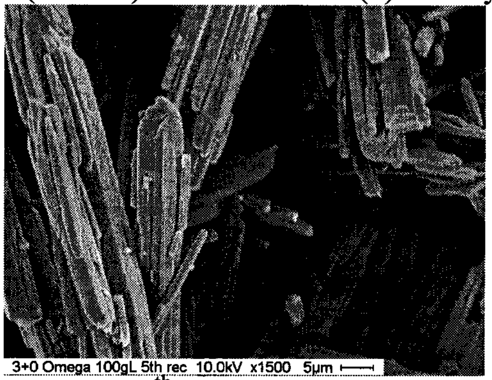

(i) 5th recycle (4 hours)

Figure 6.6. Crystal habit changes of Omega seed upon repeated recycling (3M CaCl$_2$).

Crystal size and filtration rate: The SEM images revealed not only changes with the crystal morphology but also enlargement in terms of crystal size. The latter was confirmed by particle size analysis presented in Figure 6.7. Most of the growth of the lab-made seed crystals appears to have happened during the first recycle (an increase from 20 to 60μm). Further recycling led to the mean crystal length (volume-based) to increase to 80μm after 5 recycles. In contrast, the mean crystals size of the Omega seed material increased gradually from 20 to 70μm (end of 1st recycle) and to 72μm (3rd recycle) before it started decreasing thereafter. This crystal size variation for the Omega seed material seems to correspond to the observed crystal morphology changes (Figure 6.6). Clearly the laboratory made material is a better seed in the context of the present work from a crystal growth (and morphology) point of view with optimum results (morphology and size) obtained after 3 recycles (refer to Figures 6.6g and 6.7).

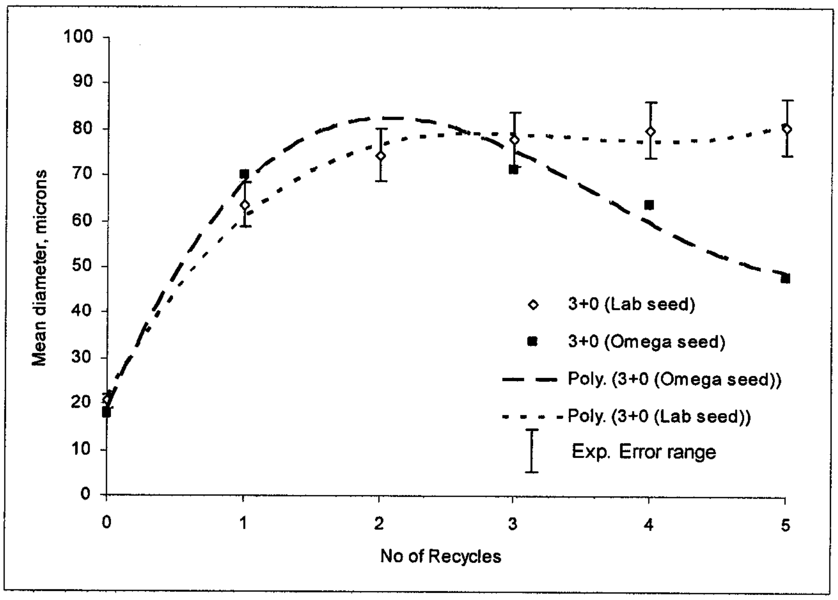

Figure 6.7. Crystal mean diameter change upon repeated recycling of Lab-made and Omega seed materials (3M $CaCl_2$, 100g/L seed).

The effect of seed recycling on the filterability of recycled products was also analysed and the data are presented in Figure 6.8. Recycling of the lab-made seed led to an increase in filtration rate (from an initial 1500 to 2200 kg/m^2/h) in concordance with the increasing mean crystal size reported in Figure 6.7. A similar trend was observed for the

Omega seed material. The erratic variation of filtration rate in the latter case most probably reflects the drastic morphological changes occurring during recycling (refer to Figure 6.6).

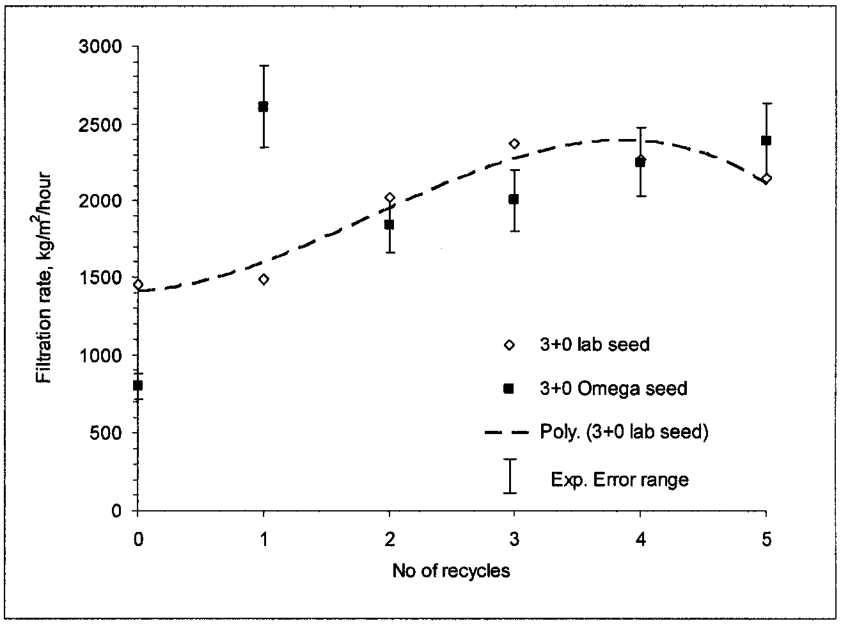

Figure 6.8. Filtration rate as a function of recycling for different seed materials (3M $CaCl_2$, 100g/L seed).

Solution Composition: It was already mentioned that monitoring the solution composition can help to separate homogeneous nucleation and growth stages (refer to Figure 6.5). In this section solution composition profile is monitored throughout the whole semi-batch crystallization run in order to obtain a better understanding of the system. Via regular sampling from the 1st recycle tests with laboratory-made and Omega seed materials the solution profiles reported in Figure 6.9 were determined. On the same figure the equilibrium and critical concentration curves (corresponding to hemihydrate), which were determined respectively by using a new OLI-based model [16] and experimentally (refer to Chapter 5), are plotted. The area between the two curves defines the metastable zone (refer to Chapter 2).

It can be seen from the plot that the $CaSO_4$ concentration stays within the metastable zone throughout the whole crystallization test with the exception of the first 30 minutes as the detailed data (magnified scale) of Figure 6.5 revealed. There seems the $CaSO_4$ concentration for the test run with lab-made seed to be higher than the respective one for the test with the Omega seed. This may relate to faster precipitation kinetics in the case of the latter due to larger surface area produced by the finer crystals of this crystallization system (refer to Figure 6.7). Finally examination of the solution composition at the end of each recycle revealed that the residual $CaSO_4$ concentration was stabilized after the 3rd recycle at about 0.15M slightly higher than the corresponding equilibrium value of 0.12M.

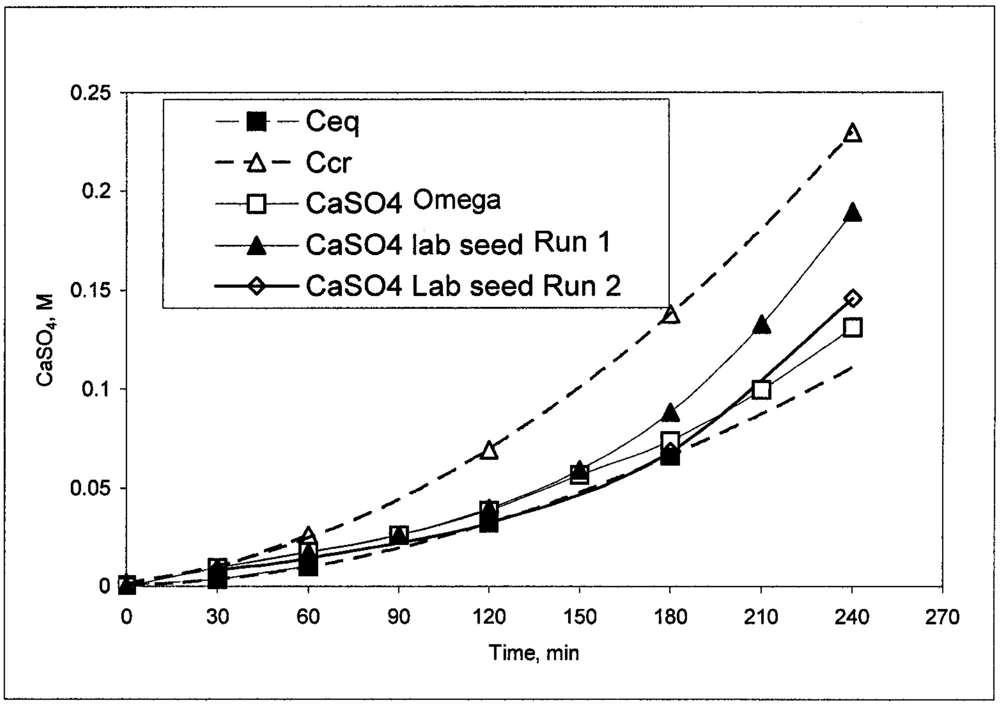

Figure 6.9. $CaSO_4$ concentration variation with reference to the metastable zone of hemihydrate crystallization (3M $CaCl_2$, 100g/L seed).

6.5. Effect of Foreign Cations

The presence of foreign cations in the form of metal chloride salts may have two effects: interference with the crystal growth process and alteration of phase or purity due to ion exchange-incorporation. These two effects are considered in this part of the work.

Crystal growth: Table 6.2 summarizes the test conditions and XRD analysis of the produced crystals after 4 hours of $CaCl_2$-H_2SO_4 reaction. XRD analysis based on the comparison of the height of the characteristic HH ($2\theta \approx 14.8$Å) and AH ($2\theta \approx 25.5$ Å) peaks revealed that the Omega seed in the presence of 1M Fe^{3+} ions underwent the most significant HH to AH transformation. Presence of Ni^{2+} ions also caused small but detectible amount of transformation. Apart from that no other sulphate phase including the sulphate salts of impurity ions was detected by XRD analysis.

Table 6.2. Summary of conditions and XRD analysis of metal chloride salt tests (80°C, 8-stage acid addition).

Initial $CaCl_2$ Conc, M	H_2SO_4 Conc, M	Impurity (1M)	Seed type	Seed Conc., g/L	Crystal phase after 4h reaction
3	5.32	None	Lab made HH	100	HH
3	5.32	None	Omega HH	100	HH
3	5.32	$FeCl_3$	Lab made HH	100	HH
3	5.32	$FeCl_3$	Omega HH	100	HH(AH)
3	5.32	$MgCl_2$	Lab made HH	100	HH
3	5.32	$MgCl_2$	Omega HH	100	HH
3	5.32	$FeCl_2$	Lab made HH	100	HH
3	5.32	$NiCl_2$	Lab made HH	100	HH(AH)

SEM images presented in Figure 6.10 show the evolution of crystal morphology of lab-made seed crystals under the effect of impurities during crystallization. It is clearly seen from the figure that the growth of seed crystals was retarded in the presence of foreign cations (compare Figures 6.10c to f with Figure 6.10b). There is evidence in the presented images that the retardation of growth occurs both in terms of elongation and thickness with the salts of Fe^{3+} (Figure 6.10c), Fe^{2+} (Figure 6.10e) and Ni^{2+} (Figure 6.10g) appearing to have the biggest effect. Lowering the metal ion concentration (Fe^{3+}) to 0.1M was found to have the same retarding effect on crystal growth as it can be deduced by comparing the SEM image of Figure 6.11a and that of Figure 6.10c. Replacement of Fe^{3+} ion by another trivalent ion, 0.1M Al^{3+}, yielded similar crystal growth retardation characteristics (Figure 6.11b). However when a monovalent metal chloride salt was used (0.1M NaCl) relatively larger, albeit still very thin crystals were obtained (Figure 6.11c). The postulated mechanism by which crystal growth retardation occurs in the presence of foreign metal chlorides is discussed at a later section.

The effect of metal chlorides on HH crystal growth was also investigated by using Omega seed crystals and the $FeCl_3$ (Fe^{3+}) and $MgCl_2$ (Mg^{2+}) salts. It was determined in section 6.4 that the prismatic morphology of Omega seed is not stable in the $CaCl_2$ – H_2SO_4 reaction environment converting to acicular type upon recycling under controlled supersaturation (staged addition of H_2SO_4). The SEM micrographs presented in Figure 6.12 reveal that the presence of foreign metal ions caused the accleration of this crystal habit transformation process. In comparison with the case, where no metal chloride salts were added (Figure 6.12b), addition of Fe^{3+} and Mg^{2+} ions (Figures 6.12c and d, respectively) resulted in the formation of fine-sized and needle-shaped crystals. The hemihydrate-anhydrite transformation as determined by XRD analysis in the case of the presence of Fe^{3+} ions was also evident in the SEM images (refer to fibre AH crystals in Figure 6.12c and d). No evidence of HH to AH transformation (appearance of fibre type crystals) was observed for Mg ions.

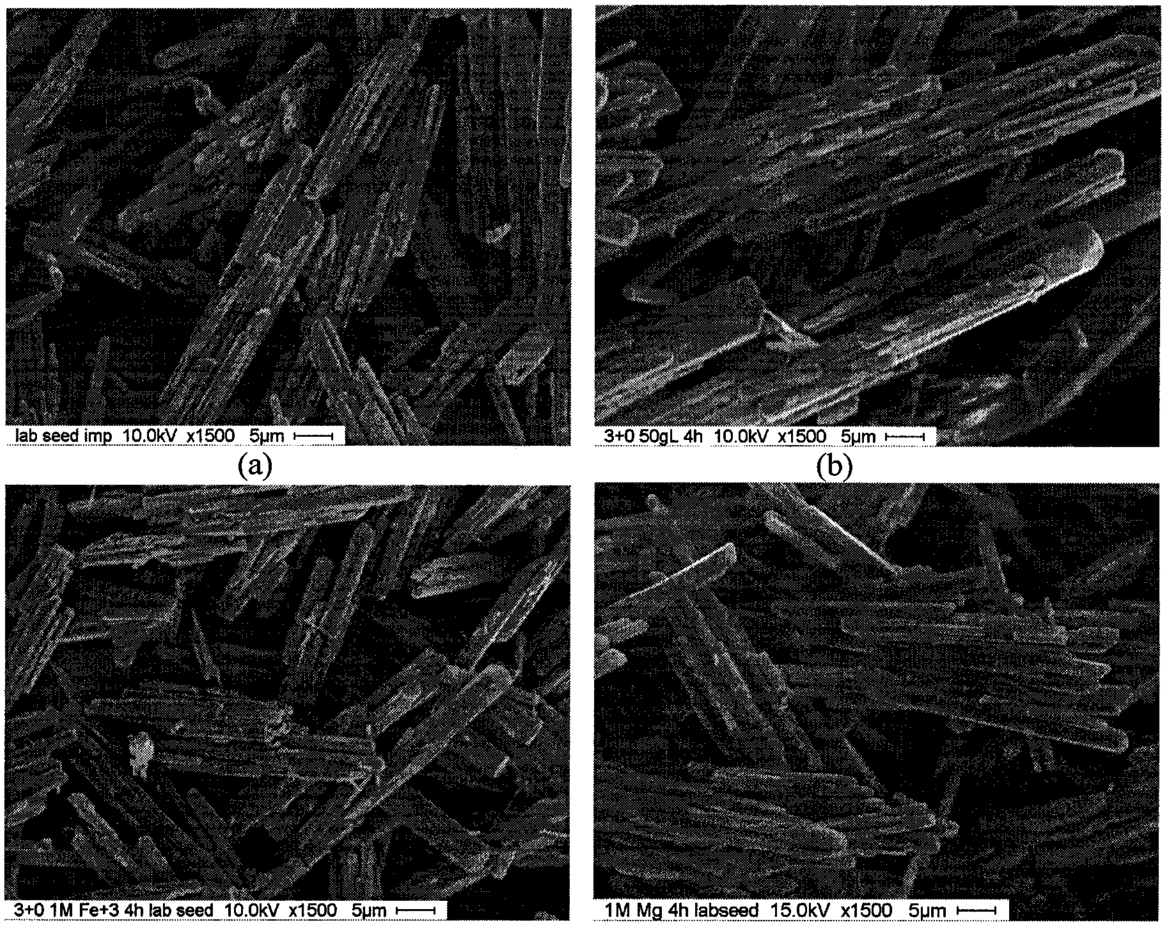

(a) (b)

(c) (d)

(e) (f)

Figure 6.10. The effect of foreign cations on HH crystal morphology (1M metal chloride salt concentration, lab-made seed); (a) Original HH seed produced in the lab, (b) 1st recycle product in the absence of impurities, (c) 1st recycle product in the presence of 1M Fe^{3+}, (d) 1st recycle product in the presence of 1M Mg^{2+} , (e) 1st recycle product in the presence of 1M Fe^{2+}, (f) 1st recycle product in the presence of 1M Ni^{2+}.

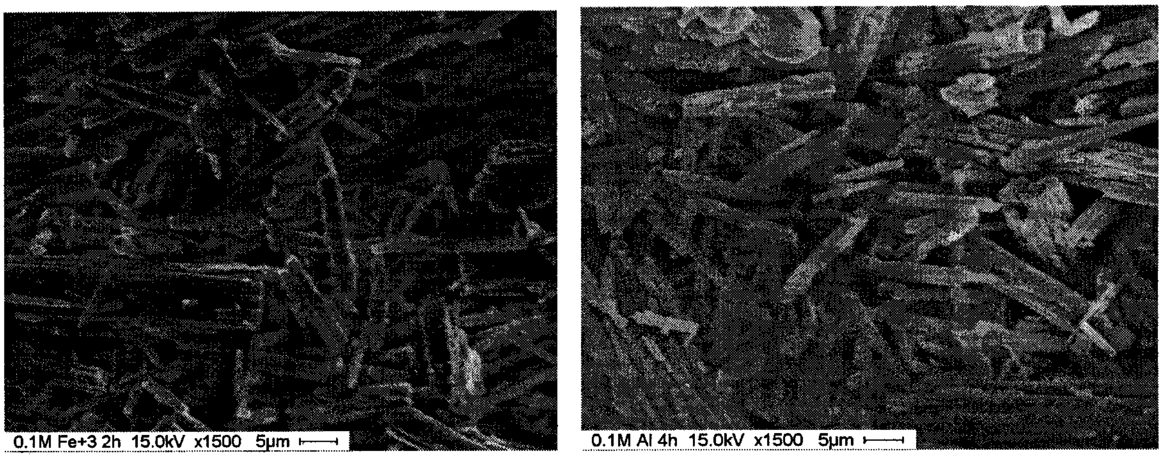

(a) (b)

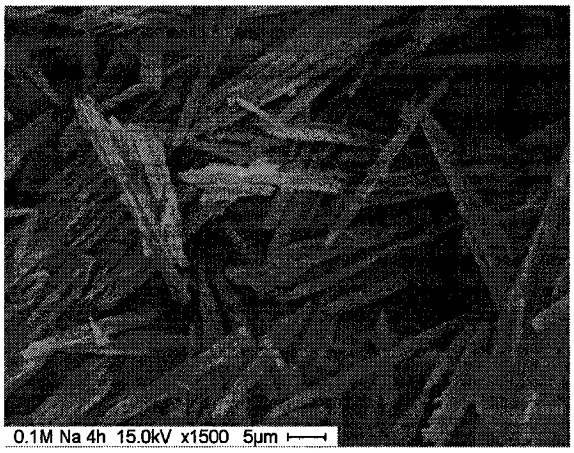

(c)

Figure 6.11. The effect of metal chloride salts on HH crystal morphology (0.1M impurity salt concentration, 100g/L lab-made seed); (a) 1st recycle product in the presence of 0.1M Fe^{3+}, (b) 1st recycle product in the presence of 0.1M Al^{3+}, (c) 1st recycle product in the presence of 0.1M Na^{+}.

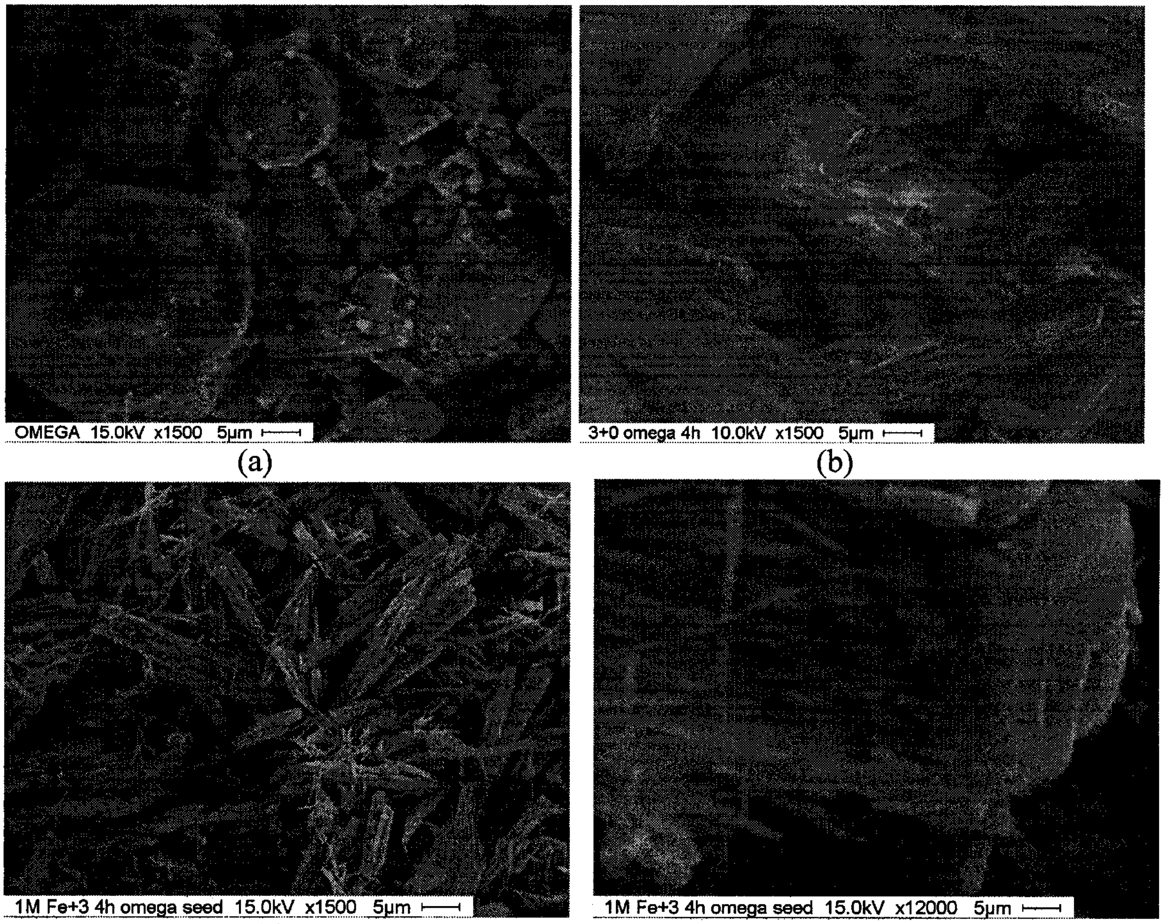

(a) (b)

(c) (d)

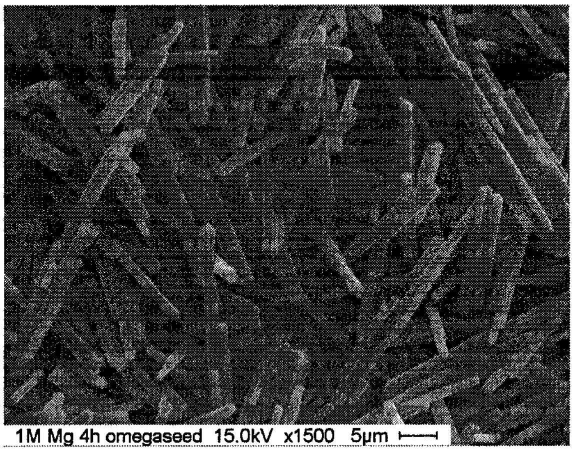

(e)

Figure 6.12. The effect of foreign cations on HH crystal morphology (1M metal cloride salt concentration, Omega seed, 1st recycle products); (a) original HH seed provided from Omega, (b) no foreign cations, (c) 1M Fe^{3+}, (d) 1M Fe^{3+}, high magnification, and (e) 1M Mg^{2+}.

The retarding effect of metal chloride salts on the growth of alpha-HH crystals was evaluated via particle size analysis. The block diagram displayed in Figure 6.13 compares the effect of different foreign metal ions on the mean diameter of the crystals produced after 1 recycle of laboratory-made and Omega seed. The mean diameters of both seed types are also indicated in the diagram (Lab-made ≈ 20.6μm and Omega seed ≈ 17.8μm). The significant growth of both seed types in the absence of foreign metal cations is also included for comparison purposes.

It is evident from the presented data that none of the foreign metal ions favoured the growth of seed crystals independent of seed type. It is clearly seen from the figure that presence of foreign metal ions either slowed down (Fe^{3+} lab seed, Mg^{2+} lab seed, Fe^{2+} lab seed) or stopped (Fe^{3+} Omega seed, Mg^{2+} Omega seed, Ni^{2+} lab seed) the growth process during the 1st recycle.

Finally measurement of the filtration rate and its correlation to mean crystal size (Figure 6.14) showed the lack of crystal growth caused by the foreign metal cations to result in some loss of filterability.

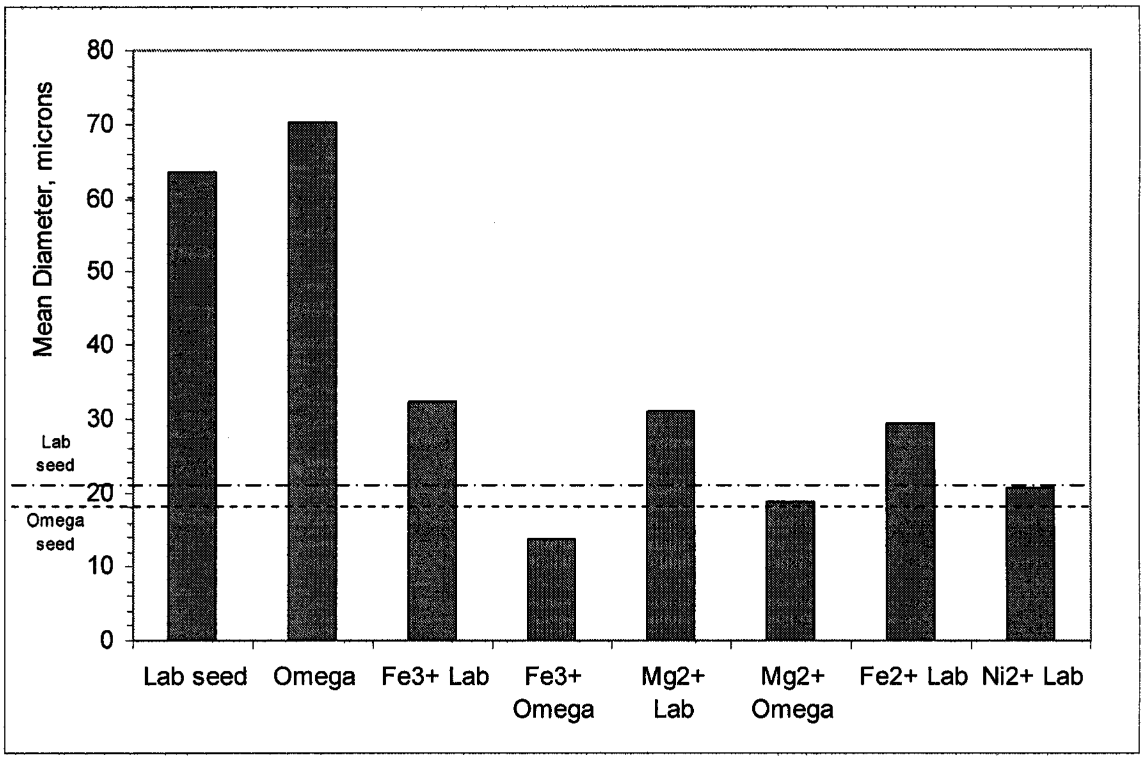

Figure 6.13. Effect of foreign cations on mean diameter of HH crystals produced after 1 recycle of 100 g/L seed.

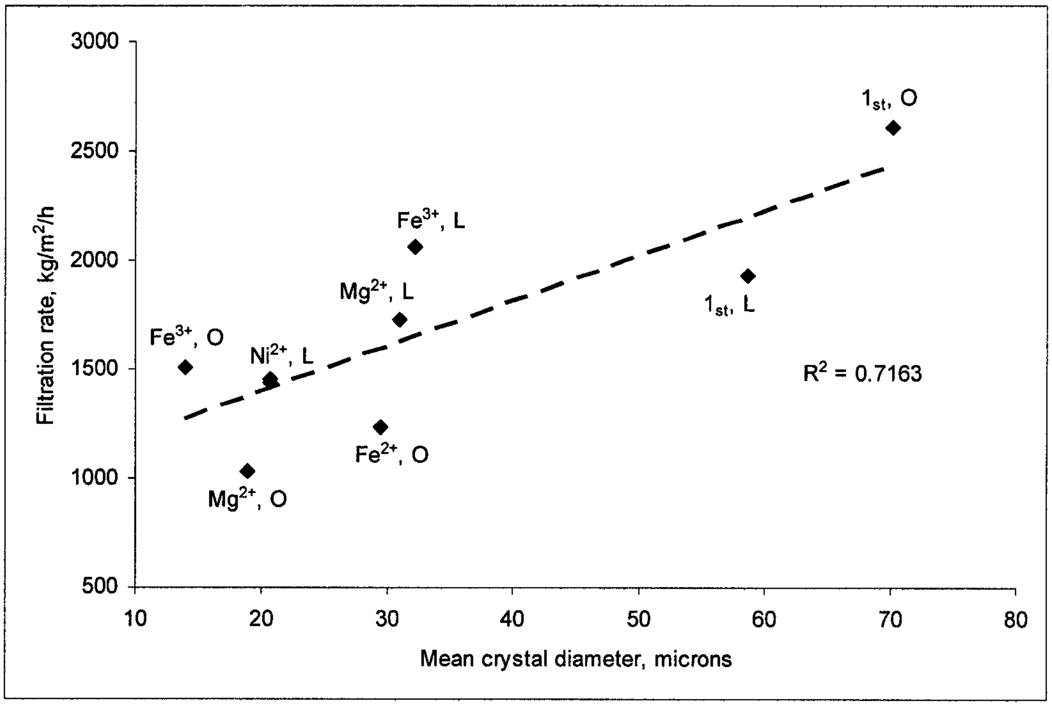

Figure 6.14. Correlation between crystal mean diameter and filtration rate.

Impurity uptake: EDS microprobe analysis was employed initially for the qualitative determination of foreign metal ion uptake by the HH crystals. According to the results presented in Figure 6.15, aluminium was the only impurity detected. It should also be noted that elemental mapping with the same equipment revealed no satisfactory information about the site of impurity incorporation and distribution.

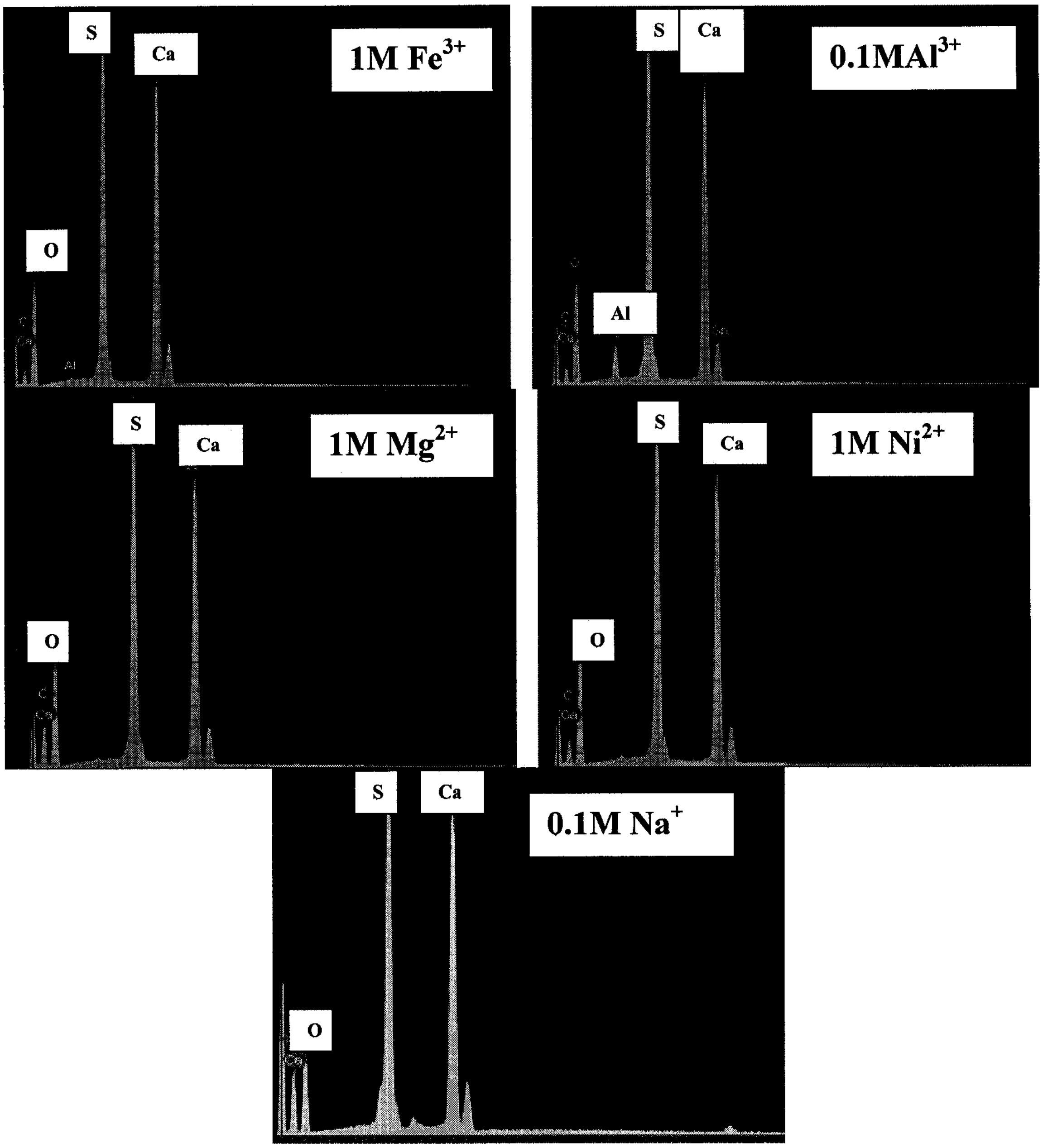

Figure 6.15. EDS microprobe analysis on crystal surface for selected foreign metal ions.

Atomic absorption analysis following the digestion of the crystals in 10% (v/v) HNO_3 solution provided quantitative data on impurity uptake. With the exception of Al, Ni and Na no incorporation of other foreign metal cations into HH crystals was detected. The detection limit was 5 ppm. The respective amounts of impurity incorporation were: 300 ppm (0.3g/t) for Na, 7000 ppm (7g/t) for Ni and 11000 ppm (11g/t) for Al. No explanation can be offered as to why these cations were incorporated but not Fe^{3+} and the other divalent ones, Fe^{2+} and Mg^{2+}. The incorporation of Na (300 ppm) in hemihydrate was significantly higher than that reported for Na in dihydrate (5 ppm) for the same $CaCl_2$-H_2SO_4 system [3]. This differentiation in the amount of Na incorporation between hemihydrate and dihydrate is in agreement with the findings of Powell's study [11], which suggests that uptake of ions into bassanite (mineral HH) is much higher than into the other $CaSO_4$ phases.

In addition to the uptake of foreign metal cations, ion chromatography was employed following the digestion of the crystals in a nitrate medium to determine the chloride ion uptake of HH crystals. The results are presented in Figure 6.16. The homogeneously crystallized product (lab-seed) contained less than 1ppm chloride. Upon recycling (3rd recycle), though, the chloride content of the crystals increased to 10ppm. On the other hand the presence of metal chlorides was found to prevent chloride uptake.

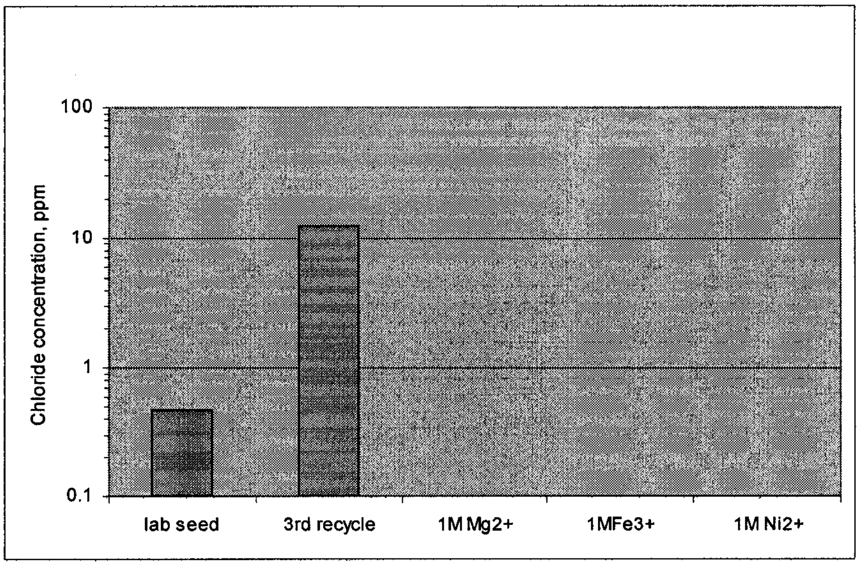

Figure 6.16. Chloride uptake of hemihydrate crystals.

Discussion: As was found in this section the presence of foreign cations in the form of metal chloride salts interfered with the stability and growth of the produced HH crystals. Thus $FeCl_3$ and $NiCl_2$ were found to induce instability to HH by accelerating its transformation to AH on one hand while all salts, with small differences caused retardation of crystal growth. Effectively, in the presence of metal chloride salts the produced crystals did not grow upon recycling but had the characteristics (morphological and size) of the lab-made seed (Figures 6.10 and 6.13). This implies that the metal chlorides acted on the surface of the seed crystals blocking the deposition of new material and hence their growth.

It was determined in section 6.4 that the mechanism of growth in this semi-batch crystallization system is via a complex agglomeration process involving the generation of fine needle-shaped crystals during the early stage of crystallization followed by parallel orientation, clustering and finally cementing ("fusion") of these agglomerates via surface deposition. Apparently the foreign cations either interfere with the clustering (attachment) of the fine needle shaped crystals or with the cementing of them by not permitting the surface deposition to occur. The SEM images of Figure 6.10 indicate that the clustering has occurred but not cementing via freshly deposited material (surface nucleation) on the loosely clustered-together aggregates.

Mullin [2] has explained this phenomenon by suggesting the accumulation of foreign ions on the surface of a seed crystal causing prevention of secondary (surface) nucleation-a perquisite for growth. Such suppression of secondary nucleation, which is associated with lowering of the surface energy of the seed crystal, has been observed in the case of $CaSO_4$ crystals. Thus Murat *et al* [17] found that foreign cations with ionic charge/ionic radius ratio higher than that of Ca^{2+} (such as Fe^{3+} and Al^{3+} with ratios respectively 44.3 and 52.6 against 18.82 for Ca^{2+} [18] retarded crystal growth due to lower surface energy thus higher homogeneous nucleation rate. In the present system, though, crystallization occurred within the metastable zone in the presence of seed (refer to Figure 6.9). It is possible, however, that a shift on the metastable zone occurred when the foreign metal chlorides were used due to their effect on $CaSO_4$ solubility. According to Li and Demopoulos [19] metal chlorides have a negative effect on $CaSO_4$ solubility hence it is conceivable that the critical supersaturation signifying the onset of homogeneous nucleation is reduced as well.

Another important aspect about the presence of metal chlorides during the crystallization of HH is their effect on $CaSO_4$ phase transition rate. As it was explained in Chapter 2, the $CaSO_4$ phase with higher solubility is thermodynamically less stable and gradually should convert to a thermodynamically more stable phase [20]. More importantly with a decrease in water activity due to the increase in electrolyte concentration, transition from a less stable (metastable) phase to more stable phase is favoured. This is suspected at least partly to occur here as well. Metal chlorides are known to lower the activity of water [21] hence the transition from HH to AH is favoured. Other facts may be responsible for the induced instability (it was observed for only Fe^{3+} and Ni^{2+} salts) but remain unknown.

6.6. Conclusions

1. Seeding was found to lead to the growth of alpha-HH crystals upon staged addition of H_2SO_4 (for maintenance of low supersaturation) into 3M $CaCl_2$ solution. As a consequence the filtration rate of the crystal slurry was improved.
2. The volume-based mean crystal size of the product was determined not to measurably depend on the amount of seed (lab-made) used.
3. The growth of needle-shaped seed crystals appeared to occur initially via agglomeration and subsequently cementing ("fusion") and outgrowth of the agglomerate.
4. Prismatic-type (columnar-shaped) seed crystals were found to initially grow over one recycle but subsequently to convert to the acicular (needle-shaped) crystal variety.
5. The laboratory (by homogeneous crystallization)-made hemihydrate variety was proven to be a superior seed in comparison to the commercially available prismatic-type variety.

6. During the early stage (30 minutes) of H_2SO_4 addition primary nucleation was observed to occur where as during the subsequent stages of acid addition, crystallization occurred within the metastable zone. Repeated recycling (up to 5 recycles) led to the production of well grown, elongated hexagonal crystals in the order of 80μm mean crystal length.
7. Metal chloride salts were found to interfere with the stability and growth of the produced HH crystals.
8. $FeCl_3$ and $NiCl_2$ salts were found to induce instability to HH by accelerating its transformation to AH on one hand while all salts ($NaCl_2$, $MgCl_2$, $NiCl_2$, $FeCl_2$, $FeCl_3$ and $AlCl_3$) with some small differences found to cause retardation of crystal growth.
9. Some of the tested foreign cations, Al^{3+}, Ni^{2+} and Na^{+}, were found to incorporate into hemihydrate crystal structure to a variable extent, from 0.3g/t for Na to 7g/t for Ni and 11g/t for Al.
10. Chloride uptake of HH seed crystals was minimum; increasing from less than 1 ppm after one cycle to 10 ppm after 3 recycles. The presence of foreign cations completely suppressed the uptake of chloride ions.

References

[1] Myerson, A.S., “Handbook of Industrial Crystallization”, 2nd Edition, Butterworth-Heinemann Ltd, Oxford, UK, 2002.

[2] Mullin, J.W., “Crystallization”, 3rd Edition, Butterworth-Heinemann, Oxford, UK, 1993.

[3] Al Othman, A., “Gypsum production and hydrochloric acid regeneration by reaction of calcium chloride solution with sulphuric acid”, M.Eng. Thesis, McGill University, Montreal, QC, 2004.

[4] Moldoveanu, G.A., “Crystallisation of inorganic compounds with alcohols”, Ph.D. Thesis, McGill University, Montreal, QC, 2005.

[5] Ling, Y., "Direct preparation of alpha-calcium sulphate hemihydrate from sulphuric acid", Ph.D. Thesis, McGill University, Montreal, QC, 2004.

[6] Tai, C.Y. and Chien, W.C., "Effects of operating variables on the induction period of $CaCl_2$-Na_2CO_3 system", Journal of Crystal Growth, 237-239, 2002, 2142-2147.

[7] Mersmann, A., "Crystallization Technology Handbook", 2nd Edition, Marcel Dekker Inc., New York, NY, 2001.

[8] Martynowicz, E.T.M.J., Witkamp, G., Rosmalen, G.M., "The effect of aluminum fluoride on the formation of calcium sulphate hydrates", Hydrometallurgy, 41, 1996, 171-186.

[9] Kubota, N., Yokota, M. and Mullin, J.W., "Supersaturation dependence of crystal growth in solutions in the presence of impurities", Journal of Crystal Growth, 182, 1997, 86-94.

[10] Kushnir, J., "Partitioning of seawater cations during transformation of gypsum to anhydrite", Geochimica et Cosmochimica Acta, 46, 1982, 433-446.

[11] Powell D.A., "Calcium sulphate hemihydrate prepared in sodium chloride solution", Australian Journal of Chemistry, 15, 1962, 868-874.

[12] College, J., "The Omega Process: Direct conversion of calcium sulphite to alpha hemihydrate", in 6th International Conference on Natural and Synthetic Gypsum, Process Research Ortech Inc., Toronto, Canada, 2000, 25-(1-11).

[13] Follner, S., Wolter, A., Preusser, A., Indris, S., Silber, C., Follner, H., "The setting behaviour of α- and β-$CaSO_4 \cdot 0.5H_2O$ as a function of crystal structure and morphology", Crystal Research and Technology, 37, 2002, 1075-1087.

[14] El Moussaouiti, M., Boistelle, R., Bouhaouss, A., Klein, J.P., "Crystallization of calcium sulphate hemihydrate in concentrated phosphoric acid solutions", Chemical Engineering Journal, 68, 1997, 123-130.

[15] El Moussaouiti, M., Boistelle, R., Bouhaouss, A., Klein, J.P, "Agglomeration kinetics of calcium sulphate hemihydrate crystals in sulpho-phosphoric solutions", Journal of Crystal Growth, 169, 1996, 118–123.

[16] Li, Z., and Demopoulos, G.P., “Development of an improved chemical model for the estimation of solubilities in the $HCl-CaCl_2-H_2O$ system up to 100°C”, Industrial and Engineering Chemistry Research, 45, 2006, 2914-2922.

[17] Murat, M., Hajjouji, A.E., Comel, C., “Investigation on some factors affecting the reactivity of synthetic orthorhombic anhydrite with water, I. Role of foreign cations in solutions”, Cement and Concrete Research, 17, 1987, 633-639.

[18] Shannon, R.D., “Revised effective ionic radii and systematic studies of interatomic distances in halides and chalcogenides”, Acta Crystallographica, A32, 1976, 751–767.

[19] Li, Z., and Demopoulos, G.P., “The effect of NaCl, $MgCl_2$, $FeCl_2$, $FeCl_3$, and $AlCl_3$ on solubility of $CaSO_4$ phases in aqueous HCl or $HCl+CaCl_2$ solutions at 298 to 353K”, Journal of Chemical Engineering Data, 51, 2006, 569-576.

[20] Nývlt, J., “The Ostwald rule of stages”, Crystal Research and Technology, 30, 1995, 443-449.

[21] Demopoulos, G.P., “Aqueous processing and its role in the production of inorganic materials and environmental protection”, Canadian Metallurgical Quarterly, 37, 1998, 1-18.

CHAPTER 7

Synopsis

7.1 Introduction

This chapter begins with global conclusions, which are the highlights from the concluding remarks drawn at the end of Chapters 4, 5 and 6. Global conclusions are followed by claims to originality, where the original contributions of this research to knowledge are identified. Finally, some recommendations for future work are given which may contribute to further development of the alpha-calcium sulphate hemihydrate production process studied in this thesis.

7.2 Global Conclusions

In this thesis, the production of alpha-calcium sulphate hemihydrate material by the controlled reaction of $CaCl_2$ solution with H_2SO_4 under atmospheric conditions was investigated in detail. The important findings of this work are as follows:

1. Through a series of stability tests, which involved the equilibration of dihydrate crystals in $CaCl_2$-HCl solutions, the kinetic stability ranges of $CaSO_4$ modifications were established under given electrolyte concentration conditions at 80°C. Accordingly, it was found anhydrite to be the only thermodynamically stable phase at 80°C, dihydrate and hemihydrate being metastable or unstable. Metastable phases were found to convert to AH within a maximum of 18 hours depending on electrolyte type and concentration. At low levels of HCl (<3M) and $CaCl_2$ (<1.5M), dihydrate was found to be metastable. Hemihydrate was found to

be metastable only in the presence of $CaCl_2$. It was also established that elevation of HCl concentration accelerates DH to HH and HH to AH conversion, while increased $CaCl_2$ concentration was found to retard HH-AH transformation.

2. Experimental and computational solubility determinations suggested that a threshold water activity (around 0.85) exists for DH-HH transition in the $CaCl_2$-HCl system at 80^oC. Theoretical estimations of the DH/HH transition with OLI Stream Analyser software were found to be in reasonable agreement with experimental findings.

3. Morphological examination of the crystals undergoing DH to HH transformation revealed that at elevated $CaCl_2$ concentration the growth of HH crystals is suppressed. Independent of the nature and concentration of electrolyte, HH was found to grow in the z-axis with acicular habit displaying a needle-shaped hexagonal crystal structure. The transition from DH to HH appears to be governed by the topochemical mechanism while that of DH to AH or HH to AH by the solid-state conversion mechanism.

4. Controlled semi-batch reactive crystallization tests involving direct reaction of $CaCl_2$ with H_2SO_4 under atmospheric conditions (at 80^oC) and $H_2SO_4/CaCl_2$ molar ratio < 0.9 demonstrated that alpha-HH can be successfully precipitated. As a result of the performed crystallization tests an operating window for HH production was established. In agreement with the stability tests, DH and HH were found to be metastable under the determined HH production conditions exhibiting variable conversion kinetics. The final HCl concentration was found to accelerate DH to HH and HH to AH conversion, while on the other hand increasing $CaCl_2$ concentration in the final solution was found to improve the kinetic stability of HH.

5. The nucleation and growth stages of the studied reactive crystallization system were successfully separated with the aid of the LaMer Diagram concept.

Supersaturation was found to decrease during reaction of $CaCl_2$ with H_2SO_4, in a semi batch reactor, due to increasing $CaSO_4$ solubility caused by decreasing $CaCl_2$ and increasing HCl concentrations. The very beginning of the reaction (i.e. first 30 minutes) is governed by high supersaturation favouring homogeneous nucleation, while for the remaining of the reaction crystallization occurs within the metastable zone favouring crystal growth. Slow rate or multiple stage (at least 8-stage) addition of H_2SO_4 was found to improve the growth and filtration rates of the produced crystals.

6. The general $CaSO_4$ precipitation sequence determined to occur, involved initial primary nucleation of dihydrate followed by transformation of dihydrate to hemihydrate (nucleation and growth) and finally transformation of hemihydrate to anhydrite upon prolonged equilibration. This sequence is in agreement with the Ostwald Rule of stages. Similar to HH produced from the curing of DH crystals, the reactive crystallization tests also produced needle-shaped hexagonal HH crystals growing along the z-axis.

7. Seeding was found to promote the growth of alpha-HH crystals upon staged addition of H_2SO_4 (for maintenance of low supersaturation) into 3M $CaCl_2$ solution. As a result of low supersaturation control and seeding the filtration rate of the crystal slurry was enhanced. Mean crystal size and filtration rate was not affected by the amount of Lab-made seed load. The growth of needle-shaped seed crystals appeared to occur initially via agglomeration and subsequent cementing ("fusion") and outgrowth of the agglomerate. In the case of the commercial Omega seed material the prismatic crystal habit was found to shift to acicular habit upon multiple recycling. The laboratory (by homogeneous crystallization)-made hemihydrate variety was proven to be a superior seed in comparison to the commercially available prismatic-type variety. Repeated recycling (up to 5 recycles) led to the production of well-grown elongated hexagonal HH crystals having typically 80μm volume-based mean crystal diameter or 100-120 μm crystal length and 10-15 μm crystal diameter.

8. Foreign metal chloride salts were found to interfere with the stability and growth of the HH crystals. In particular the chloride salts of Fe^{3+} and Ni^{2+} were found to interfere with the stability of HH by accelerating its transformation to AH. All salts tested in this study, namely NaCl, $MgCl_2$, $NiCl_2$, $FeCl_2$, $FeCl_3$ and $AlCl_3$, were found to slow down or block the crystal growth process with minor differences. In terms of metal uptake it was determined that only Al^{3+}, Ni^{2+} and Na^{+} ions to incorporate into hemihydrate crystal structure to a variable extent, from 11g/t for Al to 7g/t for Ni and 0.3g/t for Na. On the other hand the chloride uptake was limited (up to 10 ppm after 3rd recycle) while no chloride uptake was detected in the presence of foreign metal cations.

7.3 Claims to Originality

1. The crystallization behaviour of alpha calcium sulphate hemihydrate by the controlled reaction of $CaCl_2$ with H_2SO_4 is reported for the first time.

2. It is observed for the first time that $CaCl_2$ has a kinetic stabilization effect on HH.

3. Equally novel are the examination of phase transformation kinetics of $CaSO_4$ hydrates and construction of an experimental kinetics-based phase diagram in the $CaCl_2$-HCl system.

4. The growth of HH crystals via supersaturation control by staged addition of H_2SO_4 and seeding in $CaCl_2$ solutions has been studied for the first time.

5. Finally, it is the first time that the effect of metal chlorides on crystal growth and metal uptake of alpha-HH in the $CaCl_2$-HCl system is discussed.

7.4 Recommendations for Future Work

The following suggested future work aims to further development and knowledge advancement of the novel alpha-HH production technology described in this thesis for the first time.

1. The mechanical properties (i.e. mechanical-compressive strength, setting time, consistency) of alpha-HH product should be carefully investigated and improved if necessary using admixtures.

2. Although it was demonstrated in this work that HCl can be regenerated at the end of the reaction to ~4N HCl strength, further increase to 5.5N (azeotropic composition) should be sought to facilitate integration of this crystallization operation into an HCl-based hydrometallurgical process.

3. The potential residual sulphate (mainly caused by dissolved $CaSO_4$) problem (scale formation) in regenerated HCl solution after reactive crystallization has to be assesed before HCl is recycled back to the process.

4. Further improvement of crystal quality in terms of growth should be sought via the investigation of the effect of crystal habit modifiers (additives).

5. The crystallization of alpha-HH by the reaction of $CaCl_2$ with H_2SO_4 should be tested using a real process solution in a continuous reactor to measure the growth kinetics, product purity and assess the feasibility of the process.